The New Cosmology and the New Gravity

John R. Rix

First edition 1.0

ABSTRACT

Traditional cosmology and gravity feature dark matter, dark energy, and an expanding universe. These features (plus general relativity) generate predictions for observations. Recent observations by the James Webb space telescope and improved observations of the Hubble parameter have generated a tension with traditional predictions that has passed the breaking point. The time has come to consider a replacement for tradition—this document (NCNG). NCNG studies a wide range of astrophysics topics of interest. NCNG is structured as a textbook or as a series of lecture notes for graduate students. A good starting point for a new reader is Appendix A, where there is a brief history of traditional development. There is also a brief history of how my ideas for NCNG were born, and why I believe I am qualified to launch this revolution.

One cannot overturn a century of wrong physics by thinking inside the box and coloring inside the lines.

The universe is vast and ancient beyond comprehension.

TABLE OF CONTENTS

I. INTRODUCTION

Tensions between observations and theories of gravity and cosmology have existed for decades. The recent standard theory has been general relativity (GR) for gravity and Λ cold dark matter (LCDM) for cosmology. I choose to lump these together in this document (GRLCDM). There has been a decades long disagreement between astronomy and physics. Astronomers believe that GRLCDM does not allow enough time for observed large-scale organization of matter. Observations from JWST favor the astronomers. Recent observations by JWST seem to have destroyed LCDM cosmology. Tensions between observations of Hubble's parameter ([1] and [2]) and predictions using GRLCDM are well past the breaking point. I believe these problems render GRLCDM seriously suspect.

A. A model for a post relativity universe

Instead of focusing on proving that GRLCDM is a wrong theory (there are dozens of proofs), I will look at this problem in a different way. If GRLCDM is wrong, then a new theory must replace it. What form could that new theory take? In what follows, I will develop a model which is entirely different from GRLCDM—named NCNG after this document.

The main features of NCNG are simple. Cosmology has nothing to do with space-time or matter. Gravity has nothing to do with space-time. Cosmology and gravity have nothing to do with each other. NCNG is very complex but flexible. General invariance is an obvious casualty of NCNG (seriously wrong). One will discover that special relativity is a casualty as well (but an excellent approximation to reality). Appendix A has informative historical-observations and commentary about the source of the ideas leading to the NCNG revolution.

NCNG represents a new philosophy about nature and descriptive theories. GR has been popular because it is elegantly simple (beautiful)—an ancient Greek requirement. Unfortunately, GR is too simple (hence rigid). Rigidity requires special additions to arrive at the correct description (e.g., dark matter). *I believe that the universe is ugly*—lots of complex interconnections. One will discover that NCNG must be ugly as well.

In all that follows, the hypothesis is that GRLCDM is a wrong theory. Thus, any observation or theoretical conclusion that involves GRLCDM is suspect (re-examination is required). Thousands of papers from the past are suspect. That is why the NCNG bibliography is skimpy. The NCNG revolution will be very unpopular with professors, but decades of re-examinations by graduate students will be required—endless thesis topics.

B. Studying this document

I apologize for using so many acronyms (Appendix Y), but new things need new names. This document is meant to be *read and studied in the order of the contents*. All the equations and concepts are new—never seen before. One must spend many hours to understand the totality. Random examination of subsections is a recipe for confusion and misunderstandings.

The standard model date corresponds to the Appendix Z set of *universal constants* used for calculations of examples and figures in the current document. As new observations and research occur, the set of constants will be periodically updated. The new constants will be used to calculate a new set of examples and figures in a new document. Corrections and new equations will also be

added to the new document—a work in progress. It is important to keep in mind that the universal constants in Appendix Z are not independent. There are many constraints imposed on them.

II. THE NEW COSMOLOGY IN AN EMPTY UNIVERSE

Consider a (vanilla) universe that contains only two (classical) isotropic fields. The universe has four dimensions (x^0, x^1, x^2, x^3) measured in meters and a dimensionless (vanilla) metric tensor ($g_{00} = 1$ and $g_{jk} = -\delta_{jk}$ where $\delta_{JJ} = 1$ else zero). *Both fields are self-supporting*, i.e., either one can pervade all the universe without a source. Furthermore, the fields can interact with each other in a very specific manner. Each field will be dimensionless but characterized by a length.

There is no matter, so there are no observers (physicists or astronomers). There are no laws of physics—no matter and no physicist to perform experiments. There is no relativity—no pair of observers. If one finds that each field is a function only of x^0 when there is no matter, then there is no time involved in evolution (only length). Time can only result from the interaction of the two fields with matter—*matter can be thought to create the need for time*.

How does one discover the evolution of the fields? Our toolbox is nearly empty, but the principle of least action can be used,

$$0 = \delta \int dx^0 dx^1 dx^2 dx^3 \mathcal{L}. \tag{2.1}$$

$\mathcal{L}$ is the Lagrangian density (LD) for each field, and it must only be a function of universal constants, fields, and first derivatives of fields. The principle was created by a material physicist, so it uses (familiar) material units (MKS). The LD has units of $\mathrm{KS^{-1}M^{-2}}$, but the empty universe only has M—no S or K. One needs two universal constants to generate S and K from M.

I have chosen to define the needed constants as a velocity ($c = 2.99799 \times 10^8\ \mathrm{MS^{-1}}$) and a unit of action ($h = 6.62607015\text{E-}34\ \mathrm{M^2KS^{-1}}$). There are no photons in an empty universe, so any connection between photons and *c* will be deferred to subsequent sections. A constant is universal if $\partial_\mu \text{constant} = 0$, where $\partial_\mu \equiv d / dx^\mu$. In what follows, the usual conventions of tensor algebra and calculus are used. Covariant and contravariant indexes are raised and lowered using the vanilla metric tensor defined above. There are no meaningful transformations of coordinates in the empty universe.

The LD for the fields is a scalar (zero rank tensor). The apex field is a rank two tensor, and the epoch field is a scalar. The (more robust) apex field will be studied first.

A. The tensor apex field

The apex field is a dimensionless second-order symmetric tensor, $\mathrm{v}^{ax}{}_{\mu\nu}(x)$. The apex label (*ax*) and the four-coordinate (*x*) are implicit in what follows. One can define some useful scalars and vectors (first order tensors) derived from $\mathrm{v}_{\mu\nu}$: $\mathrm{S} \equiv \mathrm{v}^\lambda_\lambda$, $\mathrm{J} \equiv \mathrm{v}^\alpha_\lambda \mathrm{v}^\lambda_\alpha$, $\mathrm{S}_\mu \equiv \partial_\mu \mathrm{S}$, $\mathrm{N}_\mu \equiv \partial_\lambda \mathrm{v}^\lambda_\mu$.

There are two pieces to the apex LD, the "kinetic" density, $\mathcal{L}^{\mathrm{T}}_{\mathrm{ax}}(x)$, and a "potential" density, $\mathcal{L}^{\mathrm{V}}_{\mathrm{ax}}(x)$. The complete LD is then, $\mathcal{L}_{\mathrm{ax}} = \mathcal{L}^{\mathrm{T}}_{\mathrm{ax}} - \mathcal{L}^{\mathrm{V}}_{\mathrm{ax}}$. Each piece is defined as follows:

$$4\kappa_{ax}\mathcal{L}^{\mathrm{T}}_{\mathrm{ax}}(x) = g^{\mu\nu}\{\partial_\mu \mathrm{v}^\alpha_\beta\, \partial_\nu \mathrm{v}^\beta_\alpha - \mathrm{S}_\mu \mathrm{S}_\nu + 2\,\mathrm{N}_\mu\left(\mathrm{S}_\nu - \mathrm{N}_\nu\right)\}, \tag{2.2}$$

$$4\kappa_{ax}\mathcal{L}^{\mathrm{V}}_{ax}\left(x\right) = \mathrm{L}_{ax}^{-2}\,\mathrm{F}_{ax}\left(\mathrm{J}\right), \tag{2.3}$$

where $\kappa_{ax} = \mathrm{L}_{ax}{}^{2}\,\hbar^{-1}\mathcal{N}_{ax}{}^{-1}$ and $\mathcal{N}_{ax}$ is a dimensionless universal constant related to the energy density of the apex field. L_{ax} is a characteristic length associated with the apex field—a universal constant.

Now vary the field, $\delta\,\mathrm{v}^{\mu\nu}$, within the action integral to obtain the apex field equation *in the absence of sources*,

$$0 = \Omega^{ax}{}_{\mu\nu} + \tfrac{1}{2}\mathrm{L}_{ax}^{-2}\left(\mathrm{v}_{\mu\nu}\frac{\partial\,\mathrm{F}_{ax}}{\partial\,\mathrm{J}}\right), \tag{2.4}$$

where the coordinate *x* is implicit. Furthermore:

$$\Omega^{ax}{}_{\mu\nu} = \Xi^{ax}{}_{\mu\nu} - \tfrac{1}{2}\,g_{\mu\nu}g^{\beta\lambda}\Xi^{ax}{}_{\beta\lambda}, \tag{2.5}$$

$$2\Xi^{ax}{}_{\mu\nu} = g^{\alpha\beta}\partial_\alpha\partial_\beta\,\mathrm{v}_{\mu\nu} + \partial_\mu\partial_\nu\,\mathrm{S} - \partial_\mu\,\mathrm{N}_\nu - \partial_\nu\,\mathrm{N}_\mu\,. \tag{2.6}$$

Solve Eq. (2.4) by using an isotropic apex field that depends only on the evolution parameter, $\mathrm{v}^{ax}{}_{jk}\left(x\right) = A\left(x_0\right)\delta_{jk}$ (the other elements are zero). Furthermore, a specific three-term form for the potential is chosen,

$$\mathrm{F}_{ax}\left(\mathrm{J}\right) = -\sum_{n=1}^{3} 6d_n^{ax}3^{-n}\,\mathrm{J}^n\,, \tag{2.7}$$

where $\mathrm{J} = 3A^2$, and d_n^{ax} are a set of three dimensionless universal constants to be determined from astronomical observations. Using this potential in Eq. (2.4) leads to the following result,

$$\frac{d^2A}{(dx^0)^2} = -\,\mathrm{L}_{ax}{}^{-2}\,A\sum_{n=1}^{3} n d_n^{ax}\left(A^2\right)^{n-1}. \tag{2.8}$$

A first integral of Eq. (2.8) is as follows:

$$dA/\,dx^0 = \pm\,\mathrm{L}_{ax}{}^{-1}\left[\varsigma_0^2 - \sum_{n=1}^{3} d_n^{ax}\left(A^2\right)^n\right]^{1/2}, \tag{2.9}$$

where ς_0 is a constant of integration. Eq. (2.9) is valid only for values of *A* for which the term in brackets is not negative. This solution gives cyclic behavior with *A* endlessly oscillating between

two turning points (where $dA/dx^0 = 0$). There are two branches of Eq. (2.9). For reasons that will become clear in section III, the minus branch (decreasing *A*) is labeled as the red branch. Increasing *A* is the blue branch.

It should be clear that *the apex field is a clock,* but it does not measure time. Furthermore, one should expect that interactions between *A* and material particles will cause any material clock to have a complex relation to the apex clock.

Since $\mathrm{J} = 3A^2$, it follows that one would expect the scalar J to be invariant under a Lorenz transformation of coordinates (thus likewise for *A*). The right-hand side of Eq. (2.9) would be expected to be invariant, but the left-hand side would transform like the time-like component of a vector. This dichotomy would go away if $\mathrm{L}_{ax} \to \infty$. L_{ax} will be very large (9 billion light-years) but finite. The apex field breaks Lorentz invariance to a tiny degree and renders special relativity incorrect (but an extremely good approximation to reality). This result should be expected since the apex field embodies a special frame of reference for the universe. *General relativity is seriously wrong because special relativity is a little bit wrong*.

In all that follows, it is necessary to keep in mind that there will be no automatically invariant coordinate transformations in NG (unlike GR). There is one primary metric tensor (the rest frame for the apex field, $g_{00} = 1$ and $g_{jk} = -\delta_{jk}$) for which the equations of NCNG are meant to be applied. A coordinate transformation may introduce new physics, e.g., a rotating coordinate system plus Newtonian physics generates a Coriolis force. Furthermore, the label of scalar, vector, etc. in NCNG means the transformation label in the limit $\mathrm{L}_{ax} \to \infty$.

The energy density of the apex field (in the absence of the epoch field) is proportional to the potential density of Eq. (2.3) evaluated at a turning point,

$$\mathrm{U}_{ax} = -\tfrac{3}{2}\hbar c \mathcal{N}_{ax} \mathrm{L}_{ax}^{-4} (\zeta_0)^2. \tag{2.10}$$

Eq. (2.9) is correct if there is no source term in Eq. (2.4). If the LD for the epoch field contains *A*, then there will be an interaction term. The epoch field must be studied before finishing with the apex field.

B. The scalar epoch field

The idea of a self-supporting all-pervading scalar field with two possible vacuum states (true and false) is largely due to Sidney Coleman [3]. I have taken this idea into a different arena. In NC, the epoch field will couple with the apex field, and each vacuum state will alternate between true and false as the apex field evolves. In contrast to the situation in [3], changes will proceed with cosmologic slowness.

The epoch field (ϕ_{ep}) is dimensionless and real. The epoch field LD ($\mathcal{L}_{ep}$) has the following form:

$$\kappa_{ep} \mathcal{L}_{ep}(x) = \tfrac{1}{2} g^{\mu\nu} \partial_\mu \phi_{ep} \partial_\nu \phi_{ep} - \mathrm{L}_{ep}^{-2} \mathrm{V}_{ep}(\phi_{ep}), \tag{2.11}$$

$$\mathrm{V}_{ep}(\phi_{ep}) = -\tfrac{1}{2}\phi_{ep}^{\ 2} + \tfrac{1}{3}\lambda(A)\phi_{ep}^{\ 3} + \tfrac{1}{4}a_{ep}^{\ 2}\phi_{ep}^{\ 4}, \tag{2.12}$$

where $\kappa_{ep} = \mathrm{L}_{ep}{}^2 \hbar^{-1} \mathcal{N}_{ep}{}^{-1}$ and $\mathcal{N}_{ep}$ is a dimensionless universal constant related to the energy density of the epoch field. L_{ep} is a characteristic length and a_{ep} is a positive dimensionless factor—both universal constants associated with the epoch field. $\lambda(A)$ is a dimensionless function of the apex field,

$$\lambda(A) = -\lambda_{ep} + \beta_{ep} \tanh(\Gamma_{ep}\{A(x^0)^2 - A_{ep}{}^2\}), \tag{2.13}$$

where λ_{ep}, β_{ep}, Γ_{ep}, and $A_{ep} > 0$ are dimensionless universal constants. Eq. (2.13) is legal because *A* is a scalar, and the resulting LD does not have *explicit* dependence on x^0. There are seven universal constants for the epoch field (tabulated in Appendix Z), but all of them can be determined (in principle) from observations. Note that $\lambda(-A) = \lambda(A)$, so the resulting cosmology will be symmetric as well.

There are two possible vacuum states that correspond to local minima of Eq. (2.12), and they occur at the following values of ϕ_{ep},

$$\phi_{ep}{}^{\pm} = \{-\lambda(A) \pm [a_{ep}{}^2 + \lambda(A)^2]^{1/2}\} / 2a_{ep}{}^2. \tag{2.14}$$

If $\mathrm{V}_{ep}(\phi_{ep}{}^+) < \mathrm{V}_{ep}(\phi_{ep}{}^-)$ then $\phi_{ep}{}^+$ is the true vacuum state and $\phi_{ep}{}^-$ is the false vacuum, otherwise the reverse is true. When $\mathrm{V}_{ep}(\phi_{ep}{}^+) = \mathrm{V}_{ep}(\phi_{ep}{}^-)$ the vacuum states are degenerate, and that occurs when $\lambda(A_D) = 0$. As x^0 increases, *A* changes (very slowly), and it is possible that when *A* crosses A_D what was previously a true vacuum has become a false vacuum. In that case it is possible for the false vacuum to decay into a true vacuum. The decay process is explained in [3] and [4] and in Appendix B. This process will be important in NC and described in greater detail below. The goal in this sub-section is to develop the energy density of the epoch field and its broad behavior.

The study will start with the assumption that $\Gamma_{ep} >> 1$. Eq. (2.13) shows that the epoch field will be independent of the apex field except for a tiny region around $A(x^0)^2 = A_{ep}{}^2$ (where vacuum decay will play a role). In that case, Eq. (2.14) takes the simplified form:

$$\begin{aligned} \phi_{ep}{}^{\pm} &= \{\lambda_{ep} - \beta_{ep} \pm [a_{ep}{}^2 + (\lambda_{ep} - \beta_{ep})^2]^{1/2}\} / 2a_{ep}{}^2 \quad A^2 > A_{ep}{}^2, \\ \phi_{ep}{}^{\pm} &= \{\lambda_{ep} + \beta_{ep} \pm [a_{ep}{}^2 + (\lambda_{ep} + \beta_{ep})^2]^{1/2}\} / 2a_{ep}{}^2 \quad A^2 < A_{ep}{}^2. \end{aligned} \tag{2.15}$$

There will be constraints for λ_{ep}, β_{ep}, a_{ep}, but $\beta_{ep} > |\lambda_{ep}|$ will suffice here. If $A^2 > A_{ep}{}^2$, the true (surviving) vacuum will be $\phi_{ep}{}^-$ (< 0), and for $A^2 < A_{ep}{}^2$ the true vacuum will be $\phi_{ep}{}^+$ (> 0).

$A_{ep}{}^2$ will lie between the turning points of *A*, so *each branch of A will have two distinct epochs with different vacuums*. I choose to name the branch-epochs after seasons—red or blue summer for $A^2 < A_{ep}{}^2$ and red or blue winter for $A^2 > A_{ep}{}^2$. There are also two (very brief) transition periods for each branch when *A* is very nearly equal to A_{ep} also named after seasons—spring when

A^2 decreases through ${A_{ep}}^2$, and fall when A^2 increases through ${A_{ep}}^2$. In the new cosmology *the universe will endlessly pass in order through the eight seasons*—red spring, red summer, red fall, red-blue winter, blue spring, blue summer, blue fall, blue-red winter, red spring, etc., (a cyclic cosmology). We are in early red summer. The color tags for the seasons will be explained in section III(D).

It is helpful to relabel the vacuums as follows:

$$\begin{aligned} \phi_W &= \{\lambda_{ep} - \beta_{ep} - [{a_{ep}}^2 + (\lambda_{ep} - \beta_{ep})^2]^{1/2}\} / 2{a_{ep}}^2 \quad \text{winter,} \\ \phi_S &= \{\lambda_{ep} + \beta_{ep} + [{a_{ep}}^2 + (\lambda_{ep} + \beta_{ep})^2]^{1/2}\} / 2{a_{ep}}^2 \quad \text{summer.} \end{aligned} \tag{2.16}$$

Furthermore, it will be useful to define a linear scalar-function of ϕ_{ep} as follows:

$$\mathrm{E}(\phi_{ep}) = [\phi_{ep}(x^0) - \phi_S] / (\phi_W - \phi_S), \tag{2.17}$$

where $\mathrm{E} = 1$ in winter and $\mathrm{E} = 0$ in summer.

When matter is added to the universe, E (or any function of E and/or *A*) can be inserted anywhere in the LD for constituents. Therefore, one can have different physics in winter versus summer. Fig. C1 in Appendix C shows (red spring) E as a function of *A* for the universal constants tabulated in Appendix Z. The gap in the figure corresponds to the very brief period of active vacuum decay (what I will call the bubble era). The continuous portion is the more-lengthy "classical" part of red spring.

The epoch field energy density is given by the following forms:

$$\begin{aligned} \mathrm{U}_{ep}^{W} &= \hbar c \mathcal{N}_{ep} \, \mathrm{L}_{ep}{}^{-4} \mathrm{V}_{ep}(\phi_W) \quad \text{winter,} \\ \mathrm{U}_{ep}^{S} &= \hbar c \mathcal{N}_{ep} \, \mathrm{L}_{ep}{}^{-4} \mathrm{V}_{ep}(\phi_S) \quad \text{summer.} \end{aligned} \tag{2.18}$$

Furthermore, $\mathrm{U}_{ep}^{S} < \mathrm{U}_{ep}^{W} < 0$.

I must state the most basic aspect of NCNG at this point—the hierarchy of energy densities and ranges,

$$\begin{aligned} &\left|\mathrm{U}_{ax}\right| > \left|\mathrm{U}_{ep}\right| >> \mathrm{U}_{matter} \quad \text{all seasons,} \\ &\mathrm{L}_{ax} >> \mathrm{L}_{ep} >> \hbar / \mathrm{m}_{\mathrm{proton}} c. \end{aligned} \tag{2.19}$$

The average energy density of matter in the universe is thought to be about 250 Mev per cubic meter (a suspect value). The magnitude of the epoch field energy density will be at least eight orders of magnitude larger than average matter. The magnitude of apex energy density will be about two orders of magnitude greater than the epoch field. Thus, *matter can be considered as an insignificant froth having negligible impact on the cosmology generated by the apex and epoch fields* (despite the interaction of these fields with matter).

Neglecting matter leads to the following relations between the seasonal apex and epoch energy densities:

$$
\begin{aligned}
&\mathrm{U}_{ax}(x^0)+\mathrm{U}_{ep}(x^0)=\ \text{constant},\\
&\mathrm{U}^S_{ep}<\mathrm{U}^W_{ep}<0\Rightarrow 0>\mathrm{U}^S_{ax}>\mathrm{U}^W_{ax},\\
&\alpha^{ax}_W\equiv[(\mathrm{U}^S_{ep}-\mathrm{U}^W_{ep})/\mathrm{U}^S_{ax}],\\
&1>>\alpha^{ax}_W>0,\\
&\mathrm{U}^S_{ax}=-1.5c\,\mathrm{L}_{ax}{}^{-4}\hbar\,\mathcal{N}_{ax},
\end{aligned}
\tag{2.20}
$$

where α^{ax}_W is a universal (apex) constant tabulated in Appendix Z. The apex energy density in summer is *c* times the kinetic LD (evaluated where the potential LD is zero).

The final step in this section is the inclusion of the epoch field into a source term for Eq. (2.8). The Euler-Lagrange equation is as follows:

$$
\begin{aligned}
&0=\partial\mathcal{L}_{ep}/\partial\,\mathrm{v}^{\mu\nu}_{ax}-\partial\mathcal{L}^{\mathrm{V}}_{ax}/\partial\,\mathrm{v}^{\mu\nu}_{ax}-\partial^{\beta}[\partial\mathcal{L}^{\mathrm{T}}_{ax}/\partial(\partial^{\beta}\,\mathrm{v}^{\mu\nu}_{ax})],\\
&\frac{d^2A}{(dx^0)^2}=-\mathrm{L}_{ax}{}^{-2}\,A\sum_{n=1}^{3}nd^{ax}_n\left(A^2\right)^{n-1}+J(x^0).
\end{aligned}
\tag{2.21}
$$

A tedious calculation produces *J*,

$$
J(A)=(2\kappa_{ax}/9\kappa_{ep}\,\mathrm{L}_{ep}{}^2)\phi_{ep}(A)^3\beta_{ep}\Gamma_{ep}A\{\cosh[\Gamma_{ep}(A^2-A_{ep}{}^2)]\}^{-2}.
\tag{2.22}
$$

Reference to Appendix Z shows that Γ_{ep} is indeed very large and A_{ep} is very close to 1, so *J* is shapely peaked at $A=A_{ep}$. The following is a very good approximation for *J* :

$$
\begin{aligned}
&J=\Lambda\{\cosh[2A_{ep}\Gamma_{ep}(A-A_{ep})]\}^{-2},\\
&\Lambda=(2\kappa_{ax}/9\kappa_{ep}\,\mathrm{L}_{ep}{}^2)\phi_{ep}(A_{ep})^3\beta_{ep}\Gamma_{ep}A_{ep},
\end{aligned}
\tag{2.23}
$$

where Λ is a constant (made up from universal epoch-constants). One can make a closed form solution to Eq. (2.21) by using Eq. (2.23):

$$
\begin{aligned}
&G_{ax}(A)=d^{ax}_1A^2+d^{ax}_2A^4+d^{ax}_3A^6,\\
&(dA/dx^0)\ =\pm\mathrm{L}_{ax}{}^{-1}\,\mathcal{F}(A),\\
&\mathcal{F}(A)=\left[1+\xi(A)-G_{ax}(A)\right]^{1/2},\\
&\xi(A)=(\alpha^{ax}_W/2)\{1+\tanh[2A_{ep}\Gamma_{ep}(A-A_{ep})]\},\\
&\alpha^{ax}_W=2\Lambda\,\mathrm{L}_{ax}{}^2/A_{ep}\Gamma_{ep}.
\end{aligned}
\tag{2.24}
$$

It is convenient to feature α^{ax}_W (a tabulated universal constant) since it appears in the equation for *A* in winter. However, α^{ax}_W is also defined in two equations—the bottom element of Eq. (2.24) and the third element of Eq. (2.20). Each of the elements are constructed from some universal apex

and epoch constants. Given α_W^{ax}, there are two constraints on the construction constants—*the tabulated* Appendix Z *constants are not all independent*. In the case above, the relations are as follows:

$$\begin{aligned} \alpha_W^{ax} &= (4/9)\,\beta_{ep}\,\phi_{ep}(A_{ep})^3(\mathcal{N}_{ep}/\mathcal{N}_{ax})(\mathrm{L}_{ax}/\mathrm{L}_{ep})^4, \\ \mathrm{V}_{ep}(\phi_W) - \mathrm{V}_{ep}(\phi_S) &= (2/3)\,\beta_{ep}\,\phi_{ep}(A_{ep})^3. \end{aligned} \tag{2.25}$$

The bottom element of Eq. (2.25) is very interesting since it involves only a_{ep}, $\lambda_{ep,}$, and β_{ep}.

C. The spring and fall transitions

The duration of a transition is somewhat arbitrary since it depends on the asymptotic behavior of Eq. (2.13). I choose to define the start of spring when $\mathrm{E}(\phi_{ep}) = 0.999$ and ending when $\mathrm{E}(\phi_{ep}) = 0.001$. The fall transition has the reverse order. The epoch field vacuum becomes degenerate when $A = A_D$, where $A_D = \pm[A_{ep}{}^2 + \Gamma_{ep}{}^{-1}\mathrm{arctanh}(\lambda_{ep}/\beta_{ep})]^{1/2}$. A_D lies between the start and end of a transition since $\beta_{ep} > |\lambda_{ep}|$. Furthermore, $A = A_D$ marks the beginning of a period where active vacuum decay can occur.

The active vacuum decay period can be divided into two segments. The first segment is quiescent (included in the continuous portion of Fig. C1). The following very brief segment is explosive (the discontinuous portion of Fig. C1). It is shown in Appendix B that vacuum decay corresponds to the creation of expanding bubbles throughout false vacuum space where the true vacuum resides inside each bubble. The probability of a bubble being formed is a steep nonlinear function of $|A - A_D|$. During the lengthy quiescent period, the average probability of bubble formation is negligible. Once the first average bubble forms in a volume of space, the volume rapidly becomes filled with expanding bubbles—a true vacuum volume. In spring, the quiescent period extends from $A = A_D$ to $A = A_D - x_{Bera}$, where x_{Bera} is treated as a dimensionless universal constant tabulated in Appendix Z. The quiescent period can be three orders of magnitude longer than the explosive period. Refer to Appendix B for a review of spring bubble-formation.

One can see that the apex field is continuous during the classical period in red spring (before the red-spring bubble era). Furthermore, dA/dx^0 is continuous and only changes significantly during a very brief period around $A = A_{ep}$ (well before the chaotic bubble era). Consequently, A and dA/dx^0 (during the bubble era) will be very nearly the same on each side of a bubble wall. Thus, the bubble era will have very little effect on the apex field—the bubble era becomes marginalized. The same is true for the four bubble eras during an apex field cycle. One will learn below that I have chosen to marginalize the bubble era for summer/winter physics transitions as well (Eq. (7.4) and Eq. (7.5)).

In the empty universe there is only one interesting variable, the epoch parameter ($\mathrm{E}(\phi_{ep})$) defined in Eq. (2.17). The universe is ancient and vast in NC—at the limits of comprehension. One must expect that the universe has gone through thousands of cycles (each about 731 billion years). I have chosen to avoid the creation question. Was the universe created many cycles ago, or is it

eternal? These questions can never be answered since any evidence of a past creation is lost beyond our ability to observe.

III. THE NEW COSMOLOGY WITH MATTER ADDED

This section will couple the apex and epoch fields to matter, thus creating an interaction LD. I define matter as members of the following group: three generations of quarks and leptons, gauge vector-bosons (gluons, photons, weak bosons), the Higgs quartet, and gravitational fields—the standard model. There is no dark matter, no dark energy, no dark anything in NC. New particles or forces can be included in the future. Gravitational fields will be discussed in section IV.

There will be an important constraint on the coupling—*eliminate the cosmological pathologies of general relativity*. The cyclic cosmology of section II eliminates the one-sided pathology, but one cannot have a big bang in each cycle—no infinities. Thus, the temperature of cosmic thermal radiation must have a finite limit during each cycle (about 200^{O} k). In that case, one would expect quarks and gluons to be eternally confined (except possibly in some core-collapse supernovae) and some symmetries to be eternally broken.

NC will be the story of the first generation of composites (proton, neutron), the electron, the electron-neutrino, and the photon. The other constituents will be either virtual, rare, or ephemeral. This section will illustrate the coupling of the apex and epoch fields to photons and (charged and neutral) fermions.

Unless noted, physics is assumed to be described in the rest-frame of the apex field in all that follows. The rest-frame of the cosmic microwave background should coincide with the rest-frame of the apex field.

The epoch field coupling is defined through use of the epoch parameter, $E(\phi_{ep})$. The Lagrangian density for matter (LDM) contains many universal constant parameters, e.g., masses and coupling constants. These constants have (known) present-day values (corresponding to the summer epoch). I propose that the NC version of the LDM is generated by substituting NC values of the constants in place of the present-day constants.

$$\text{NC constant} = (1 - K(E)) * \text{present-value} + K(E) * \text{winter-value}, \tag{3.1}$$

where K is a function to be determined.

The winter value of each constant is to be determined, but only a few will differ from the summer value. Specifically, the strong and electromagnetic interactions will be the same in all seasons. The gravitational fields will be slightly different in winter, and the weak interactions will be significantly different in winter.

The Higgs quartet plays a puzzling role in NC. Are they independent (massive) epoch fields or should the epoch field modify the parameters of the quartet? In either case, the quartet would be made stable. I have chosen to evade this question by decoupling the quartet from the apex and epoch fields. Where necessary, the epoch field will over-ride the quartet to make masses or coupling constants have seasonal values.

A. Coupling the apex field to photons and fermions

In what follows here, recall that the NC labels scalar, vector, etc., are mushy. The apex field is a "tensor", so a coupling tensor can be generated. I propose the following two connector "tensors", $\Delta_{\mu\nu}$ and $\sigma_{\mu\nu}$.

$$\begin{aligned}
&\Delta_{\mu\nu} \equiv \mathcal{P}\, \mathrm{g}_{\mu\nu} + \mathrm{v}_{\mu\nu}\left(apex\right)W, \\
&\mathrm{v}_{jk}\left(apex\right) = A\delta_{jk} \text{ (only non-vanishing elements)} \\
&\mathcal{P} = [\mathrm{J}(A, \mathrm{E}(\phi_{ep}))]^{-1/2} \\
&W = (\mathcal{P} - 1)/A \\
&\sigma^{\mu\lambda}\Delta_{\lambda\nu} = \delta^{\mu}_{\nu},
\end{aligned} \tag{3.2}$$

where $\delta^{\mu}_{\nu} = 1$ if $\mu = \nu$ else $= 0$. $\mathrm{J}(A, \mathrm{E})$ is an arbitrary real function of A and E, but there are some constraints. $\mathrm{J}(-A, \mathrm{E}) = \mathrm{J}(A, \mathrm{E})$, $\mathrm{J}(0,0) = 1$ and $\mathrm{J}(A, \mathrm{E}) > 0$ for all A and E attainable during each cycle. As a result, W is well behaved at mid-summer when $A = 0$. J will be defined in subsection F below. Eq. (3.2) insures that $\Delta^0_0 = \mathcal{P}$, $\Delta^k_k = 1 = \sigma^k_k$, and $\sigma^0_0 = \mathcal{P}^{-1}$, and the constraints will eliminate any pathology. $\mathcal{P}$ is a scalar since E and A are scalars, and it is a function of fields without any explicit dependence on x^0. Thus, $\Delta_{\mu\nu}$ and $\sigma_{\mu\nu}$ can be inserted (anywhere and in any manner) into the LDM.

The apex field can be thought of as a master clock. One can create an LDM for a field of interest. Using Eq. (2.1), the equation of evolution for the field results, but the evolution is relative to x^0 (the apex clock). There is another clock. We measure evolution (physical time) by using devices (clocks) that operate according to physical laws of matter. There must be a relationship (transformation) between physical time (τ) and x^0 —subject to important constraints. The transformed physical time equations must have the same speed limit for all constituents (and for all x^0)—the universal constant $c = 2.99799\,\mathrm{x}10^8$ MS^{-1}. Furthermore, the transformed equation must be the same familiar version except for corrections. The corrections must be so tiny that they could only be measured by an experiment that ran for a (extremely) long physical time.

It is useful to introduce a notation that distinguishes between apex and physical clocks:

$$\begin{aligned}
&\partial'_0 = \partial/\partial x^0;\ \partial'_k = \partial/\partial x^k, \\
&\partial_0 = \partial/\partial c\tau\ ;\ \partial_k = \partial/\partial x^k.
\end{aligned} \tag{3.3}$$

The procedure is clear enough. The first step is to form the "bare" primed LDM—just the familiar LDM with primes for the fields and their derivatives (and Dirac matrixes). Next, form a "dressed" primed LDM by inserting delta, sigma, and theta tensors (shown below) to form an interaction with the apex field. Next, obtain the primed equation of motion from the Euler-Lagrange equation (by variation of the primed field of interest). Finally, use a set of transformations to the unprimed equation of motion using the delta, sigma, and theta tensors.

The method of dressing and transforming may seem arbitrary. However, the desired result is that the unprimed equation of motion will look exactly like the familiar equation except for (possibly) a tiny correction and $c\tau$ in place of x^0. I have chosen to use τ in place of the customary t as a reminder. What we think of time has a hidden structure.

The ratio of the physical clock evolution to the apex clock evolution is given as a power series in $c\tau\,\mathrm{L}_{ax}^{-1}$,

$$d(c\tau)/dx^0 \equiv \mathrm{f} = \mathcal{P} - (\partial_0{}' \ln \mathcal{P}) c\tau + \cdots . \tag{3.4}$$

The leading terms in Eq. (3.4) are a first order differential equation for $\tau(x^0)$, and there will be an arbitrary constant of integration that can be chosen so that $\tau = 0$ *corresponds to now for an observer*. The solution of Eq. (3.4),

$$c\tau(x^0) = \mathcal{P}(x^0)^{-1} \int_0^{x^0} dx^{0\prime} \mathcal{P}(x^{0\prime})^2, \tag{3.5}$$

fixes now as corresponding to $x^0 = 0 = \tau$. Thus, the present-day value of the apex field $A_{now} = A(x^0 = 0)$. A_{now} will be determined in Appendix C, but it is not a universal constant. In what follows, the tiny corrections will be of order L_{ax}^{-1} and smaller corrections will be ignored. The final transformation of derivatives follows:

$$\begin{aligned} &\partial_0{}' = \mathrm{f}\,\partial_0 \;;\; \partial_k{}' = \partial_k, \\ &\partial_\mu{}' = \Sigma_\mu^\lambda \partial_\lambda, \\ &\Theta_\mu^\lambda \Sigma_\lambda^\nu = \delta_\mu^\nu, \end{aligned} \tag{3.6}$$

where $\Sigma_0^0 = \mathrm{f}$, $\Sigma_k^k = 1 = \Theta_k^k$, and $\Theta_0^0 = \mathrm{f}^{-1}$. Note that $\partial_0 \Theta_0^0 = 0$ (order L_{ax}^{-2}). Σ is not quite a Lorenz invariant tensor because the speed of light in the apex clock system is not a constant. The transformation will make light-speed seem constant but possibly with tiny deviations. A (theoretically perfect) Michelson interferometer (with unequal-length arms) will not have a null result, but over a long time it will measure Hubble's parameter. In NC, Lorenz invariance is slightly broken. It is possible to add higher power terms in Eq. (3.4) to marginalize any mischief generated by multiples of the leading term—no evaporating fermions.

B. Coupling method for fermions

The units used for electromagnetism (EM) are MKSQ, where electric charge (Q) is measured in coulombs. The four-potential (A_μ) has units $\mathrm{KMS^{-1}Q^{-1}}$, and the vacuum-permittivity has units $\mathrm{Q^2S^2K^{-1}M^{-3}}$ ($\varepsilon_0 = 8.854\,\mathrm{x}10^{-12}$). The dressed primed LD for a fermion that could have electrical charge is chosen as follows:

$$\mathcal{N}_F^{-1}\mathcal{L}_F = (i/2)(\bar{\psi}'\Gamma^\mu \partial_\mu{}'\psi' - \mathrm{c.c.}) - \kappa \mathrm{A}_\mu{}' \bar{\psi}'\Gamma^\mu\psi' - \mathrm{L}_F^{-1}\bar{\psi}'\psi', \tag{3.7}$$

where $\kappa = \mathrm{q}/\hbar$, q is the electric charge of the fermion, $\mathrm{L}_F{}^{-1} = \mathrm{m}_F\, c/\hbar$, and $\mathcal{N}_F$ is a constant normalization factor. The transformations are governed by minimal EM coupling as follows:

$$\begin{aligned} \psi' &= \psi, \\ \mathrm{A}_\mu{}' &= \Sigma_\mu^\lambda\, \mathrm{A}_\lambda . \end{aligned} \tag{3.8}$$

The usual (constant) Dirac matrices are used as follows:

$$\begin{aligned} \{\gamma^\mu, \gamma^\nu\} &= 2g^{\mu\nu}, \\ \bar{\psi} &= \psi^\dagger \gamma^0, \\ \Gamma^\mu &= \Theta_\lambda^\mu \gamma^\lambda . \end{aligned} \tag{3.9}$$

Next, the primed equation of motion follows from a variation ($\delta\bar{\psi}'$),

$$0 = i\Gamma^\mu \partial_\mu{}' \psi' + (i/2)(\partial_\mu{}' \Gamma^\mu)\psi' - \kappa\, \mathrm{A}_\mu{}'\, \Gamma^\mu \psi' - \mathrm{L}^{-1}\psi'. \tag{3.10}$$

The unprimed equation results by using Eq. (3.2) to (3.10) *and then taking* $\tau \to 0$ *to obtain the now equation*,

$$0 = i\gamma^\mu \partial_\mu \psi - \kappa\, \mathrm{A}_\mu\, \gamma^\mu \psi - \mathrm{L}^{-1}\psi, \tag{3.11}$$

which is the familiar Dirac equation *without explicit reference to the apex field*. There is a conserved current ($\partial_\mu \bar{\psi}\gamma^\mu \psi = 0$), and a source term for primed EM,

$$\partial \mathcal{L}_F / \partial\, \mathrm{A}_\mu{}' = -\kappa \mathcal{N}_F \Theta_\lambda^\mu (\bar{\psi}\, \gamma^\lambda \psi). \tag{3.12}$$

Eq. (3.12) will be useful in the following subsection.

C. Coupling method for electromagnetism

The dressed primed LD for EM is

$$\begin{aligned} \mathcal{N}_{EM}{}^{-1} \mathcal{L}_{EM} &= \sigma_\varepsilon^\alpha \sigma_\delta^\beta\, \mathrm{F}_{\alpha\beta}{}'\, \sigma_\gamma^\varepsilon \sigma_\lambda^\delta\, \mathrm{F}^{\gamma\lambda\prime}, \\ \mathrm{F}_{\mu\nu}{}' &= \partial_\mu{}'\, \mathrm{A}_\nu{}' - \partial_\nu{}'\, \mathrm{A}_\mu{}', \end{aligned} \tag{3.13}$$

where $\mathcal{N}_{EM} = -\varepsilon_0 c/4$. The primed Euler-Lagrange equation for photons and charged fermions has the following form,

$$0 = (\partial \mathcal{L}_F \,/\, \partial\, \mathrm{A}_\nu{}') - \partial_\mu{}' [\partial \mathcal{L}_{EM} \,/\, \partial(\partial_\mu{}'\, \mathrm{A}_\nu{}')]. \tag{3.14}$$

Next, obtain the primed equation from Eq. (3.14):

$$\partial_\mu{}'[\sigma^\mu_\varepsilon\sigma^\nu_\delta\sigma^\varepsilon_\gamma\sigma^\delta_\lambda \mathrm{F}^{\gamma\lambda\prime}] = \kappa\mathcal{N}_{FEM}\Theta^\nu_\lambda\bar{\psi}\gamma^\lambda\psi, \tag{3.15}$$

where $\mathcal{N}_{FEM} = -\mathcal{N}_F \,/\, 4\mathcal{N}_{EM}$. Since $\partial_k\mathcal{P} = 0$, only time-like derivatives of Δ, σ, Σ, and Θ will survive. Note that Δ, σ, Σ, and Θ are diagonal. Convert Eq. (3.15) to the unprimed version using the transformations above,

$$\begin{aligned} \mathrm{F}_{\mu\nu}{}' &= \Sigma^\alpha_\mu\Sigma^\beta_\nu \mathrm{F}_{\alpha\beta}, \\ \mathrm{F}_{\mu\nu} &= \partial_\mu \mathrm{A}_\nu - \partial_\nu \mathrm{A}_\mu . \end{aligned} \tag{3.16}$$

Eq. (3.15) can be rewritten,

$$\Sigma^\nu_\kappa\Sigma^\chi_\mu\partial_\chi[\sigma^\mu_\varepsilon\sigma^\kappa_\delta\sigma^\varepsilon_\gamma\sigma^\delta_\lambda\Sigma^\gamma_\alpha\Sigma^\lambda_\beta \mathrm{F}^{\alpha\beta}] = \mu_0 J^\nu, \tag{3.17}$$

where $\mu_0 J^\nu = \kappa\mathcal{N}_{FEM}\bar{\psi}\gamma^\nu\psi$ and $\partial_\mu J^\mu = 0$. Eq. (3.17) can be rewritten as well,

$$\mathrm{A}^{\chi\nu}_{\alpha\beta}\,\partial_\chi \mathrm{F}^{\alpha\beta} + \mathrm{B}^\nu_{\alpha\beta}\mathrm{F}^{\alpha\beta} = \mu_0 J^\nu. \tag{3.18}$$

As $\tau \to 0$, $\Sigma^\nu_\mu \to \Delta^\nu_\mu$, and $\partial_0\Sigma^0_0 \to 0$. Thus, $\mathrm{A}^{\chi\nu}_{\alpha\beta} \to \delta^\chi_\alpha\delta^\nu_\beta$, $\mathrm{B}^\nu_{\alpha\beta} \to -2[\partial_0 \ln(\mathcal{P})]\delta^0_\alpha\delta^\nu_\beta$, and the *now equation* results,

$$\partial_\mu \mathrm{F}^{\mu\nu} - 2[\partial_0 \ln(\mathcal{P})]\,\mathrm{F}^{0\nu} = \mu_0 J^\nu. \tag{3.19}$$

Unlike the fermion equation, Eq. (3.11), the EM Eq. (3.19) has an *explicit reference to the apex field* and x^0. However, for the electric field of a point charge (a stationary charged fermion) the $\partial_0 \ln(\mathcal{P})$ term of Eq. (3.19) vanishes identically, and $\partial_\mu \mathrm{F}^{\mu 0} = \mu_0 J^0$. Thus, *the energy level of a stationary state of the charged fermion equation will be independent of* x^0—a universal constant. This fact will be important in what follows.

The relative size of the $\partial_0 \ln(\mathcal{P})$ term of Eq. (3.19) for typical radiation calculations will be of order $\lambda / \mathrm{L}_{ax}$, where λ is the wavelength of the radiation. For example, if $\lambda = 1$ meter (low temperature thermal radiation), the $\partial_0 \ln(\mathcal{P})$ term would be of order 10^{-26}—safely ignored. The only case where the $\partial_0 \ln(\mathcal{P})$ term can be significant is when free photons travel for eons from source to observer.

Thermal radiation is created at the same time in the current cosmology (GRLCDM). In NC, thermal photons and some portions of background x-rays and gamma rays are relic in nature. These relic photons could have traveled for hundreds of billion years—from the preceding winter or summer.

D. Cosmological red shift

An observer today of distant objects will observe shifted spectrums. That shift has two components—a cosmological shift toward red and a doppler shift. The doppler component is due to the velocity of the source relative to the observer, and it is generally unknown and neglected. This subsection focuses only on the cosmological component.

Consider a (polarized and monochromatic) electromagnetic wave-train moving through empty space in the x^1 direction in the first half of red summer. The vector potential will have one component, $\mathrm{A}_2(x^1,\tau)$, and Eq. (3.19) will take the following form,

$$0=\partial_0{}^2\,\mathrm{A}_2-\partial_1{}^2\,\mathrm{A}_2-2(\partial_0\,\mathrm{A}_2)[\partial_0\ln(\mathcal{P})]. \tag{3.20}$$

Assume that the wave-train has a length of N+1 crests, and that the vector potential has a form (accurate near the center of the train), $\mathrm{A}_2=\cos(2\pi\lambda^{-1}\xi)$, and $\xi=x^1-c\tau$. The center of the train corresponds to $\xi=0$. In the limit $\xi\to 0$, Eq. (3.20) requires the following constraint,

$$\partial_0\ln(\lambda)=-\partial_0\ln(\mathcal{P}). \tag{3.21}$$

The train was created at a certain time in the past (then) and observed in the observer's now. Eq. (3.21) causes a connection between then and now.

$$\lambda_{now}/\lambda_{then}=\mathcal{P}_{then}/\mathcal{P}_{now}, \tag{3.22}$$

where λ_{now} is the λ of A_2 in Eq. (3.20). During the first half of red summer $\partial_0\mathcal{P}<0$, and $\lambda_{now}>\lambda_{then}$. *Now* for an observer can be at any value of x^0 (or $\mathcal{P}$), and one can define a red shift parameter (z) for a distant source in the usual fashion,

$$1+\mathrm{z}=\lambda_{observer}/\lambda_{source}\ . \tag{3.23}$$

The red shift can be connected directly with the apex field,

$$1+\mathrm{z}=\mathcal{P}_{source}/\mathcal{P}_{observer}. \tag{3.24}$$

Consider two observers (both in the rest-frame of the apex field) widely separated in space but observing the same wave-train from the same source. Each observer can measure the wavelength at the center of the train. The velocity of the center of the train can be established by measuring the physical time lag ($\Delta\tau$) for the center to travel a known distance (Δx^1). The velocity of the center is independent of the wavelength, so $\Delta x^1/\Delta\tau=c$ *for both observers*. If observer1 is closer to the source than observer 2 then $\mathrm{z}_1<\mathrm{z}_2$.

If a monochromatic wave-train is N+1 crests long, then the length (and volume) of the train will be proportional to $\mathcal{P}^{-1}$. The electromagnetic energy density is proportional to $\mathcal{P}^2$, so the total energy of the photons within the volume is proportional to $\mathcal{P}$. The total number of photons within

the volume is constant since photons cannot be created or destroyed in flight through a vacuum. Therefore, the energy of a single photon in flight is determined,

$$E_{\gamma} = E_{source}\mathcal{P} \,/\, \mathcal{P}_{source} \ . \tag{3.25}$$

The free photon will always be observed to move with velocity c (the universal constant), and it can directly gain energy from or lose energy to the apex field in flight.

An observer today looking into the past at a distant object will observe a red shifted spectrum—i.e., the observer is in the red branch. An observer in early blue summer looking into the past will see blue shifted spectrums. Blue and red people will use the same physics to explain experiments—the only tangible difference will be cosmological in nature. During the last half of red summer an observer looking into the past will see blue shifted spectrums for nearer objects and red shifts for more distant objects. The corresponding blue situation will be the opposite.

E. Clocks and durations

What is the relationship between the apex clock and the physical clock? The evolution of cosmology is governed by the apex clock while our lives march by the physical clock. Eq. (3.4) gives the appropriate relation,

$$d(c\tau) / dx^0 = \mathcal{P}, \tag{3.26}$$

where $\tau \to 0$ (the physical clock is being continuously reset). Since observers are interested in the evolution of distant physical systems, it is necessary to use *physical time* to describe the evolution of the universe. In NCNG the *universe is not expanding*, so the distance to an observed object will always be $c\Delta\tau$. The duration of physical time between two values of the apex field is

$$\int_{\tau_1}^{\tau_2} d\tau = \int_{A_1}^{A_2} dA(dc\tau / dx^0)(dA / dx^0)^{-1} c^{-1}. \tag{3.27}$$

As an example, the number of years between now and the middle of the current summer,

$$\Delta\tau = \mathrm{L}_{ax}\, c^{-1} \int_0^{A_{now}} dA[\mathrm{J}(A,0)]^{-1/2}[1 - G_{ax}(A)]^{-1/2}, \tag{3.28}$$

can be evaluated once the universal constants in Eq. (3,28) have been established. That task will be relegated to Appendix C.

F. Physical clock functions

I have chosen the following form for the J function,

$$\begin{aligned} &\mathrm{J}(A,\mathrm{E}) = N(A)(1-\mathrm{E}) + M(A)\,\mathrm{E}^2, \\ &N(A) = 1 - A\tanh(\Gamma_{cl} A), \\ &M(A) = (1-\kappa_{cl})\exp[\beta_{cl}(1-A^2)], \end{aligned} \tag{3.29}$$

where $1>>\kappa_{cl}>0$, $\beta_{cl}>>1$, and $\Gamma_{cl}>>1$ are universal clock constants. This arcane form for J results from various requirements for a consistent cosmology.

Eq. (3.29) satisfies the criteria of Eq. (3.2), and it is well-behaved over the whole cycle and continuous except for tiny slices during bubble eras. J has the simplest form ($\mathrm{J}=1-|A|$) during summer (E=0) except for tiny regions near $A^2=1$ and $A=0$.

For reasons that will become clear in the section about reverse nucleosynthesis, it is necessary that each winter season needs to last about $33\,\mathrm{L}_{ax}\,c^{-1}$ years. That constraint requires the following relation,

$$33\sim 2\int_1^{A_W} dA[\mathrm{J}(A,1)]^{-1/2}[1+\alpha_W^{ax}-G_{ax}(A)]^{-1/2}, \tag{3.30}$$

where $G_{ax}(A_W)=1+\alpha_W^{ax}$. The integrand of Eq. (3.30) has two factors. The *G* factor is determined by observations that have nothing to do with winter. If the J factor is of order unity, the integral will be too small. The only way to satisfy Eq. (3.30) is if J can be very small in winter—hence the exp beta term of J.

In red spring after the bubble era, there is a maximum value of z. The size of $\mathrm{z}_{\max}$ is influenced by the *M* term of Eq. (3.29). Using E^2 instead of E and the kappa factor keeps $\mathrm{z}_{\max}$ in the proper range—larger than the highest observed z, but not too big ($\mathrm{z}_{\max}\sim 15$).

I have gone into extra detail here to illustrate a recurring theme in NCNG. There are new universal constants and new functions that seem as if they could have any form or value, but consistency and observability will lead one to the best choice.

Every aspect of NCNG can be verified by observations *in principle*, but there is a proviso—if one has a big enough telescope with low enough noise. Unlike GRLCDM, NCNG has no dark side since z is always in a cool range. Furthermore, the cool range of z eliminates the first pathology of GR—infinite z at the origin of time.

G. Bubble wall speed versus photon speed

Eq. (3.26) shows that a bubble wall moves at light speed only when $\mathrm{J}=1$, e.g., when $A=0$. In general, $|\mathbf{v}_{wall}|/|\mathbf{v}_{photon}|=\mathcal{P}$. On the summer side of the wall, Eq. (3.29) will generate $\mathcal{P}>>1$, and on the winter side $\mathcal{P}>1$. In (red or blue) spring, inside is summer and a photon inside will move much slower than the receding wall that surrounds it. Such a photon will never cross back into winter during the bubble era. On the winter side, photons are moving slightly slower than the wall, and the wall can overtake photons. Thus, *any spring photon will only cross a bubble wall once*.

The situation in (red or blue) fall is similar. Inside is winter and a photon inside will move slightly slower than the receding wall that surrounds it, and the photons on the summer side can be overtaken by the much faster moving wall. There are no observers in winter, so this case is moot. Any photon (existing before the spring bubble era) that arrives at a summer observer's telescope will have crossed only one bubble wall.

What happens when a photon crosses a bubble wall? That question depends on the forces that can interact with a photon traveling in a vacuum—there are two. If the bubble wall is moving

through a gravitational field, there could be a discontinuity across the wall. If so, the photon could be deflected crossing the wall. That possibility will be eliminated in section VII(B). The second "force" is the interaction of a photon with the apex field via Eq. (3.19). In that case, there would be an insignificant change in the cosmological red shift of the photon across the wall. Thus, each relic photon making the necessary single wall crossing will not be affected. *The bubble era is transparent for relic photons.*

H. The Hubble parameter

Now that $\mathcal{P}$ has been given form, The Hubble parameter (H_0) can be formulated in red summer. The definition of H_0 is

$$\mathrm{H}_0 = -(dz / d\tau)_{now}, \tag{3.31}$$

where now corresponds to $\mathrm{E} = 0$, and $\mathrm{J} = 1 - A$. Eq. (3.24) gives z as a function of A,

$$z = -1 + [(1 - A_0) / (1 - A)]^{1/2}, \tag{3.32}$$

where A_0 is the present-day value of A. Eq. (3.31) can be rewritten,

$$\mathrm{H}_0 = -c[(dz / dA)(dA / dx^0)(dc\tau / dx^0)^{-1}]_{A=A_0}. \tag{3.33}$$

Eq. (3.26) and Eq. (2.24) give the final form,

$$\mathrm{H}_0 = 0.5c\,\mathrm{L}_{ax}{}^{-1}(1 - A_0)^{-1/2}[1 - G_{ax}(A_0)]^{1/2}. \tag{3.34}$$

The most accurate value (in obsolete units) is $\mathrm{H}_0 = 73.8$ (km/sec) per mega-parsec from [1] and [2]. A more useful version is $\mathrm{H}_0 = c\,\mathrm{L}_H{}^{-1}$, where $\mathrm{L}_H = 13.26 \times 10^9$ LY. An important relationship results,

$$\mathrm{L}_{ax} = 0.5\,\mathrm{L}_H(1 - A_0)^{-1/2}[1 - G_{ax}(A_0)]^{1/2}. \tag{3.35}$$

Since L_{ax} is a universal constant (see Appendix Z) and G_{ax} is formed from universal constants, it follows that $\mathrm{L}_H \Rightarrow A_0$. This is important because all cosmological red shift information springs from a knowledge of A_0.

I. Cosmic microwave background-radiation and cosmological frequency shift

Cosmic microwave background-radiation (CMB) has been observed and identified as black body thermal radiation. CMB accurately matches the Planck distribution, $B(\nu, T)$, giving a present-day temperature of $2.7250\ ^{\circ}\mathrm{K}$. The physical expansion of the universe in GR allows the use of thermodynamic relations to establish how the characteristic temperature of the radiation (T)

changes as the universe expands—an avenue not available in NC. In NC the thermal photons in flight can lose or gain energy via Eq. (3.25). Each photon will have the following change between two physical times,

$$\nu / \nu' = \mathcal{P}(\tau) / \mathcal{P}(\tau') \equiv \xi, \tag{3.36}$$

where ξ can be treated as a constant in what follows. The Planck distribution has the following constraints,

$$\begin{aligned} &B(\nu,T) = 2h\nu^3 c^{-2}[\exp(h\nu / kT) - 1]^{-1}, \\ &\int_0^\infty d\nu B(\nu,T) = \pi^{-1}\sigma T^4, \\ &\int_0^\infty d\nu' B(\nu',T') = \pi^{-1}\sigma (T')^4. \end{aligned} \tag{3.37}$$

If one substitutes Eq. (3.36) into the first of the integrals of Eq, (3.37), one obtains the following,

$$\begin{aligned} &T' = T\xi^{-1}, \\ &T(\tau') / T(\tau) = \mathcal{P}(\tau') / \mathcal{P}(\tau), \end{aligned} \tag{3.38}$$

where $\mathcal{P}(\tau)$ is established using the techniques of subsections 3(E) and 3(F) above.

IV. THE NEW GRAVITY

This section will add gravity to the universe. The provisions of section III(A) apply with the addition of the Newtonian gravitational (universal) constant ($G = 6.67430 \text{x} 10^{-11}\ \text{M}^3\text{K}^{-1}\text{S}^{-2}$). There is *one kind of graviton* (a massless tensor-boson) in GR, but it is *not a gauge boson*.

In the new gravity (NG), *gravitons are tensor gauge-bosons*, and there are more than one kind. Thus, a new universal constant is added to Appendix Z (N_q defines the number of NG graviton kinds). There is no limit to N_q—only sufficient to agree with observations. For reasons that will become clearer below (see V(L)), I have chosen $N_q = 5$, where each kind has a different (extremely tiny) mass.

There are eight (small mass) gauge-bosons for the strong interaction and six (massive) gauge-bosons for the weak interaction. Thus, NG *joins the standard model of particle physics*. The only outlier is the electro-magnetic force with one massless gauge-boson (photon). One is lead to wonder if perhaps there should be two or more photons with different (extremely tiny) masses like NG?

A. The tensor gravity fields

As mentioned in section II, there is one primary metric tensor (the rest frame for the apex field, $g_{00} = 1$ and $g_{jk} = -\delta_{jk}$) for which the equations of NCNG are meant to be applied.

Each of the five gravity fields is a dimensionless second-order symmetric tensor, $\mathrm{v}_{\mu\nu}(q,x)$, where $q=1...N_q$. In each case, the four-coordinate (x) will be implicit and the usual contravariant, covariant, and contraction algebra is used.

One can define some useful scalars and vectors derived from $\mathrm{v}_{\mu\nu}(q)$: $\mathrm{S}(q) \equiv \mathrm{v}^{\lambda}_{\lambda}(q)$, $\mathrm{J}(q) \equiv \mathrm{v}^{\alpha}_{\lambda}(q)\,\mathrm{v}^{\lambda}_{\alpha}(q)$, $\mathrm{S}_{\mu}(q) \equiv \partial_{\mu}\,\mathrm{S}(q)$, $\mathrm{N}_{\mu}(q) \equiv \partial_{\lambda}\,\mathrm{v}^{\lambda}_{\mu}(q)$. There are two pieces to the Lagrangian density (LD) for each of the five gravity fields, the "kinetic" density, $\mathcal{L}^{\mathrm{T}}_{g}(q,x)$, and a "potential" density, $\mathcal{L}^{\mathrm{V}}_{g}(q,x)$. The complete LD for each gravity field is then, $\mathcal{L}_{g} = \mathcal{L}^{\mathrm{T}}_{g} - \mathcal{L}^{\mathrm{V}}_{g}$. Each piece is defined as follows:

$$\begin{aligned} 4\kappa_q \mathcal{L}^{\mathrm{T}}_{g}(q,x) = g^{\mu\nu}\{&\partial_{\mu}\,\mathrm{v}^{\alpha}_{\beta}(q)\partial_{\nu}\,\mathrm{v}^{\beta}_{\alpha}(q) - \mathrm{S}_{\mu}(q)\,\mathrm{S}_{\nu}(q) \\ &+2\,\mathrm{N}_{\mu}(q)\big(\mathrm{S}_{\nu}(q) - \mathrm{N}_{\nu}(q)\big)\}, \end{aligned} \tag{4.1}$$

$$4\kappa_q \mathcal{L}^{\mathrm{V}}_{g}\left(q,x\right) = \mathrm{L}^{-2}_{gq}\{\mathrm{J}(q,x) - \tfrac{1}{2}\mathrm{S}(q,x)^2\}, \tag{4.2}$$

where $\kappa_q = 8\pi G\,\mathrm{Z}_{gq}\,c^{-3}$ and Z_{gq} is a dimensionless universal constant related to the strength of each gravity field. L_{gq} is a characteristic length associated with each gravity field—universal constants. I have chosen the following lengths,

$$\mathrm{L}_{gq} = q\,\mathrm{L}_{g1}. \tag{4.3}$$

These lengths are vast—L_{g1} will be about one million light years. The strength multipliers will be discussed below.

The Euler-Lagrange equation for each field in the absence of sources yields:

$$\begin{aligned} &0 = \Omega^{gq}{}_{\mu\nu} + \tfrac{1}{2}\mathrm{L}^{-2}_{gq}\{\mathrm{v}_{\mu\nu}(q) - \tfrac{1}{2}g_{\mu\nu}\,\mathrm{v}^{\lambda}_{\lambda}(q)\}, \\ &\Omega^{gq}{}_{\mu\nu} = \Xi^{gq}{}_{\mu\nu} - \tfrac{1}{2}g_{\mu\nu}g^{\beta\lambda}\Xi^{gq}{}_{\beta\lambda}, \\ &2\Xi^{gq}{}_{\mu\nu} = \partial^{\varepsilon}\left(T^{gq}{}_{\varepsilon\mu\nu}\right), \\ &T^{gq}{}_{\varepsilon\mu\nu} = \partial_{\varepsilon}\,\mathrm{v}_{\mu\nu} + \tfrac{1}{2}\left(g_{\varepsilon\mu}S_{\nu} + g_{\varepsilon\nu}S_{\mu}\right) - \left(g_{\varepsilon\mu}N_{\nu} + g_{\varepsilon\nu}N_{\mu}\right). \end{aligned} \tag{4.4}$$

Eq. (4.1) and Eq. (4.4) are relative to the x^0 evolution parameter, i.e., the apex clock. These equations correspond to the primed LD of section III when $A=0$. The gravity fields need to interact with the apex field.

The central field will be studied below. In that case, polar coordinates are useful, so $g_{00}=1$, $g_{rr}=-1$, $g_{\theta\theta}=-r^2$, $g_{\phi\phi}=-r^2\sin^2\theta$. In Eq. (4.1) and Eq. (4.4), $\partial_{\lambda}\to D_{\gamma}$ (D_{λ} is the usual covariant derivative) and $D=r^2\sin\theta$. The invariant volume element is $dV^4 \equiv D\,d^4x$, where $D \equiv \left(-\det\left(g\right)\right)^{1/2}$.

B. Gravity and the apex field

The five gravity-fields just represent another form of matter, and they couple to the apex field using the same method that was developed in section III. In this case, the details of the method are different from the photon method, which was different from the fermion method as well. Furthermore, the gravity method is far more complex. The following set of new tensors are useful:

$$\begin{aligned}
&\psi_{\mu}^{\alpha} = \sigma_{\lambda}^{\alpha}\Sigma_{\mu}^{\lambda},\\
&\omega_{\mu}^{\alpha} = \psi_{\lambda}^{\alpha}\psi_{\mu}^{\lambda},\\
&\tilde{\psi}_{\lambda}^{\alpha}\psi_{\mu}^{\lambda} = \delta_{\mu}^{\alpha},\\
&\tilde{\omega}_{\lambda}^{\alpha}\omega_{\mu}^{\lambda} = \delta_{\mu}^{\alpha},\\
&\psi_{0}^{0} = 1 - c\tau[\partial_{0}\ln(\mathcal{P})],
\end{aligned} \tag{4.5}$$

where σ and Σ are defined in Eq. (3.2) and Eq. (3.6). The five bare primed LDs are just Eq. (4.1) and Eq. (4.2) with fields and derivatives primed. The dressed LD is obtained using the following substitutions:

$$\begin{aligned}
&\mathrm{v}_{\mu\nu}(q)' \underset{dress}{\rightarrow} \psi_{\mu}^{\alpha}\psi_{\nu}^{\beta}\,\mathrm{v}_{\alpha\beta}(q)',\\
&\partial_{\mu}' \underset{dress}{\rightarrow} \sigma_{\mu}^{\alpha}\partial_{\alpha}'.
\end{aligned} \tag{4.6}$$

Great care must be applied to constructing the dressed LD ($\bar{\mathcal{L}}_g$) since there will be many terms. There is a useful third rank tensor, $\Lambda_{\mu\nu\lambda}' = \partial_{\mu}'\,\mathrm{v}_{\nu\lambda}'$, that illustrates this problem. The dressed version of Λ' is

$$\begin{aligned}
&\Lambda_{\mu\nu\lambda}' \underset{dress}{\rightarrow} \mathrm{F}_{\mu\nu\lambda}^{\alpha\beta\gamma}\,\Lambda_{\alpha\beta\gamma}' + \mathrm{E}_{\mu\nu\lambda}^{\beta\gamma}\mathrm{v}_{\beta\lambda}',\\
&\mathrm{F}_{\mu\nu\lambda}^{\alpha\beta\gamma} = \sigma_{\mu}^{\alpha}\psi_{\nu}^{\beta}\psi_{\lambda}^{\gamma},\\
&\mathrm{E}_{\mu\nu\lambda}^{\beta\gamma} = \sigma_{\mu}^{\alpha}\partial_{\alpha}'(\psi_{\nu}^{\beta}\psi_{\lambda}^{\gamma}).
\end{aligned} \tag{4.7}$$

E is a tiny correction (of order L_{ax}^{-1}) that must be included. The E factor of Eq. (4.7) will cause an unusual contribution to the source-free Euler-Lagrange equation (first term),

$$0 = \partial\bar{\mathcal{L}}_g^{\mathrm{T}} / \partial\,\mathrm{v}^{\mu\nu\prime} - \partial\bar{\mathcal{L}}_g^{\mathrm{V}} / \partial\,\mathrm{v}^{\mu\nu\prime} - \partial^{\varepsilon\prime}\left(\partial\bar{\mathcal{L}}_g^{\mathrm{T}} / \partial\Lambda^{\varepsilon\mu\nu\prime}\right). \tag{4.8}$$

The solution of Eq. (4.8) can be written as follows,

$$0 = \xi^{\alpha\beta\gamma}_{\mu\nu}\,\Lambda_{\alpha\beta\gamma}{}' - \tfrac{1}{2}\,\mathrm{L}^{-2}_{gq}\,\omega^{\alpha}_{\mu}\omega^{\beta}_{\nu}\,\mathrm{v}_{\alpha\beta}{}' - \partial^{\varepsilon\prime}\left(G^{\alpha\beta\gamma}_{\varepsilon\mu\nu}\Lambda_{\alpha\beta\gamma}{}' + \mathrm{M}^{\beta\gamma}_{\varepsilon\mu\nu}\mathrm{v}_{\beta\gamma}{}'\right), \tag{4.9}$$

where *G* is a series of five contractions of two F's. M and ξ are each a series of five contractions of E and F. These are too lengthy to exhibit, and there is another step! The last step requires the following substitution to convert Eq. (4.9) into a now equation that involves only physical time,

$$\begin{aligned} \mathrm{v}_{\mu\nu}(q)' &= \tilde{\omega}^{\alpha}_{\mu}\tilde{\omega}^{\beta}_{\nu}\,\mathrm{v}_{\alpha\beta}(q), \\ \partial_{\mu}{}' &= \Sigma^{\alpha}_{\mu}\partial_{\alpha}. \end{aligned} \tag{4.10}$$

The resulting equation can be written as follows,

$$0 = \mathrm{T}^{\alpha\beta\gamma}_{\varepsilon\mu\nu}\,\partial^{\varepsilon}\Lambda_{\alpha\beta\gamma} + \mathrm{L}^{-2}_{gq}\{\mathrm{v}_{\mu\nu} - \tfrac{1}{2}\,g_{\mu\nu}\,\mathrm{v}^{\lambda}_{\lambda}\} + \mathrm{U}^{\alpha\beta\gamma}_{\mu\nu}\,\Lambda_{\alpha\beta\gamma} + \mathrm{W}^{\alpha\beta}_{\varepsilon\mu\nu}\,\partial^{\varepsilon}\,\mathrm{v}_{\alpha\beta}, \tag{4.11}$$

where U and W are tiny corrections (of order $\mathrm{L}_{ax}{}^{-1}$). T is a series of seven terms involving both ω, $\tilde{\omega}$, and the metric tensor. U involves a derivative of T and a contraction of ξ. W involves a contraction of M and of *G*.

The now equations for the five fields are analogous to Eq. (3.11) for fermions or Eq. (3.19) for photons and are obtained in the same manner—the limit as $c\tau \to 0$ in Eq. (4.5). The now limit of psi is $\psi^{\alpha}_{\mu} \to \delta^{\alpha}_{\mu}$ and $\partial_0\psi^{\alpha}_{\mu} \to -\delta^{\alpha}_{0}\delta^{0}_{\mu}[\partial_0 \ln(\mathcal{P})]$. Using these limits in Eq. (4.11) gives the source free form,

$$0 = \Omega_{\mu\nu}(q) + \tfrac{1}{2}\,\mathrm{L}^{-2}_{gq}\{\mathrm{v}_{\mu\nu}(q) - \tfrac{1}{2}\,g_{\mu\nu}\,\mathrm{v}^{\lambda}_{\lambda}(q)\} + \delta\Omega_{\mu\nu}(q), \tag{4.12}$$

where Ω is given in Eq. (4.4) with $\partial_0 = \partial/\partial c\tau$, and $2\delta\Omega_{\mu\nu}$ is the U and W parts of Eq. (4.11). The tiny correction term has too many terms to display in general, so I will limit the analysis to three cases of general interest.

Case 1 corresponds to a static-weak field without symmetry. The non-zero fields will be $\mathrm{v}_{00}\left(q, x^1, x^2, x^3\right)$, and Λ_{k00} will be non-zero. Only U^{k00}_{00} and W^{00}_{k00} can contribute, but they are both zero. Thus, $\delta\Omega_{\mu\nu} = 0$.

Case 2 corresponds to a static central field of any strength. The non-zero fields will be $\mathrm{v}_{00}\left(q, x^1\right)$ and $\mathrm{v}_{11}\left(q, x^1\right)$, and both Λ_{100} and Λ_{111} will be non-zero ($x^1 = r$). Only U^{100}_{00}, U^{111}_{00}, U^{100}_{11}, U^{111}_{11}, W^{00}_{100}, W^{11}_{100}, W^{00}_{111}, W^{11}_{111} can contribute, but they are all zero. Thus, $\delta\Omega_{\mu\nu} = 0$.

Case 3 corresponds to a plane-transverse gravitational wave. The non-zero fields will be $\mathrm{v}_{23}\left(q, x^0 = c\tau, x^1\right)$, and both Λ_{023} and Λ_{123} will be non-zero. Only U^{023}_{23}, U^{123}_{23}, W^{23}_{023}, W^{23}_{123} can contribute, but only one (U^{023}_{23}) is non-zero. Since $\mathrm{U}^{023}_{23} = (\partial_0\omega^0_0)_{now} = -2[\partial_0 \ln(\mathcal{P})]$, the correction will be $2\delta\Omega_{23} = \mathrm{U}^{023}_{23}\,\Lambda_{023} = -2[\partial_0 \ln(\mathcal{P})]\partial_0\,\mathrm{v}_{23}$. If one substitutes the correction into Eq. (4.12) and

neglects the infinitesimal L_{gq}^{-2} term, the equation of motion for a gravitational wave is the following,

$$0 = \partial_0{}^2\,\mathrm{v}_{23} - \partial_1{}^2\,\mathrm{v}_{23} - 2(\partial_0\,\mathrm{v}_{23})[\partial_0 \ln(\mathcal{P})]. \tag{4.13}$$

Eq. (4.13) is the same as Eq. (3.20) for an electromagnetic wave. Thus, the apex field treats gravitons in flight in the same manner as photons. A gravitational wave train will appear to move with the same velocity (= *c*) for observers regardless of distance from the source, and the wavelength of the train will be red shifted (in early red summer) to the same degree as a photon. The apex field can directly add or subtract energy from a graviton in flight.

C. Coupling matter to the new gravity

The second pathology of GR is due to the strong field limit of the Schwarzschild solution. In the new gravity, one demands that the orbit equation for a gravitational source of finite mass should be well-behaved—no infinities or zeroes. That constraint will require a new set of dimensionless coupling tensors. I have chosen the following form,

$$\begin{aligned} &\mathrm{V}_{\mu\nu}(x) \equiv \sum_{q=1}^{N_q} Q_{GC}(q,\mathrm{E})\,\mathrm{v}_{\mu\nu}(q,x), \\ &\tilde{G}_{\mu\nu} = g_{\mu\nu} + H_{\mu\nu}\left(\mathrm{V}_{\alpha\beta}\right), \\ &G^{\mu\lambda}\tilde{G}_{\lambda\nu} = \delta^{\mu}_{\nu}, \end{aligned} \tag{4.14}$$

where $Q_{GC}(q,\mathrm{E})$ is the gravitational charge (defined in the following section). The *H* tensor is a power series in V (which takes a simple form when V is diagonal):

$$\begin{aligned} &H_{\mu\nu} = \sum_{n=1}^{\infty} a_n h_{\mu\nu}(n), \\ &h_{\mu\nu}(n+1) = \mathrm{V}^{\lambda}_{\mu}\, h_{\lambda\nu}(n), \\ &h_{\mu\nu}(1) = \mathrm{V}_{\mu\nu}. \\ &H^{\nu}_{\mu} = \delta^{\nu}_{\mu}\sum_{n=1}^{\infty} a_n (\mathrm{V}^{\mu}_{\mu})^n \equiv \delta^{\nu}_{\mu} H(\mathrm{V}^{\mu}_{\mu}) \ \text{ if V is diagonal.} \end{aligned} \tag{4.15}$$

The leading coefficient must be $a_1 = 1$ to give the correct weak field limit. If V is diagonal, *H* can be an arbitrary continuous-function—subject to the constraint $\partial H(V)/\partial V = 1$ when $V = 0$. The form for this function will be developed in section VI(D).

The method of coupling will be illustrated for three cases. First, consider a (fictitious) scalar boson (possibly having large mass). The LDM is modified, $g^{\mu\nu}\partial_\mu\phi^*\partial_\nu\phi \to G^{\mu\nu}\partial_\mu\phi^*\partial_\nu\phi$, and the Klein-Gordon equation of motion follows,

$$0 = \partial_\mu (G^{\mu\nu} \partial_\nu \phi) + (m_B c / \hbar)^2 \phi. \tag{4.16}$$

Eq. (4.16) is very useful because it yields the correct relativistic version of Hamilton's principle function. Thus, Hamilton-Jacobi theory is available for the classical orbit of a featureless object of mass m moving in a static gravitational field. This methodology will also work for $m = 0$ giving a simple method for photon ray tracing, *all valid for the new gravity*. Refer to Appendix E for central field details.

Next, consider a fermion. The modification is indirect,

$$\{\gamma^\mu, \gamma^\nu\} = 2g^{\mu\nu} \rightarrow \{\Gamma^\mu(x), \Gamma^\nu(x)\} = 2G^{\mu\nu}(x), \tag{4.17}$$

and the Dirac matrixes are no longer constants. The Dirac equation follows,

$$0 = i\Gamma^\mu \partial_\mu \psi + (i/2)[\partial_\mu (\Gamma^\mu)]\psi - (m_F c / \hbar)\psi. \tag{4.18}$$

Eq. (4.17) demonstrates a clear necessity for *G* to be well-behaved.

Finally, consider electromagnetism in the absence of a source. The modification of $\mathcal{L}_{EM}$ is $\mathrm{F}_{\mu\nu}\, g^{\mu\alpha} g^{\nu\beta}\, \mathrm{F}_{\alpha\beta} \rightarrow \mathrm{F}_{\mu\nu}\, G^{\mu\alpha} G^{\nu\beta}\, \mathrm{F}_{\alpha\beta}$, and the equation of motion follows,

$$0 = \partial^\varepsilon [\left(G^\alpha_\varepsilon G^\beta_\mu - G^\alpha_\mu G^\beta_\varepsilon\right) \mathrm{F}_{\alpha\beta}]. \tag{4.19}$$

Eq. (4.19) is required to obtain the correct gravitational red shift for weak fields.

The sources for Eq. (4.12) for gravitational systems of interest are as follows,

$$J_{\mu\nu}(q) = \Omega_{\mu\nu}(q) + \tfrac{1}{2} \mathrm{L}^{-2}_{gq} \{\mathrm{v}_{\mu\nu}(q) - \tfrac{1}{2} g_{\mu\nu}\, \mathrm{v}^\lambda_\lambda(q)\} = \kappa_q \partial \mathcal{L}_M / \partial\, \mathrm{v}^{\mu\nu}(q), \tag{4.20}$$

where $\delta\Omega$ is neglected for these systems, and Eq. (4.20) is for physical time ($x^0 = c\tau$).

Eq. (4.20) can be rewritten in a more transparent form using the unprimed version of Eq. (4.4),

$$\begin{aligned} &\Theta_{\mu\nu} \equiv 2\Xi_{\mu\nu} + \mathrm{L}^{-2}_{gq} \mathrm{v}_{\mu\nu}, \\ &\Theta_{\mu\nu} = 2\{J_{\mu\nu} - \tfrac{1}{2} g_{\mu\nu} J^\lambda_\lambda\}, \\ &J_{\mu\nu}(q, x) = \kappa_q \partial \mathcal{L}_M / \partial\, \mathrm{v}^{\mu\nu}(q, x). \end{aligned} \tag{4.21}$$

For each *q* one has the following:

$$\partial^\varepsilon \partial_\varepsilon\, \mathrm{v}_{\mu\nu} + \tfrac{1}{2}\left(\partial_\mu S_\nu + \partial_\nu S_\mu\right) - \left(\partial_\mu N_\nu + \partial_\nu N_\mu\right) + \mathrm{L}^{-2}_{gq} \mathrm{v}_{\mu\nu} = 2\{J_{\mu\nu} - \tfrac{1}{2} g_{\mu\nu} J^\lambda_\lambda\}. \tag{4.22}$$

The systems of interest can be characterized by three qualifiers: weak/strong field, local/distal, and Newtonian/relativistic dynamics. Weak fields have $\mathrm{V}_{00} < 10^{-3}$. Local means that the range term in Eq. (4.22) can be ignored. Strong field systems are always local. In the next sections a wide range of systems will be examined.

The source term of Eq. (4.22) is a single particle defined by Eq. (4.16) or Eq. (4.17). However, *the left-hand side of* Eq. (4.22) is linear in $\mathrm{v}_{\mu\nu}(q,x)$ so the superposition principle is applicable (unlike GR). The gravitational field of a group of particles is the sum of the individual fields generated by each member of the group—each (atom-sized) particle has a tiny contribution despite a possibly large *G* factor on the right-hand-side. Appendix J outlines the application of superposition for some problems of interest.

D. Gravitational charge

For each of the five gravitons there are two universal constants, Z_{gq} and L_{gq}. These two are independent of seasons. However, it will be necessary for gravity to be different in winter than in red or blue summer for all types of matter. That chore is handled by the gravitational charge in Eq. (4.14) where E is defined in Eq. (2.17).

In summer. $\mathrm{E}=0$, and $Q_{GC}(q,0)=1$. In winter, $\mathrm{E}=1$, and the five charges ($Q_{GC}(q,1)$) are universal constants tabulated in Appendix Z. The change of season is found in Eq. (7.5). I believe that it is prudent for the epoch and Higgs fields to be oblivious of gravity ($Q_{GC}(q,\mathrm{E})=0$).

E. Gravitons

Since Eq. (4.13) looks the same as Eq. (3.20) for an electromagnetic wave, the discussion of waves versus particles in electromagnetism should apply to gravity as well. There are five gravitons with different, extremely tiny masses.

For most applications, one can treat each graviton as a massless spin 2 particle with energy $h\nu$ and momentum $h\nu/c$. The only difference between electromagnetism studies and (the much weaker) gravity studies would be smaller numbers of gravitons. The importance of these observations is that *there can be a significant graviton background radiation that we are completely unaware of*. Unlike CMB, this radiation will be a function of τ and $\mathbf{x}$.

V. THE WEAK FIELD LIMIT OF THE NEW GRAVITY

There are many systems in the universe that fall into the weak category. The first topic is the most basic.

A. Newtonian dynamics and the new gravity

The weak field limit of static-matter sources and their gravitational fields is basic to an understanding of both local and distal systems. The non-relativistic motion of traceable matter in these fields provides a measure of their form. Eq. (4.16) will be central to the quest.

The weak field limit has $G^{00}=1-\mathrm{V}^{00}(\mathbf{x})$, $G^{jk}=g^{jk}$, then one can convert Eq. (4.16) to the Schrodinger equation by substituting $\phi\left(x^0,\mathbf{x}\right)=\psi\left(\tau,\mathbf{x}\right)\exp\left(ix^0mc/\hbar\right)$ and keeping the leading terms in *c* ($x^0=c\tau$). The connection between the Newtonian potential (V_N) and V^{00} results,

$$\hbar i(\partial\psi/\partial\tau)+(\hbar^2/2m)\nabla^2\psi\equiv\mathrm{V}_N\psi=(mc^2/2)\mathrm{V}^{00}\psi. \tag{5.1}$$

Use the Ehrenfest theorem to obtain Newtonian dynamics for a (neutral) particle moving in the five gravitational fields,

$$m(d^2\mathbf{x}/d\tau^2) = -\nabla \mathrm{V}_N(\mathbf{x}), \tag{5.2}$$

$$\mathrm{V}_N(\mathbf{x}) = m\sum_{q=1}^{N_q} \mathcal{A}_N(q,\mathbf{x}), \tag{5.3}$$

$$\mathcal{A}_N(q,\mathbf{x}) = \tfrac{1}{2}c^2\, \mathrm{v}_{00}(q,\mathbf{x}), \tag{5.4}$$

The next step is to adapt Eq. (J.5) in Appendix J to a situation where the source is a static collection of (atom-sized) particles that are defined by a mass density ($\rho(\mathbf{x})$). Eq. (5.2) requires only $\mathrm{v}_{00}(q,\mathbf{x})$—justifying the neglect of other gravitational components in Eq. (J.5). The static version of Eq. (J.5) has a right-hand side that is proportional to a sum of delta functions for the location of each member of the collection. Auto-correlate both sides of Eq. (J.5), i.e., integrate over volume elements that contain very many sources, but are small compared to the inverse of the logarithmic derivative of v_{00}. Divide both sides by the volume of the element. The right-hand side will be proportional to the number of particles per unit volume ($\rho(\mathbf{x})/m$). Rearrange the terms to obtain the desired equations,

$$\begin{aligned} &4\pi G Z_{gq} Q_{GC}(q,\mathrm{E})\rho(\mathbf{x}) = \nabla^2 \mathcal{A}_N(q,\mathbf{x}) - \mathrm{L}_{gq}^{-2}\, \mathcal{A}_N(q,\mathbf{x}), \\ &d^2\mathbf{x}/d\tau^2 = -\sum_{q=1}^{N_q} \nabla \mathcal{A}_N(q,\mathbf{x}), \end{aligned} \tag{5.5}$$

where ρ is the mass density of the source. Eq. (5.5) will be used primarily for the study of galaxy-sized objects or larger. For clarity, there is no dark matter, dark energy, or dark anything in the NCNG universe. Rho is the density of ordinary matter (stars, gas, dust, white dwarfs, neutron stars, and the NCNG version of black holes of all masses)—usually called visible matter.

B. Newtonian field of a point source

The solution of Eq. (5.5) for a point source of mass *M* is given,

$$\mathcal{A}_N(r) \equiv \sum_{q=1}^{N_q} \mathcal{A}_N(q,r) = -\frac{MG}{r}\sum_{q=1}^{N_q} Z_{gq} Q_{GC}(q,\mathrm{E}(\phi_{ep}))\exp\left(-r/\mathrm{L}_{gq}\right), \tag{5.6}$$

where I have included the full seasonal dependence of Q_{GC}.

In summer, one requires that the acceleration potential ($\mathcal{A}_N(r)$) must reduce to Newton's Law when $r << \mathrm{L}_{g1}$. Since $Q_{GC}(q,0) = 1$ for matter in summer, there is a constraint,

$$\sum_{q=1}^{N_q} Z_{gq} = 1 \tag{5.7}$$

There is another constraint for all seasons. The gravitons can represent either attractive or repulsive forces. Therefore, I choose the following:

$$\begin{aligned} Z_{g1} &< 0 \ \text{(repulsive)}, \\ Z_{g2} &> 0 \ \text{(attractive)}, \\ Z_{g3} &< 0 \ \text{(repulsive)}, \\ Z_{g4} &> 0 \ \text{(attractive)}, \\ Z_{g5} &< 0 \ \text{(repulsive)}, \end{aligned} \tag{5.8}$$

where the current values of these universal constants (Z_{gq}) are listed in Appendix Z and used throughout NCNG. Appendix Z tabulates all the universal constants that define NCNG. Since NCNG is a work in progress, Appendix Z will be periodically updated as more accurate observations constrain the predictions of NCNG.

Each $Q_{GC}(q,0)$ can be different from 1 during winter, and they are also universal constants tabulated in Appendix Z. The analog of Eq. (5.8) follows,

$$\sum_{q=1}^{N_q} Z_{gq} Q_{GC}(q,1) = 0 \ \text{(winter)}. \tag{5.9}$$

There is no local gravity in winter, so there can be no stars, no white dwarfs, no core-collapse cinders, and no NCNG versions of supermassive black holes in winter. This subject will be revisited in the section about physics in winter.

The Yukawa form of Eq. (5.6) has far-reaching consequences in all seasons. The most obvious consequence is that $r\mathcal{A}_N(r) \to 0$ for finite *r*. Furthermore, the point-source gravitational force becomes weakly repulsive at large distances. The Green's function for Eq. (5.5) has a structure that requires a knowledge of ρ for all values of *r* to calculate $\mathcal{A}_N(r)$ for small *r*—a serious complication. Since Eq. (5.6) does not represent an inverse-square force law, the *virial theorem* (a frequently used tool in astrophysics) is only useful for stars and *unreliable for galaxies and larger objects*.

C. The sequestration of matter

The fact that NG gravitation has finite range brings a new perspective of scale for matter organization. The five graviton types defined in Appendix Z give rise to a specific point source gravitational field. Using Eq. (5.6), one finds that the summer force is attractive for $r < R_1$, repulsive for $R_1 < r < R_2$, and attractive for $r > R_2$, where $R_1 = 11.6$ MLY and $R_2 = 20$ MLY. Furthermore, R_2 is *the same in winter*. R_1 and R_2 are *independent of the source mass*. There is a

small repulsive bump centered on R_1 and a very shallow gravitational well centered on R_2. This shallow well slightly favors two sources to be 20 MLY apart. The consequences of this result will be examined in section V(L).

The source of an object of interest is a collection of matter located near the center of the object. The resulting gravitational field at large distances is well approximated by the point source above. The gravitational field contains the matter, so *I call the object a canister*. The sources for a canister are gas molecules, stars, stellar cinders, galaxies, and clusters of galaxies. The size of a canister is finite, but two canisters will be oblivious of each other only when separated well beyond R_2. If so separated, the canister source matter within will evolve undisturbed.

Canisters can move and they can (rarely) collide. When two canisters collide, the final state depends on the mass and matter distribution of each. The collision will be inelastic. The final state will be one or more canisters and possibly a splattering of unconfined matter contributed to the local inter-canister space. It is assumed that the matter within a canister is concentrated near the center, then the impact parameter for the collision would have to be smaller than $2R_1$ for a significant disruption of the sources.

The second level of sequestration is the division between gas, stellar, galactic, or cluster mass objects within a canister. For some (massive) canisters the intergalactic gas is thought to contribute much more mass to the canisters than the galaxies.

The intergalactic gas is a mixture of hydrogen, helium, and fusion nuclides (stirred in from galaxies moving through the gas), and it is not visible using optical photography. This extremely diffuse gas is very hot (10^6 $^\circ$K) and clearly seen using soft Xray photography (0.4 Kev). Furthermore, gas is found to be concentrated in a spherically symmetric *massive diffuse gas object* (MDGO). The radius of a MDGO can be several million light years, and the mass can be as small as a dwarf galaxy or as great as 100 heavy galaxies. Appendix F has information about MDGOs and their gravitational fields.

After a collision, a canister could have two or more MDGOs as well as galaxies. This N body orbit problem would be extremely complex. The simplest canister would have one galaxy and one much heavier MDGO. The center of the canister would be at the center of the MDGO, and the galaxy would orbit around the center. Appendix K has information about galaxy orbits within a MDGO, and Section V(L) has a study of our own milky way (MW) canister.

Even a huge mass MDGO still has a weak-field gravitational potential and an extremely tiny density. Thus, a MDGO cannot support any pressure differential—e.g., order one millionth atmospheres between the center and the outer edge two million light years above! This fact supports the model of Appendix F, where the gas pressure, temperature, and density are constant out to a radius (and zero beyond).

There are two examples of two MDGOs in a canister. Chandra Xray photography shows that Abell 399 and Abell 401 are headed for a collision in the future. The centers of the MDGOs for these *two clusters* are currently 10 MLY apart—clearly within the *same canister*. NG would consider these two clusters as one object (accounting by canisters). A Chandra photo of Abell 2744 shows two co-orbiting MDGOs (unequal size) close enough to be in the same canister.

It is likely that there is an NG version of a super-massive black hole near the center of each MDGO. When such an object is active, it becomes a very bright source of high energy (10 Kev) photons. The faint cosmic Xray background is thought to come from such distant sources.

Many Xray studies are for containers that have MDGOs in collision. Such collisions cause compression shock waves moving at sub-light velocities that are much hotter and brighter than an

unperturbed MDGO. Furthermore, the photons from the compressed zone move ahead of the shock waves and heat the unperturbed gas (a chaotic evolving temperature map).

The past or future of canisters with two or more co-orbiting MDGOs is very difficult to predict from present day observations. However, viscosity shear forces are independent of gas density, so one should expect that viscosity would play a big role with the tiny-density MDGOs. I believe that the eventual fate of a multi MDGO canister is a one MDGO canister. The mass of the MDGO would be conserved, but the size, density, and temperature would change,

There is an important fact that will end this subsection. The soft Xray emissions of a MDGO are powered by Kelvin (and Helmholtz) contraction (Appendix F). Therefore, *soft Xray emissions from a canister in winter will also be observable*. The only direct information about winter must come from soft Xray astronomy.

D. Large scale structure

There is a significant difference between the NCNG explanation and the GRLCDM explanation for large-scale structure (LSS). With GRLCDM, LSS *must be created* in the earliest stage of the Big Bang. NCNG *does not require any explanation* for LSS—it is what it is. Canisters eternally move about. Their contents evolve independently. Rarely, there are canister collisions—new canisters moving in different directions replace the two colliders.

Canisters can only be identified using high resolution soft Xray telescopes to see the MDGO sources (none exist now). Thus, NCNG has a hidden order that cannot be observed using (the many) longer wavelength telescopes. What one sees is a snapshot of a slowly changing vista that might make more sense using soft Xray astronomy.

There is another important difference. The GRLCDM version of structure is created at the same time, and the statistical nature of the proposed creation mechanism makes correlations universal. For example, the correlation-coefficient for the relative positions of galaxies in GRLCDM is thought to be a function only of the (scalar) distance between any two galaxies—independent of their location or orientation. In NCNG, the correlation-coefficient is not universal (a pathological function instead) and has no useful application for LSS. This difference cannot be tested directly since that would require two observers communicating over a vast distance. There is another important scale structure developed in section V(L).

E. General relativity version of Newtonian gravity

For purposes of comparison, the general relativity summer version of Eq. (5.5) follows,

$$\begin{aligned} &4\pi G[\rho_{VM}(\mathbf{x})+\rho_{DM}(\mathbf{x})]=\nabla^2\mathcal{A}_{GR}(\mathbf{x}),\\ &d^2\mathbf{x}/d\tau^2=-\nabla\mathcal{A}_{GR}(\mathbf{x}). \end{aligned} \tag{5.10}$$

The ρ_{VM} factor is the density profile for visible matter. The ρ_{DM} factor represents the density profile of what is called dark matter—an unknown gaseous substance that is thought to surround gravitating visible masses in a halo.

For spiral galaxies, there are various shapes for ρ_{DM} in the literature. A common choice is a three-parameter spherically symmetric profile,

$$\rho_{DM}(r) = \rho^0_{DM}[1+(r/r_{DM})^2 + \lambda_{DM}(r/r_{DM})^4]^{-1}. \quad (5.11)$$

Note that $\lambda_{DM} > 0$, otherwise the volume integral of ρ_{DM} will be infinite—not acceptable. Other shapes also require three parameters for finiteness [6].

There are important consequences of Eq. (5.10) and Eq. (5.11). If $\rho_{DM} = 0$, then there is no choice for ρ_{VM} that will come even remotely close to providing a correct rotation velocity profile for any spiral galaxy. GR *can be a candidate for a correct gravitational theory only if dark matter exists*.

The GR solution for rotation always requires using the *three extra parameters* of Eq. (5.11) compared to Eq. (5.5). Worse yet, the dark matter parameters are adjustable (*different for each galaxy*), and they cannot be predicted by using a knowledge of the shape of ρ_{VM}. In contrast, the constants that define all aspects of NG gravity are universal constants—the same for all galaxies, for all times, and for all locations in the universe.

It should be clear that dark matter is a fudge-factor that allows one to pretend that GR is a correct gravitational theory, not an actuality. The correctness of NG or GR can be determined by (existing and new) observations.

F. Spiral galactic rotation

While all galaxies exhibit some degree of angular momentum and a rotational velocity distribution, very few are suitable objects for study. References [7] and [8] detail part of the selection process, the velocity measurement process, and the velocity profiles of a set of candidate suitable spiral galaxies. Appendix D has all the information of interest for the NCNG version of this topic. The following is a brief review of what I believe are the requirements for a suitable study to compare NCNG with GRLCDM predictions.

The observatory must be an array of numerous radio telescopes (there are only four). The observation is the (relative) doppler shift of the 21 cm line of H1. This is the most accurate measure for velocities at large distances from the galactic center where there are few stars, and where the deviations from Newtonian rotation are expected to be greatest.

The distance to the candidate spiral galaxy must be accurately known. I consider observations of cepheid variables within the candidate as the only reliable method. The ladder of distances is unreliable and subject to considerable disagreement. There are very few such observations.

The candidate galaxy must have a flat and thin circular disk oriented between face-on and edge-on. Bars should be faint, and arms should be faint and confined within the circular disk. A bulge at the center is ok, but significant lumps or imbedded dwarf galaxies are not ok. It is also necessary that there are no oddities in the observed rotation velocity profile, e.g., a band which has negative angular momentum compared to the remainder of the profile. Once again, there are few galaxies that satisfy this set of constraints.

There is only one galaxy that I know about that satisfied all these conditions, NGC 3198. In Appendix D, A hypothetical galaxy which is similar to NGC 3198 was used to calculate an apples to apples set of NCNG and GRLCDM rotation velocity profiles. FIG. D2 and FIG. D3 illustrate these two profiles. The NCNG profile was chosen to resemble the observed profile of NGC 3198. The figures show that the GRLCDM profile is not even remotely close to the NCNG profile—a dismal failure.

There are many rotation profiles that are based on visible wavelengths instead of the 21 cm wavelength. These profiles are not as accurate nor extensive as the 21 cm profiles, but they may extend beyond the distance from the galactic center where the NCNG and GRLCDM profiles start to diverge. If some of these galaxies also happen to have cepheid variable distances tabulated, then one can generate figures like those in Appendix D. This method resembles a catalogue search. I believe that any additional information will end up destroying GRLCDM as a viable theory.

G. The central field

In this subsection, the gravitational field will be local, static, and spherically symmetric. Eq. (4.20) will be solved in polar coordinates within the region where the spherically symmetric source is zero—a point source. The purpose of this study is to develop the relativistic corrections to weak field orbits. The distances will be local, and the season will be red summer. Omega is a linear function of $\mathrm{v}_{\mu\nu}(q,r)$. Local and summer mean that one can rewrite (unprimed) Eq. (4.4) in terms of the compound five gravitational fields,

$$\begin{aligned}
&\mathrm{V}_{\mu\nu} = \sum_{q=1}^{N_q} \mathrm{v}_{\mu\nu}(q,r),\\
&2\Xi_{\mu\nu} = D^{\varepsilon}\left(T_{\varepsilon\mu\nu}\right),\\
&0 = \Omega_{\mu\nu} = \Xi_{\mu\nu} - \tfrac{1}{2} g_{\mu\nu} g^{\beta\lambda}\Xi_{\beta\lambda},\\
&T_{\varepsilon\mu\nu} = D_{\varepsilon}\,\mathrm{V}_{\mu\nu} + \tfrac{1}{2}\left(g_{\varepsilon\mu}S_{\nu} + g_{\varepsilon\nu}S_{\mu}\right) - \left(g_{\varepsilon\mu}N_{\nu} + g_{\varepsilon\nu}N_{\mu}\right),\\
&S_{\mu} = \partial_{\mu}\,\mathrm{V}^{\lambda}_{\lambda},\\
&N_{\mu} = D_{\lambda}\,\mathrm{V}^{\lambda}_{\mu}.
\end{aligned} \tag{5.12}$$

Eq. (5.12) is solved by using two potentials and careful application of the covariant derivatives for polar coordinates,

$$\begin{aligned}
&\mathrm{V}_{00} = V(r)\\
&\mathrm{V}_{rr} = U(r)\\
&0 = \Omega_{00} = (\partial_r U + U r^{-1}) r^{-1},\\
&0 = \Omega_{rr} = -(\partial_r V + U r^{-1}) r^{-1},\\
&0 = \Omega_{\theta\theta} = -(r/2)(r\partial_r^2 V + \partial_r V + \partial_r U),\\
&0 = \Omega_{\phi\phi} = \Omega_{\theta\theta}\sin^2\theta.
\end{aligned} \tag{5.13}$$

Eq. (5.13) is solved as follows,

$$\begin{aligned} U &= V = -b/r, \\ b &= 2GMc^{-2}, \end{aligned} \tag{5.14}$$

where *M* is the mass of the source and *G* is the universal gravitation constant. The b length factor comes from Eq. (5.2) and Eq. (5.6)—known in GR as the Schwarzschild radius. Eq. (5.14) is correct for strong fields as well, and it will be revisited in the strong-field limit section. Eq. (4.14) and Eq. (4.15) can be solved using Eq. (5.14),

$$\begin{aligned} G^{00} &= [1+H(V)]^{-1}, \\ G^{rr} &= -[1+H(-U)]^{-1}, \\ G^{\theta\theta} &= -r^{-2}, \\ G^{\phi\phi} &= -r^{-2}\sin^{-2}\theta, \end{aligned} \tag{5.15}$$

where *H* is an arbitrary function of *V* except for the following constraints. The physical region is for $-\infty < V < 0$, and in that region $-1 < H < 0$. Furthermore, $\partial H/\partial V = 1$ at $V = 0$. The orbits for the potentials of Eq. (5.14) are developed in Appendix E using the weak-field limit of Eq. (5.15).

This problem is the first instance of the need for gravitational components beyond $\mathrm{v}_{00}(q,x)$. The orbit solutions of Appendix E illustrate important facts. Even though V_{00} and V_{rr} have the same strength, V_{00} causes the Newtonian orbit for a non-relativistic object, but V_{rr} causes only the tiny advance of perihelion. This fact is the rationale for neglecting the nine gravitational components (beside V_{00}) for non-relativistic objects. The story for photons (or relativistic objects) is very different—V_{rr} is responsible alone for the defection of photons. Thus, one must have more than one gravitational component to describe the path of a photon in a gravitational field.

H. Canisters

If the mass of a canister is dominated by a MDGO, the galaxies can be ignored in this subsection. The goal is to develop an equation for the potential well using Eq. (5.5) for a canister with one MDGO. Refer to Appendix F for details of the solution for Eq. (5.5) and other important information. A MDGO is like an elephant in the living room—vitally important but often ignored.

Since the MDGOs and galaxies are made up of non-relativistic matter, Eq. (5.5) is sufficiently accurate as noted in the preceding subsection. The path of photons through a canister is much more complex (see VI(F)).

Figure 1 shows the dimensionless (red summer) NG gravity field ($\mathrm{V}_{00} = 2\mathcal{A}_N(r)c^{-2}$) for an example constant-density MDGO having a size $\mathrm{R}_{MDGO} = 2\,\mathrm{x}10^6$ LY and a mass $\mathrm{M} = 10^{14}$ solar masses. The NG gravitational constants are found in Appendix Z. This gravity well is very deep. The escape velocity for an object at R_{MDGO} is 15013 km/s, and an object must have a radial velocity greater than 1480 km/s to get over the repulsive barrier (enter the canister during summer).

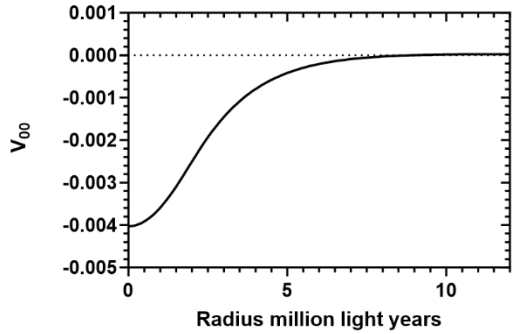

Figure 1. The dimensionless NG gravitational potential (for the example canister described above) versus distance from the canister center. The peak of the weak repulsive barrier is at the right side of the figure.

The dimensionless NG gravitational potential (for the example canister described above) versus distance from the canister center. The peak of the weak repulsive barrier is at the right side of the figure.

No compact object is likely to enter or leave a canister of this mass, but another canister can enter. Given the gravitational constants, the dimensionless field ($V_{00}(r)$) is a function of M and R_{MDGO}.

I. Galaxies within canisters

The orbital motions of individual galaxies within a canister are determined in a stepwise manner. The mass of a contained MDGO is assumed to be significantly greater than the mass of the galaxies associated with that MDGO. Thus, the galaxies can be considered as perturbation.

The first step is to obtain the orbit for an object in the radially symmetric field of a single MDGO using the equations of Appendix F and the techniques of Appendix E. This step will provide useful information (the subsequent steps are beyond the scope of this document).

One can use the example model MDGO of section V(H) to calculate the example orbit of a galaxy. The orbit will lie in a plane containing the center of the MDGO (with arbitrary orientation). The orbital information is summarized by studying two extremes of angular momentum. Case one is for a circular orbit of radius *R* (maximum angular momentum), and case two is for a linear orbit (angular momentum = 0) with turning points at *R* and -*R*. Figure 2 shows the orbital periods for the two cases as a function of *R*.

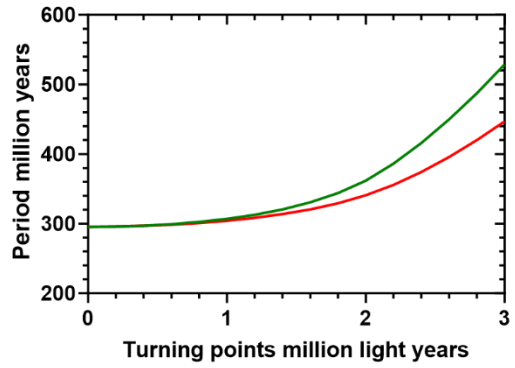

Figure 2. Periods of a galaxy orbiting within an example MDGO. Circular orbit (green) and zero angular momentum (red).

The period for any angular momentum will lie between the two curves of Figure 2. The primary observation for this subsection is that the orbits for this model will have periods of order 350 million years—small compared to the average canister collision frequency. Thus, considerable evolution of the relative positions of the MDGO galaxies will occur between potentially disruptive collisions.

J. Ultra-diffuse galaxies

Ultra-diffuse galaxies (UDGs) can have significant size (like the milky way) but faint luminosity (like a dwarf galaxy). UDGs of large size are found in distant clusters of galaxies, generally nearer to the center. There could be smaller UDG's in a distant cluster that are too small and faint to be observed. The UDG velocity dispersion suggests a robust gravitational force, but the faint luminosity suggests a small visible mass. Using GRLCDM to explain their structure via Eq. (5.10) yields *absurdly high ratios* of dark-matter mass / visible mass—not acceptable. The NG explanation is plausible but extremely complex.

The most dramatic difference between GR and NG is illustrated by a simple example distribution of (visible) matter. Consider a thin radial shell of radius R_S having constant density,

$$\begin{aligned} \rho(r) &= \sigma\,\delta(r-\mathrm{R}_S), \\ \mathrm{M}_S &= 4\pi\sigma\,\mathrm{R}_S{}^2, \end{aligned} \tag{5.16}$$

where δ is the Dirac delta function and M_S is the shell mass. The shell is an approximation for a group of galaxies distributed at a constant distance from a center. For GR, there is *no gravitational force within the shell* (constant potential). For NG inside the shell vacuum, there is a gravitational potential bulge (*repulsive force supported by no matter inside the shell*).

Using Eq. (5.16) in Eq. (F.1) yields the NG potential:

$$\begin{aligned} \mathrm{V}_{00}(r) &= -2\,\mathrm{M}_S\,G\,(\mathrm{R}_S\,c^2)^{-1}\,\mathrm{F}(r), \\ \mathrm{F}(r) &= \sum_{q=1}^{N_q} \mathrm{Z}_q\,\mathrm{L}_{gq}\,r^{-1}\sinh(r\,\mathrm{L}_{gq}{}^{-1})\exp(-\mathrm{R}_S\mathrm{L}_{gq}{}^{-1}), \end{aligned} \tag{5.17}$$

where the constants are tabulated in Appendix Z. Eq. (5.17) is presented as an example comparison of NCNG and GRLCDM. A real canister can have many galaxies orbiting about the MDGO center with perturbations between each other. At any point where the vector NG force of all the orbiting galaxies is zero, there will be the maximum of a vacuum repulsive gravitational potential (a peak). One should expect that there will be many peaks. Since the galaxies are moving, the peaks will move, wax or wane, appear or disappear. I believe that the force from the MDGO can be neglected since it is canceled by the acceleration of each orbiting galaxy.

If a peak lies within a galaxy, there will be a consequence depending on the size and strength of the repulsive volume and the size and mass of the galaxy (if it was outside the repulsive volume). The attractive force of the NG galactic matter is countered by the repulsive volume.

A UDG results only if the repulsive volume is large enough and strong enough to hold all the mass of the galaxy with significantly smaller density. Otherwise, the galaxy would be largely intact, but it would contain a small lower density volume within (difficult to observe).

All of this represents a very complex evolution. There are peaks wandering about and galaxies moving as well. A UDG can only exist when a peak and a galaxy coincide (*their paths cross*). Thus, one should expect that *a specific galaxy could have a UDG appearance during a brief period* (likely less than 100000 years), and after the appearance the galaxy would be largely the same as before the appearance. The NCNG version of a UDG is radically different compared to the (failed) GRLCDM version. The complexities of this topic are beyond the scope of this document.

K. The Milky Way canister

Our own canister (MWC) has the virtue of relative simplicity. What is known as the local group consists of two massive galaxies (MW and M31—Andromeda) and many lesser objects (negligible mass). These objects are associated with a MDGO of unknown mass and location. There are not any other candidate MDGOs within ten million light years, so one may assume that MWC has only one MDGO. In that case, gravitation within the canister devolves into a three-body problem (MDGO, M31, MW). This is an example of *the elephant in the living room problem* since studies of interactions between M31 and MW have been treated as a two-body problem, e.g., the erroneous notion that MW and M31 will collide in the future.

Direct evidence about our MDGO is problematic. The gas associated with our MDGO has been observed but misidentified as a wisp of warm-hot intergalactic matter (WHIM) —the defunct dark cosmology. These observations indicate that both M31 and the MW are within the boundary of our MDGO. Therefore, the center of our MDGO is within (roughly) 2 MLY of both massive galaxies. It is likely that MDGOs have a NCNG version of a super-massive black hole near their center, but that object would only be observable when ingesting an occasional star—not the case for MWC now.

The distance between MW and M31 is accurately known now (0.770 Mpc—cepheid), but the GRLCDM mass (including dark matter) of M31 is very poorly known. The rotation velocity profile of M31 has been established [17], so an accurate NCNG mass can be established using the methods of Appendix D. MW rotates, but the velocity profile is not accurate enough to get a good NCNG mass.

I believe that the warping of the rotating discs of MW and M31 are both caused by our MDGO instead of each other. Therefore, it could be possible to establish a direction toward our MDGO—an exercise for the reader, A good MDGO direction would simplify the search for a NG version

of a super massive black hole near the center of the MDGO. Such an object (even if inactive) would likely emit radiation observable by the JWST.

MWC gravitation includes the three massive objects plus many dwarf satellite galaxies. There could be several (very small) UDGs near MW and M31 (as described in section V(J)). If there are genuine UDGs, their locations would constrain the mass and locations of the three massive objects. A possible candidate UDG would be And II [Ra(1,16,29.8), Dec(33,25,9)]—a satellite of M31.

Spectral red shifts are another source of information about the members of the MWC. However, red shift has three components (cosmologic, doppler, gravitational) and then only for the line-of-sight portion of information. Gravitational red shift in NG is a larger factor than in GR, thus making doppler determinations less reliable. One does not know where the center of our MDGO is located. For a plausible set of parameters, the extremes of the gravitational contribution to the apparent doppler velocity are ± 41 km/s (either MW or M31 is at the center of our MDGO). M31 is thought to be moving toward Milky Way at 110 km/s. The actual receding velocity could be -110 ± 41 km/s—a major uncertainty due to NG. Furthermore, MW and M31 have different orbits about the MDGO center (see Appendix K). The risible notion of a near-future collision is not supported.

NCNG can yield an impressive crop of accurate information about MWC, whereas GRLCDM can yield only question marks.

L. Largest scale structure

This topic is by far the most complex application of both NC and NG. NG astronomy up to this point has been all about canisters. Canisters are all about MDGOs, and MDGOs are all about soft Xray astronomy. There is no soft Xray astronomy now, and the two toy observatories of the past were hopelessly inadequate. Conventional astronomy of interest here is all about galaxies (Their orbits are influenced by MDGOs *that cannot be located*). The next step-up is the organization of canisters on a larger scale—*filaments of canisters*.

This subsection is also the most important one of section V because this is the first case where knowledge of the winter seasons is important. Filaments of galaxies (residing in canisters) are considered as the largest structures in the universe. They are billions of light years in size and appear as long *kinky lines* in the sky. It is difficult to understand how filaments had enough time to organize a form in a GRLCDM universe. This problem does not exist in NCNG since thousands of cycles are available—*evolution during all seasons*. What one sees today is just a snapshot of an evolution that has continued for eons.

The rationale for my choice of five gravitons in NG will now become clear. A minimum of five gravitons is required so that the NG gravitational potential of a point source (Eq. (5.6) where $V_{00} = 2c^{-2}\mathcal{A}_N$) will have a single shallow attractive gravitational well centered at a distance D_W from the source. D_W (R_2 of subsection V(C)) is independent of the mass of the source. Thus, point sources of any mass can become trapped when they are about D_W apart. D_W is a universal constant since it is calculated using the universal constants of Appendix Z. Can one find a value for D_W?

A study of four nearby major galaxies and their satellites (M81, M94, NGC5128, and Sculptor) lead to an interesting result. The distance from earth of the four major galaxies are known and in the same distance ladder slot. The directions are very accurate, so the distance between any pair of the four major galaxies is known. They are far enough apart so that *there are four separate single major-galaxy and single* MDGO *canisters*. The location of each canister center is unknown but likely to be within a million light years of each major galaxy. Of the six possible pairs, four have

nearly the same separation (19.95 ± 0.77 million light years), and the other two are significantly different. The four major galaxies do not lie in a plane, so one has four possible equilateral triangles (defining a plane) and one outlier not in the plane. I have chosen the equilateral triangle (M81, NGC5128, and Sculptor) and M94 as the outlier. In that case, $D_W = 20.081$. There is another canister of interest (MWC is a two major-galaxy and one MDGO canister). MWC is too close to the triangle to be part of the connectivity.

The gravitational constants of Appendix Z are constrained by this choice of distance. If future data requires a different distance, the reasoning below will not be changed, but details will change (*for every topic in* NG). I also believe that smooth evolution is best served by having *the same distance* (D_W) *in winters*—a constraint on winter NG constants in Appendix Z. Using point sources for this study is a good approximation at the distances of interest. The point source coincides with the center of mass for a canister. The gravitational well is shallow but large enough to hold a MDGO and all the galaxies of a canister. It will be important to keep in mind that a canister source in the well can orbit about the center of the well. An observed galaxy in the well will orbit within the canister (which in turn will orbit within the well). The lack of information about canister MDGOs will be a persistent problem—no soft Xray astronomy.

It should be obvious that a *chain* of sources separated by D_W could form the *frame* for a filament. There will be individual galaxies and canisters that are not part of the chain-frame connectivity but move in orbits within the gravitation of the chain-frame (I call them rogues). For example, MWC could be a rogue. There are also rare interlopers that pass through the chain-frame gravitation without being trapped. MWC could also be an interloper—a question of unknown velocities.

Rogues can (rarely) interact with frame sources and possibly dislodge them, thus breaking the chain. Rogues can also conspire to replace a missing frame source, thus repairing the chain. An interloper can also knock out a frame source. The replacement frame source can be a newly formed canister or the old, displaced canister. Once again, one sees an extremely complex evolution with details beyond the scope of this document. However, some examples will give one an insight into the stability of a filament.

Consider a very long linear-filament consisting of equal mass canister-sources separated by D_W. The NG dimensionless gravitational potential surrounding the filament is $V_{00}(r,z)$, where z the position along the line joining the centers of the sources, and r is a radial distance perpendicular to z. V_{00} is independent of the radial angle, ϕ—cylindrical symmetry. There is another symmetry, $V_{00}(r, z+D_W) = V_{00}(r,z)$.

The origin ($r = z = 0$) is at the center of an arbitrary source in the linear filament. There are two separate orbits of interest. The orbit of a rogue is determined by the sum of the NG potentials (Eq. (5.6)) of *all* the filament canister sources. The orbit of a filament-source (near the origin) is determined by the total sum *excluding the potential of the source at the origin*. V_{00} is well approximated by summing the two or three source-potentials of the sources near the origin. Refer to Appendix G for some details of this study.

The main discovered factor in this study is that the period of an orbiting canister-source is measured in tens of billions of years (up to trillions). Thus, canister sources in a linear frame are very weakly bound, and an observed filament is favored by having the heaviest possible canister sources. Furthermore, rouges are the only candidates for dislodgement, so the lightest possible rogues are favored. In that case, a single pass of a rouge close to a canister source will provide an impulse that is small enough so that the source is still bound in the future when another pass occurs (providing an impulse in a different direction). The dislodgement mechanism is significantly

slowed by the randomness of the impulse directions. I believe that a linear filament can last for tens of billion years—very slow evolution.

An observed filament has galaxies closer together than D_W. The extra galaxies are rogues with orbits favoring the z axis between canister sources. Motion along that axis is agonizingly slow—hundreds of million years. This topic deserves much study.

VI. THE STRONG FIELD LIMIT OF THE NEW GRAVITY

The primary goal of this section is to determine the function $H_{\mu\nu}$ (defined in Eq. (4.15)) which governs the strong field limit for NG. I have chosen a specific form for *H* that is simple, especially when $V_{\mu\nu}$ is diagonal. There are more complex possibilities that could be considered as possible perturbations—beyond the scope of this document.

Strong gravitational fields can only occur close to sources that are massive and compact. Only three types of sufficiently compact sources are known—white dwarfs, neutron stars (pulsars), and black holes. New equations are needed to develop the NCNG version of these objects.

A. Static central field orbit equations

One requires an inhomogeneous version of Eq. (5.14) as the starting point for this study. Assume that the source of the local central field is a spherically symmetric mass distribution contained within radius R_{sorce}. Since the source is assumed to be static, the only change to Eq. (5.14) is that $\Omega_{00}(r) \neq 0$ for $r < R_{sorce}$. The Hamilton-Jacobi solution follows:

$$\begin{aligned} &\partial I / \partial E = 0 = \tau + \partial \mathrm{f} / \partial E, \\ &\partial I / \partial A = 0 = \phi + \partial \mathrm{f} / \partial A, \\ &[1 + H(-U)]^{-1} \left(\partial_r \mathrm{f}\right)^2 = [1 + H(V)]^{-1} c^{-2} E^2 - A^2 r^{-2} - m^2 c^2, \end{aligned} \tag{6.1}$$

where *E* is the conserved (total) energy of the orbiting object, *A* is the conserved angular momentum, *m* is the orbiting object mass, and τ is physical time in the rest frame of a far-distant observer and the source. If $E < mc^2$, the object is bound to the source. The weak field limit requires that $H(0) = 0$.

For orbits that lie outside of the source, $U = V = -b/r$. As the mass of the source (and *b*) goes to infinity, there will be a range ($R_{sorce} + \varepsilon > r > R_{sorce}$) for which *V* can go to minus infinity as well. Such a source *cannot grow* unless there are orbits which intersect with the source—f *is real* for $V \to -\infty$. Thus, one requires $H(V) > -1$ for $V \leq 0$ (the physical region) otherwise a source cannot accrete mass. If orbits are to have the observed advance of perihelion and bending of starlight, it is necessary that $\partial H / \partial V = 1$ at $V = 0$. Thus, $H > 0$ at least in a portion of the unphysical region ($V > 0$). In GR, $V = -1$ is the point where a singularity arises (dividing the physical region into two subregions). $H(V)$ is a continuous function for all values of *V* in NG, but $V = -1$ will still represent a (nonpathological) boundary dividing the physical region into two sectors.

Eq. (6.1) gives rise to the orbit equations,

$$dr/d\tau = -[\partial(\partial_r \mathrm{f})/\partial E]^{-1},$$
$$d\phi/d\tau = -(dr/d\tau)[\partial(\partial_r \mathrm{f})/\partial A]. \tag{6.2}$$

Eq. (6.2) can be rewritten:

$$dr/d\tau = \pm[1+H(-U)]^{-1/2}[1+H(V)]E^{-1}c^2K,$$
$$K = \{[1+H(V)]^{-1}c^{-2}E^2 - A^2r^{-2} - m^2c^2\}^{1/2}, \tag{6.3}$$
$$d\phi/d\tau = -AE^{-1}c^2[1+H(V)]r^{-2},$$

where plus means the orbiting object is moving away from perihelion and minus is toward perihelion. Note that the advance of perihelion depends on A^2—independent of counterclockwise or clockwise observed motion.

B. The strong central field source

The strong (red summer) source for Eq. (5.14) is given by one change,

$$\Omega_{00} = 8\pi G c^{-2}\rho(\partial G^{00}/\partial V),$$
$$G^{00} = [1+H(V)]^{-1}. \tag{6.4}$$

Eq. (5.14) with alteration Eq. (6.4) represents the inhomogeneous central field equations that will be used in what follows. These equations are approximations. The L_{gq} terms have been neglected since $r << \mathrm{L}_{gq}$ for examples of interest. The effects of pressure (P) within the source are neglected since $(\mathrm{P}/\rho c^2) << 1$ for most examples of interest. The resulting equation for V is nonlinear and represents what the source does to the field.

C. Hydrostatic equilibrium

What does the field do to the source? The field defined by modified Eq. (5.14) exists inside the source. In turn, the orbit equation for a particle within the source is given by Eq. (6.3). The source particle is stationary ($dr/d\tau = 0$), but it is subject to a force ($d^2r/d\tau^2 \neq 0$). This force is countered by a pressure gradient,

$$\partial \mathrm{P}/\partial r = \rho a_g,$$
$$a_g = -0.5c^2(\partial V/\partial r)[\partial H(V)/\partial V][1+H(-U)]^{-1}. \tag{6.5}$$

The radial acceleration (a_g) is calculated using Eq. (6.3) for zero angular momentum,

$$a_g = \left[\frac{\partial}{\partial\tau}\left(\frac{dr}{d\tau}\right)\right]_{dr/d\tau=0} = \left[\left(\frac{dr}{d\tau}\right)\frac{\partial}{\partial r}\left(\frac{dr}{d\tau}\right)\right]_{dr/d\tau=0} . \tag{6.6}$$

In the weak field limit, $a_g \to -\partial\mathcal{A}_N / \partial r$. Eq. (6.5) is also an approximation—valid when $(\mathrm{P}/\rho c^2) << 1$.

D. Equation of state and boundary conditions

The (summer) field/source equations can be summarized,

$$\begin{aligned} &U = -r(\partial V / \partial r), \\ &\partial V / \partial r = 8\pi G c^{-2} r^{-2} \int_0^r dr' r'^2 \{\rho(\partial H / \partial V)[1 + H(V)]^{-2}\}_{r'} , \\ &\partial \ln(\rho) / \partial r = -0.5 c^2 (\partial \mathrm{P}/\partial\rho)^{-1} (\partial V / \partial r)(\partial H / \partial V)[1 + H(-U)]^{-1}, \end{aligned} \tag{6.7}$$

and they will need boundary conditions. The equation of state (EOS) for matter within the source allows the elimination of one unknown (pressure).

The thermodynamics of the source material comes into play if the EOS depends on temperature. An additional equation is required in that case:

$$\partial \mathrm{T}/\partial\tau = r^{-2}\partial_r (r^2 \mathrm{K}_T \rho^{-1} \mathrm{S}_T{}^{-1} \partial_r \mathrm{T}) + \mathrm{J}_T \rho^{-1} \mathrm{S}_T{}^{-1}, \tag{6.8}$$

where $\mathrm{T}(r,\tau)$ is the temperature of the source material ($^\circ$kelvin). Eq. (6.8) must be well-behaved as $r \to 0$, and $\partial \mathrm{T}/\partial\tau \to 0$ for all applications of interest *except core collapse*. K_T is the heat conductivity of the source material, and S_T is the specific heat capacity—both can depend on temperature and composition of the source material. J_T is the sum of the (positive) power/volume of any nuclear fusion within the source and the (negative) heat loss caused by any neutrinos fleeing the source. It is possible for a small amount of proton-proton fusion to occur where hydrogen material abuts helium material in the source, but this heat source can be neglected. There are conditions where a zone in the source can have protons (in the underlying nuclides) undergo electron capture (producing a neutron and an electron flavor neutrino). This heat loss can be significant. The asymptotic static version of Eq. (6.8) follows,

$$\partial_r \mathrm{T} \propto -r^{-2} \rho \mathrm{S}_T \mathrm{K}_T{}^{-1} \text{ as } r \to r_{edge} \tag{6.9}$$

One should expect that K_T could be large near the center of the source and very small near the outer edge.

Static means that the source composition, temperature profile, mass, gravitational field, etc., change *very* slowly after the brief formation era of the source—evolution. The solution of Eq. (6.7) is a snapshot of an instant in the lengthy object evolution.

The method of solution starts with forming an EOS that spans a large range of densities and corresponding pressures (providing $\partial \mathrm{P}/\partial\rho$). The EOS can have phase changes, so $\partial \mathrm{P}/\partial\rho$ can

have discontinuities. The source composition profile will depend upon the age of the object, so some plausible evolution is needed.

The three strong-gravitational source types are all formed during the death of a star. In NCNG there are only three kinds of source material, electron degenerate matter (EDM), neutron degenerate matter (NDM), and proton-neutron matter (PNM) —known as neutron pasta. EDM also includes partial degeneracy as does NDM. EDM has been well understood for more than eighty years. A white dwarf is made of EDM, and I believe that NGNC will not provide any useful (observable) white dwarf information about the strong limit. The pulsar and black-hole objects are a different story. These two objects are created in a very similar manner—core collapse. They are cinders remaining from the death of a summer-time star.

The NCNG versions of the two types need new names: CCNS (*core collapse neutron star*) replaces pulsar and CCBO (*core collapse boundary object*) replaces black hole. A boundary takes the place of an event horizon—described below. The composition of CCNS and CCBO is a mixture of EDM, PNM, and NDM. A CCNS or CCBO can exist for billions of years during summer, so one must expect evolution.

There is a third NCNG type of interest, MBO (*massive boundary object*), which replaces the super massive black hole. An MBO is just a CCBO that has grown in a special manner to a very large mass. The evolution of a MBO and the fate of all cinder types in winter are discussed in sections VI(G) and VII(E).

Returning to the method of solution, one can cobble together an EOS that spans a large range of densities and corresponding pressures (providing $\partial \mathrm{P}/\partial\rho$). The integrations start at the center (r = 0) with initial conditions,

$$\begin{aligned} &U(0) = 0, \\ &V(0) = V_0 < 0, \\ &\rho(0) = \rho_0. \end{aligned} \tag{6.10}$$

The integrations using Eq. (6.7) continue until $r = r_{stop}$, where $\varepsilon = 1 - U(r_{stop})/V(r_{stop})$ and epsilon is positive and sufficiently small (e.g., 10^{-7}). If $\rho(r_{stop})/\rho_0$ is sufficiently small, then one has a plausible solution for that choice of V_0 and ρ_0:

$$\begin{aligned} &R_{source}(\rho_0) = r_{stop}, \\ &\mathrm{M}_I(\rho_0) = M_{inertial}(r_{stop}), \\ &\mathrm{M}_G(\rho_0) = M_{gravity}(r_{stop}), \end{aligned} \tag{6.11}$$

otherwise, a different ρ_0 must be chosen (for the same V_0) and the integration procedure repeated until a plausible solution is found. The inertial and gravitational masses are accumulated during the integration process—not necessarily the same due to the *H* factor on the right-hand side of Eq. (6.4). There is only one solution per V_0, but there could be two different solutions per ρ_0. Appendix H has details for the summer solutions of Eq. (6.7) for objects of interest.

Eq. (6.7) represents the NCNG version of the TOV (Tolman, Oppenheimer, Volkoff) equation which can be found as Eq. (11) of [9]. TOV is still in use today—use a modern EOS for nuclear

matter to obtain $\mathrm{M}_I(\rho_0)$. Even if GR could be a correct theory of gravity, TOV would still be a crude approximation. TOV is derived using a simple two parameter model of the source energy-momentum tensor (an ideal fluid). Source material *is not an ideal fluid due to (second degree) phase changes and an inhomogeneous consistency*. Furthermore, a "cold" temperature is used for the EOS in [9]. *The assumption that the internal temperature is cold is suspect*. The cooling time for a white dwarf cinder is measured in billions of years. There is no reason to believe that neutron star *cinders* would cool significantly faster despite some (zonal) neutrino cooling *during the actual core collapse*.

The only *observable* consequence of Eq. (6.7) is the gravitational mass of the source object (which determines the orbit of an object distant from the source). The fields for the distant orbiting object are $U = V = -b/r$, where $b = 2G\,\mathrm{M}_G c^{-2}$. The central density ($\rho_0$) can only be inferred by using Eq. (6.7). The only (observable) information that can determine $H(V)$ are the *ranges of mass for certain classes of source and the rate of accretion during their formation*.

The mass spectrums of two classes in summer (CCBO, CCNS) give rise to an important clue for the form of $H(V)$. There appears to be a gap between the heaviest mass (observed) for a CCNS and the lightest mass for a CCBO. Within the source for each type, $\partial H/\partial V > 0$ (an inward gravitational force). If this condition is met for all $V < 0$, there would be no expectation for a mass gap. Therefore, one must expect that there is a (small) region where $\partial H/\partial V < 0$ (a repulsive barrier). I have chosen to place this boundary at $V = -1$. In essence, NG replaces the event horizon of GR with a (finite) repulsive boundary. The boundary form for $H(V)$ is as follows:

$$\begin{aligned} &H(V) = \theta_{SL}(V)h_{>}(V) + (1-\theta_{SL}(V))h_{<}(V), \\ &\theta_{SL} = 0.5\{1+\tanh[\Gamma_{SL}(V+1)]\}, \end{aligned} \tag{6.12}$$

where Γ_{SL} is a universal constant ($\Gamma_{SL} >> 1$). Both $h_{>}$ and $h_{>}$ are continuous functions defined for all V, and H is continuous as well.

A cinder cannot be stable if there is a repulsive boundary within the source. Therefore, there will be two classes separated by the boundary. The heaviest CCNS will have $V(0) = -1$, while the lightest CCBO will have $V(R_{source}) = -1$. There are no reliable observations of low candidate CCBO masses (largely due to controversy and uncertainty about their distances). The TOV models [9] give maximum CCNS masses in the range (1.8-2.25) solar masses, but there are observations as high as 2.4 solar masses (also with controversy and uncertainty).

It is more convenient to use the following definition:

$$\begin{aligned} &Q(V) \equiv 1 + H(V), \\ &Q(V) = \theta_{SL}(V)q_{>}(V) + (1-\theta_{SL}(V))q_{<}(V), \end{aligned} \tag{6.13}$$

where $0 < Q(V) < 1$ for $V < 0$, $Q(0) = 1$, and $\partial Q/\partial V = 1$ at $V = 0$. The following functions satisfy these conditions:

$$\begin{aligned} &q_{>}(V) = (1+V+\varepsilon_{SL}V^2)(1+0.5V^2+\gamma_{SL}V^4)^{-1}, \\ &q_{<}(V)^{-1} = \delta_{SL}{}^{-1} - 1 - \alpha_{SL} - V + \alpha_{SL}V^{-2}, \end{aligned} \tag{6.14}$$

where ε_{SL}, γ_{SL}, δ_{SL}, α_{SL}, and Γ_{SL} are *universal constants*. The universal constants are subject to constraints: $0<\varepsilon_{SL}<1$, $0<\gamma_{SL}<<1$, $0<\delta_{SL}<1$, $\alpha_{SL}<0$, and $\Gamma_{SL}>>1$, Furthermore, *these constants control different observable aspects*. Γ_{SL} and δ_{SL} control the flow of matter and photons across the boundary at $V=-1$. ε_{SL} controls the mass of the heaviest neutron star. α_{SL} controls the mass of the lightest CCBO, γ_{SL} controls the maximum size of a MBO source. The universal constants are determined in Appendix H for a set of observable aspects (gravitational mass spectrum). The mass spectrum is not well known at present, so I have chosen plausible values to establish the strong-field-limit component of a *standard* NCNG *model* (Appendix Z),

$$\begin{aligned}\varepsilon_{SL}&=0.487,\\ \gamma_{SL}&=2.8\text{x}10^{-7},\\ \alpha_{SL}&=-1.9,\\ \delta_{SL}&=0.95\ .\end{aligned} \tag{6.15}$$

The limits are based on a maximum CCNS mass =2.406 solar masses, minimum CCBO mass = 4.093 solar masses, and maximum MBO source size $=1.597\text{x}10^{7}$ km. The required rate of flow across the boundary is an extremely complex subject since it involves the details of core collapse—visited in a subsection below. Therefore, my choice for δ_{SL} represents a starting assumption. Appendix H has Figures showing size and gravitational mass as functions of the central density for the CCNS, CCBO, and MBO.

There are situations of interest where time dependence and thermodynamics are important—formation and seasonal changes in physics. These situations will be discussed in various sections.

E. Core collapse and cinder formation

Core collapse and the resultant formation of central dense objects (cinders to be) is the most challenging problem in astrophysics. NG (with the new strong field limit) does not simplify this problem. Instead, NG significantly complicates core collapse because one must carry the calculations through any boundary all the way to the center. Furthermore, composition and thermodynamics of the forming central object within any boundary must be considered as well. In NC, core collapse can only occur during summer—no stars in winter.

How will NG change the current model of core collapse evolution? A detailed study of this subject is beyond the scope of this document, but I can make the following observations. Refer to Appendix M for what follows. Using Eq. (M.2), one obtains the velocities—$c\beta_{>}$ is the material velocity on the $V>-1$ side of the boundary, and $\beta_{<}$ is the velocity on the $V<-1$ side. The velocity on each side has the same sign, positive for outbound particles and negative for inbound.

If the core is not spinning, the velocity profile of material will be radial ($\mathcal{V}(r,\tau)$), where $\mathcal{V}(0,\tau)=0$. A boundary is only a few meters thick. The gravitational potential, $V(r,\tau)$, will not be directly connected to the velocity profile. The radius of a boundary, $V(R_B(\tau),\tau)=-1$, *can move. A boundary can come into existence at any radius or vanish at any time*. This evolution is very complicated—many moving parts.

The time evolution of gravitational systems has not been developed in this document. However, I believe that Eq. (M.2) can be applied to a special instant in time during core collapse (τ_{cc}). That instant occurs when there is a boundary, $\mathcal{V}(R_B(\tau_{cc}),\tau_{cc})=0$, and $\partial_\tau \mathcal{V}(R_B(\tau_{cc}),\tau_{cc})=0$ —the region near the boundary is quasi-static (in the frame where the boundary is stationary). Thus, $c\beta_< = 0$ and $c\beta_> = \pm c\,a^{1/2}$. There can be a sudden reversal of material flow: $c\beta_> = -\,ca^{1/2}$ (inbound) when $\tau = \tau_{cc} - \varepsilon$, and $c\beta_> = c\,a^{1/2}$ (outbound) when $\tau = \tau_{cc} + \varepsilon$ (epsilon is a very small time). *The inbound matter is bounced off the (moving) boundary*. If the boundary is inbound $\mathcal{V}_B < 0$, then the bounce can develop into a very robust outbound shockwave that will start with $\mathcal{V}_{SW} = -2\mathcal{V}_B$ and move upstream into a nearby region where there is fusion fuel available.

The creation of an outbound shockwave is also a feature of present-day models. Once this shockwave enters a region where fusion is ongoing, it could radically increase the rate of fusion (if it is sufficiently robust)—create a new shockwave. The new shockwave would have two fronts, outbound and inbound. The outbound side could set off a runaway increase in fusion (a type II supernova). The inbound side could increase the mass of the source and perhaps create a new bounce.

I believe that a comprehensive study of the moving parts in NCNG will reproduce the basic elements of the scenario above. However, there will be a significant difference from present-day models. The NG version of the boundary is very dynamic. A boundary with a specific behavior is required to have a robust bounce, otherwise the (weaker) bounce will depend on the properties of the source EOS. Is the source a CCNS or a CCBO? The NG answer is simple. If there is a static boundary after the source becomes isolated, it is a CCBO, otherwise a CCNS. I also believe that the present-day models have used the incorrect strong field limit of GR to produce suspect results.

The composition profile of a *newly formed* CCBO or CCNS summer-cinder is governed by the environment of the center of the collapse at its end—iron at ($\mathrm{T}(r=0) \sim 2.7\,\mathrm{x}\,10^9\ ^\circ\mathrm{k}$). T(0) is the burn-temperature of the last fuel to be exhausted (Silicon). The EOS of *new cinder* material causes the composition profile to have three or less spherical layers. An *aging cinder* may have extra layers due to growth. Each layer represents a different (second order) phase or composition of the EOS, but the EOS is continuous.

The number of layers in a *new cinder* (and their thickness) depends on the gravitational mass of the new cinder. The density, pressure, and temperature all decrease moving outward from the center for all possible sources that do not have fusion within. A small amount of fusion is possible only in summer for a growing cinder with a very specific temperature profile.

The outermost layer of a *new cinder* consists of iron EDM. This EDM layer is always present for all *new cinders* of any mass. In many cases it is the only layer (heavy CCBOs or light CCNSs). The amount of degeneracy and free-electron velocity decline moving outward in this layer. One should expect that the heat conductivity will decline as well.

A second layer of PNM (proton neutron matter) for a *new cinder* can form inside the EDM layer for lighter CCBOs or heavier CCNSs. The EOS undergoes a (second degree) phase change at the EDM-PNM boundary when the pressure rises above the maximum pressure for a fully degenerate electron gas. Furthermore, the protons in the iron nuclides that underly the electron gas of the EDM layer can undergo electron capture and turn into neutrons (and fleeing neutrinos). Thus, the matter transitions into an underlying solid of protons and neutrons and a depleted degenerate electron gas. As pressure increases toward the origin, the proton density and electron gas density decline and can vanish. The PNM material is a solid.

A third layer of NDM (neutron degenerate matter) for a *new cinder* can form inside the PNM layer for the lightest CCBOs or heaviest CCNSs. The EOS undergoes a (second degree) phase change at the NDM-PNM boundary. The NDM material is a liquid.

I have used the EOS of [9] to calculate the mass spectrums of Appendix H (despite questions of accuracy). The results of Appendix H should be viewed as a comparison of the strong field limit of NCNG versus GR, rather than the correctness of the EOS. The source-density at the EDM-PNM edge is $3.6883\text{x}10^{14}$ (MKS) and $1.3038\text{x}10^{17}$ (MKS) at the PNM-NDM edge. The figures of Appendix H give rise to summer-time observations. All CCNS cinders have all three layers. All CCBO objects that are heavier than 10^5 solar have only one layer (EDM). All CCBO objects lighter that roughly 30000 solar have all three layers and the remainder have two layers (EDM and PNM).

F. Gravitational lensing

The path of photons through an NG gravitational field containing a source is an important subject today. This discussion will be limited to static central fields of all strengths—an excellent approximation for canisters and ellipsoidal galaxies.

The necessary equations are derived from the Hamilton-Jacobi procedure outlined in Eq. (6.1). One simply takes the limit where the mass of the orbiting object goes to zero. The essential difference between NG and GR is that *a photon can never be trapped within a gravitational well*. A photon can be created at the surface of a source, and it will *always* trace a path that will end up at infinite radius. A photon can come from infinite radius and trace a path that leads it to be absorbed by the surface of the source. A photon can come from infinite radius and trace a path that never intersects with the surface of the source and returns to infinite radius. All three possibilities have a single common identifier, the impact parameter of scattering theory.

The orbit equation for a photon is obtained from Eq. (6.3) by setting $m = 0$,

$$\begin{aligned} &Q(V) = 1 + H(V), \\ &dr / d\phi = \pm r^2 Q(-U)^{-1/2} [Q(V)^{-1} (E^2 / c^2 A^2) - r^{-2}]^{1/2}, \\ &(E^2 / c^2 A^2)_{m=0} = R_{impact}{}^{-2}. \end{aligned} \tag{6.16}$$

The conserved angular momentum (A) of the photon (relative to the origin) is $A = R_{impact} E / c$, where $E = h\nu(\infty)$. The impact parameter is given by the closest distance from the origin of the vector momentum of the photon at infinity extended as a straight line to the vicinity of the origin. There is a turning point (closest approach to the origin),

$$R_{TP} Q(V(R_{TP}))^{-1/2} = R_{impact}. \tag{6.17}$$

There are two categories of interest. The first is for local opaque sources surrounded by a vacuum (stars, NSs, and BOs). In this case, orbits of interest have $U = V = -b / r$, where $b = 2GM_{source} c^{-2}$. For stars, the potential is weak, and Eq. (6.14) yields Eq. (E.7) and the GR result. For a neutron star, the field is strong with more complex optics. For a boundary object, the field is even stronger, and the obits can cross the boundary with even more complex optics. The second category is for vast weak fields (galaxies and canisters). The most interesting problem is the optical characteristics of a canister.

The primary object of study for *category one* is the MBO at the center of our galaxy, where the mass is $4.1\text{x}10^6$ solar masses, $b = 1.2109\text{x}10^7$ km, and $R_{source} = 1.3767\text{x}10^5$ km. The numerical values that follow are based on these three source constants and Eq. (6.13). One can simplify Eq. (6.14) for photon orbits *that do not intersect the source* for this case,

$$\begin{aligned} &dV / d\phi = \pm Q(-V)^{-1/2}[Q(V)^{-1}\xi^2 - V^2]^{1/2}, \\ &V = -b / r, \\ &\xi = b / R_{impact}\ . \end{aligned} \tag{6.18}$$

A (non-intersecting) photon can cross the boundary but cannot be trapped within. All solutions of Eq, (6.16) start and end with $r = \infty$ ($V = 0$), and the orbit lies in a plane defined by the origin and the two locations at $r = \infty$. The only observable is the angle of deflection ($\Delta\phi_D$), which is given by $\mathbf{n}_{in} \cdot \mathbf{n}_{out} = \cos(\Delta\phi_D)$. The unit vectors correspond to the direction of motion of the photon at infinity inbound and outbound. A numerical solution of Eq. (6.16) starts at the turning point ($V = V_{TP} < 0,\ \phi = \pi / 2$) and continues along the – branch ($dV > 0,\ d\phi < 0$) until ($V = 0,\ \phi = \phi_{end} < 0$). There is a discontinuity in $dV / d\phi$ at $V = -1$, so it is necessary to break the process into two portions using $Q_<$ for the inner part and $Q_>$ for the outer. The orbit is symmetric about the turning point, so only the outbound part needs to be calculated. For large R_{impact} (weak field), $\Delta\phi_D$ is small and positive—the inbound photon is bending toward the source. For the photon to avoid intersecting the source, the turning point must be $V_{TP} > -87.9556$. Note that $\xi^2 = V_{TP}{}^2 Q(V_{TP})$, and the boundary is assumed to have infinitesimal thickness.

There are three zones for solutions of Eq. (6.16),

$$\begin{aligned} &\text{external}\ \ \xi < 0.56979 \text{ and } V_{TP} > -1, \\ &\text{bounce}\ \ 0.56979 < \xi < 0.97468 \text{ and } V_{TP} = -1, \\ &\text{crossing}\ \ 0.97468 < \xi \text{ and } -87.9556 < V_{TP} < -1.6734. \end{aligned} \tag{6.19}$$

The external zone is familiar—small positive deflections. The bounce is new. Bounce photons have too much angular momentum to penetrate the boundary, so they bounce off it. Bounce calculations should use $Q_>(V)$.

The crossing zone is also new. Inbound (crossing) photons have small enough angular momentum to cross the boundary. They spiral inward toward the turning point, then spiral outward and recross the boundary outbound toward infinity. The spiral nature of the inner photons can cause $\Delta\phi_D > 2\pi$ and so require the observed deflection to be $\text{mod}_{2\pi}(\Delta\phi_D)$. $\Delta\phi_D$ is a single-valued function of R_{impact} for crossing photons. As R_{impact} decreases, $\Delta\phi_D$ increases steeply—there are shrinking slices of R_{impact} within which $0 \le \text{mod}_{2\pi}(\Delta\phi_D) < 2\pi$. There are 1025 slices for our MBO. Fig. 3 shows the first three slices.

It should be clear that photons from a distant star occulted by our MBO would have negligible probability of ending up in a telescope since they can be moving in any direction—invisible star. The apparent motion of a star moving toward occultation with our MBO would be a direct

observation of the strong field limit of NG (or GR). All other possibilities have *b* too small or the MBO is too distant. Unfortunately, an infrared (2.2 micron) interferometer with a base of order 100 km would be required for accurate measurements of this best case!

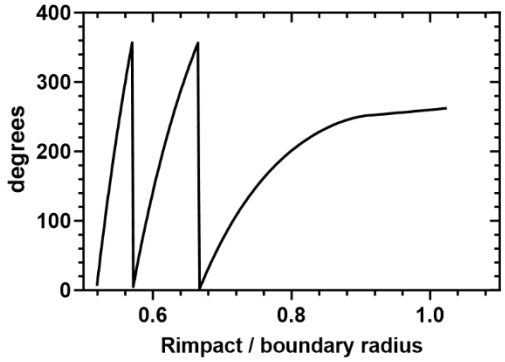

Figure 3. Degree of spiraling of a photon that crossed the boundary of our MBO (then exited) versus impact parameter.

The second category (canister lensing) is developed in part of Appendix K. A solution of Eq. (K.12) gives the photon deflection angle (radians) as a function of impact parameter (million light-years) for a given MDGO. The geometry of a photon path through a canister and the impact parameter is explained as well.

Fig. 4 illustrates an example deflection profile for an MDGO having $M = 10^{14}$ solar within a radius (R_E) of 2 million light-years. R_{impact} is given in million light-years and θ_D in radians.

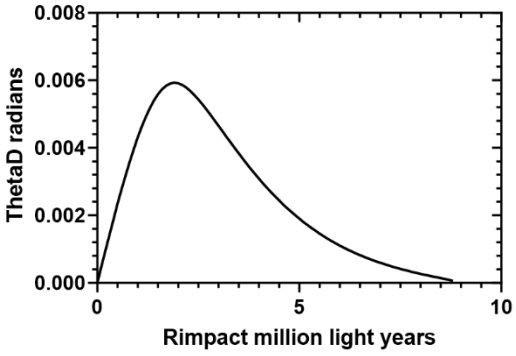

Figure 4. The deflection of a photon that passed through the example canister defined above.

The optical properties of a canister (isolated and containing a single MDGO) are completely determined by the function θ_D. The resulting observations can be complex. A simple example will illustrate an observation. Suppose that a camera is aimed at the center of the canister of Fig. 5 which is located at a distance F_{camera} (million light-years) from the camera. Suppose that there is a point photon-source (radiating uniformly in all directions) located on a line joining the canister-

center and the camera-lens at a distance of F_{source} (same units) from the canister-center (opposite to the camera). The only photons that can arrive at the camera lens must bend through a specific angle,

$$\begin{aligned} R_{impact} &= F_{source} \sin\alpha, \\ R_{impact} &= F_{camera} \sin\psi, \\ \alpha + \psi &= \theta_D(R_{impact}). \end{aligned} \tag{6.20}$$

Due to the cylindrical symmetry of this arrangement, the image of the source on a photograph would be a circle with a radius corresponding to ψ. A more realistic source would have size, shape, and a spectrum. The image would be an annular ring with average radius ψ.

Fig. 5 shows the annular radius in radians versus $\log_{10}(F_{source})$ when F_{camera} is 700 million light-years (for this example canister). Each portion of the annulus would have the same spectral characteristics—a smeared-out image of a single object. In general, F_{source} and F_{camera} can be established through the cosmological red shift of the source and canister galaxies. The size and the location of the center of the canister MDGO can be determined by soft-Xray photography. Thus, a knowledge of ψ leads to a determination of the mass of the container for this type of arrangement.

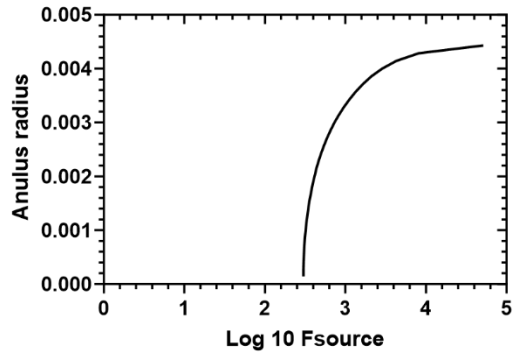

Figure 5. The radius of the anulus image in radians versus log 10 of F_{source} defined above in an example.

The camera image is far more complex when the source is not in line with the canister and camera. As the angle of the source increases, the annular ring breaks up into a diminishing number of displaced partial segments. These blobs can be identified as images of the same object because they will have the same spectrum. Furthermore, the path-distance of the photons for each image will be slightly different (but calculable). In that case, there will be an arrival time difference of observable events between images of the same object, thus leading to a knowledge of the distance of the source that is independent of cosmological red shift. It should be clear that using NG to study canisters and lensing will lead to a more precise ladder of distance versus red shift, mass distribution of canisters, and the universal constants of Eq. (5.10).

G. Growth of a massive boundary object during summer

The formation and growth of a massive boundary object (MBO) is yet another NCNG topic that is extremely complex (beyond the scope of this document), but I can outline an evolution model. I will focus on the MW MBO—the best-known object.

NCNG requires that there will be no relic MBOs in any galaxy at the end of any winter (when local gravity is turned on). Otherwise, the universe could become filled with MBO debris.

Section VII(E) deals with the fate of a MBO at the end of any summer in any galaxy (when local gravity is turned off). NCNG requires that a MBO must disintegrate in such a manner that the debris can be efficiently recycled during the following winter—no buildup of MBO debris.

The evolution model must start (local gravity turned on) with no MBO, newly borne Kelvin contraction stars, and a stable (small) amount of relic iron debris, The evolution ends (local gravity turned off) when a MBO begins to disintegrate (in the right manner). The growth model will use information from the following sections: VI(C), VI(F), VII(B), Appendix H, and Appendix M.

The early evolution model will have an *important event*. Fusion will be turned on about one million years after the start—see VII(B). Some of the newly borne Kelvin contraction stars will be heavy and hot enough to ignite and form a stellar cinder. The newly created CCBO that is closest to the galaxy center is most likely to be the seed that will grow to become the MW MBO today (about 21 billion years after the start).

How does a boundary object grow? The MW MBO would have to gain *an average* of one solar mass per 5100 years—cross the MW MBO boundary. This robust diet can only be sustained by a bombardment of material objects (projectiles) at the growing MW MBO *boundary* (target). Thus, one needs to understand many applicable topics—a scattering theory problem.

What are the projectiles? The environment near the center of MW consists of stars, stellar cinders, gas and gravitational fields. Gas as a projectile can be neglected since gas crossing the target boundary is an inefficient equilibrium problem (Appendix M). Stars are the largest projectiles and easily observed. There is a zoo of stellar cinders: WDs, CCNSs, CCBOs, and even fledging MBOs. Cinder projectiles are much smaller than stars and not observable (a major problem). Gravitational fields are important but difficult to calculate, and they change as the MW MBO grows.

What happens when a projectile collides with the target boundary? There is no simple answer to this important question. The fate of the projectile depends strongly on the type and velocity of projectile and the mass of the target. None of the alternatives have been studied. Some examples will illustrate the problem. The target boundary is safely assumed to be stationary at the center of MW. The radius of the target boundary is $R_{MBO} = 2.9533\ M_{MBO} / M_{\odot}$ km. Suppose the projectile is the sun moving at 1200 km/s—a typical star near the center of MW today. Furthermore, assume that the projectile is aimed at the center of the target.

The first example has 1000 solar target mass (5906 km diameter) in the early red summer. The diameter of the projectile is 1.39 million km, and the target is within the projectile for 19.3 minutes. Although the gravitational force of the target is large compared to that of the projectile, the force is an impulse that reverses as the center of the projectile crosses the center of the target. It should be clear that the collision will have negligible effect on the projectile, and the target will be left with a (small) fraction of the projectile mass in an accretion halo on the target boundary. The mass of the accretion halo, and the amount of that mass that stays inside the target boundary needs to be calculated—extremely difficult.

The second example has 235600 solar target mass in later summer. Then the target is the same size as the projectile, and the projectile is completely destroyed. The target will be left with a

(larger) fraction of the projectile mass in an accretion halo, and the rest of the projectile mass will be gas released into the environment (where it can contribute to the creation of new projectiles). This calculation is much more difficult.

When the projectile is a cinder, the result is orders of magnitude more complex than a star because one must calculate the effects of the collision on the projectile source. For example, a CCBO projectile can cross the target boundary in a special manner because the target and projectile boundaries can merge, and the projectile will not actually cross a boundary. However, the source of the CCBO will be subject to severe tidal forces and become distorted or even dispersed. If that is not difficult enough, the projectile can be in an orbit that will take the (wrecked) projectile back outside of the target boundary! This topic requires a huge amount of study.

What happens to the source of the target after a collision? This topic requires the thermodynamics of the target source and the projectiles that formed it—also requiring a huge amount of study. The source is all the matter that is trapped inside the boundary. The source is layered by phase. Innermost is the solid phase (EDM), surrounded by an ocean (liquid phase). Outermost is an atmosphere (gas phase). The EDM ball has most of the source mass.

EDM is well studied and has important features: the EOS is independent of temperature, the formative nuclides are largely retained, and the heat conductivity is dominated by the temperature and density of the electron gas. The layers are in thermodynamic equilibrium. I believe that the EDM nuclides are also organized so that the nuclide mass decreases as the radius increases. When a projectile permanently crosses the target boundary, the equilibrium is briefly unbalanced.

There will only be a few formative nuclides: iron, carbon, oxygen, helium, and hydrogen. A collision with a star will provide hydrogen and helium. A collision with a WD will most likely provide carbon and oxygen. A collision with a CCNS or CCBO will provide iron. A collision with a MBO can provide all five.

The formative nuclides will slowly diffuse through the EDM toward the center until they reach an equilibrium zone. The zones would be an iron zone at the center (then moving outward), an oxygen zone, a carbon zone, a helium zone, and a hydrogen zone. Each zone would have a small flux of heavier nuclides moving inward.

The heat conductivity of each zone would be proportional to the mass of the zone nuclides and decline as the temperature declines. The temperature at the center (iron zone) would be extremely high (burn temperature of silicon) and would decline to a low value where the hydrogen EDM meets the liquid phase. Modest temperature hydrogen EDM is an excellent insulator.

The high temperature at the center of the iron zone is because the original MBO to be CCBO was created in the environment where the temperature would be the burn temperature of the last available fuel element (silicon)—about $3\text{x}10^{9}\ ^{\odot}\text{k}$. The rapid early growth of this cinder would cover the center with layers of EMD that would act as insulation. The center would not have an opportunity to cool significantly.

Now, one comes upon the joker in this deck. It is summer and fusion is turned on. *Fusion can occur in any zone except the iron zone*. The topic of fusion within layered EDM needs to be developed, but I believe that the heat energy released into the EDM ($E(r)$) will take the familiar form, $\log E(r) = \alpha(r, T(r)) \log T(r)$, where r is the distance from the center of the EMD ball. NCNG requires that the thermal radiation from the MW MBO today (and at the end of summer) to be small enough to be difficult to observe. That would require $T(r)$ to be small enough through all zones except the iron zone.

The answers to these questions will form the required model for growth after a huge effort of study. Furthermore, the resulting model will set the initial conditions for section VII(E).

VII. PHYSICS IN EACH WINTER PER CYCLE

The familiar laws of physics that govern both red and blue summer evolution have processes that go in only one direction. Nuclear fusion (nucleosynthesis) steadily changes the universal mixture of nuclides, Kelvin contraction causes canister MDGOs to steadily shrink, etc. To have a viable (eternal) cyclic cosmology, it is necessary to have *unfamiliar* laws of physics during each winter that *undo some of the results of evolution* during the other seasons.

The most important winter task is to return the universal mixture of nuclides (averaged over suitably large volumes) to the same initial state at the beginning of each red and blue spring—reverse nucleosynthesis (RN). This section will examine various topics that will define the difference between winter and summer physics.

A. Particle census

As a prelude to a discussion of RN, it is useful to consider a simple model for the most important material constituents of the universe (proton, neutron, electron, and the electron-flavor neutrino and antineutrino). Furthermore, the model will consider only two weak-interaction red and blue summer processes:

$$\begin{aligned} p^+ &\to n^0 + e^+ + \nu(e) \quad \text{(fusion)}, \\ n^0 &\to p^+ + e^- + \overline{\nu}(e) \quad \text{(beta decay)}. \end{aligned} \tag{7.1}$$

Next, define mean densities (number of particles per unit volume averaged over sufficiently large volumes of space) which will depend only on time. Eq. (7.1) and electrical charge conservation require the following constraints:

$$\begin{aligned} N_p(\tau) + N_n(\tau) &= N_{RN}, \\ N_n(\tau) - N_\nu(\tau) + N_{\overline{\nu}}(\tau) &= \vartheta_{RN} N_{RN}, \\ N_p(\tau) &= N_e(\tau). \end{aligned} \tag{7.2}$$

For NCNG, N_{RN} and ϑ_{RN} are *universal constants*. Let $\tau = 0$ correspond to the start of the red or blue spring transition. I have chosen $N_\nu(0)$ and $N_{\overline{\nu}}(0)$ to be very small. It is thought that our early universe (start of red summer) consisted of about seven protons per neutron, in which case $\vartheta_{RN} = 0.125$. It is also thought that $N_{RN} = 0.25/\mathrm{m}^3$ based on LCDM (now suspect). These values represent the desired initial state of each half-cycle. During summers $dN_\nu(\tau)/d\tau > 0$ and $dN_{\overline{\nu}}(\tau)/d\tau > 0$. Winter requires $dN_\nu(\tau)/d\tau < 0$ and $dN_{\overline{\nu}}(\tau)/d\tau < 0$.

B. Winter changes

The task of returning the winter universe to its initial state does not require changing the winter strong and electromagnetic forces from their summer version—these forces are independent of season. Only the weak interactions and gravitation will change.

In winter, fusion must be stopped. One way to stop fusion is the elimination of high temperatures and pressures needed—turn off local gravity. Another way to stop the processes of Eq. (7.1) is to favor a reverse,

$$\begin{aligned} \bar{\nu}(e) + p^{+} &\rightarrow n^{0} + e^{+}, \\ \nu(e) + n^{0} &\rightarrow p^{+} + e^{-}. \end{aligned} \tag{7.3}$$

Eq. (7.3) requires a winter change in the weak interactions.

I believe the following changes in the winter version of the weak interactions will be sufficient: (1) The PMNS matrix (U_{FM}) will be diagonalized. (2) The electron-flavor neutrino mass will be increased. (3) The W boson mass will be decreased. (4) The weak coupling-constant, g_W, (W-fermion vertex) will be increased. (5) The Z boson coupling-constant and mass will retain their summer values. These changes are summarized:

$$\begin{aligned} U_{FM} &= U_{FM}^{S}\left(1-\mathrm{K}_W(\phi_{ep})\right) + \delta_{FM}\,\mathrm{K}_W(\phi_{ep}), \\ m_{\nu e} &= m_{\nu e}^{S}\left(1-\mathrm{K}_W(\phi_{ep})\right) + m_{\nu e}^{W}\,\mathrm{K}_W(\phi_{ep}), \\ m_W &= m_W^{S}\left(1-\mathrm{K}_W(\phi_{ep})\right) + m_W^{W}\,\mathrm{K}_W(\phi_{ep}), \\ m_Z &= m_Z^{S}, \\ g_W &= g_W^{S}\left(1-\mathrm{K}_W(\phi_{ep})\right) + g_W^{W}\,\mathrm{K}_W(\phi_{ep}), \\ g_Z &= g_Z^{S}, \\ \mathrm{K}_W(\phi_{ep}) &= 0.5\left(1-\tanh\{\Gamma_W[\mathrm{E}(\phi_{ep})-\mathrm{E}_W]\}\right), \end{aligned} \tag{7.4}$$

where Γ_W and E_W are universal constants (tabulated in Appendix Z) that govern when and how rapidly the weak interaction values change between winter and summer.

It is important to understand that Eq. (7.4) represents a list of *what is necessary for* RN, *not how the goal is achieved*. The weak interactions are radically different in winter compared to the existing theory for summer. An entire reformulation of the weak interactions is necessary,

The S superscript is the summer value and W superscript is for winter. The winter electron-flavor neutrino mass is chosen to be $m_{\nu e}^{W} = 30$ Mev. The tiny $m_{\nu e}^{S}$ will be neglected in what follows. The winter W boson mass (m_W^{W}) and the winter coupling-constant (g_W^{W}) are chosen so that the universal neutron conversion processes of Eq. (7.3) can proceed at a rate sufficient to return the universe to the desired initial state during the physical time allotted to winter. The rationale for these choices will be clarified below.

Note that there are 2856 nuclides ($\leq$ Pu245) that have been studied theoretically or observed by experiment, of which 273 are stable against all decay mechanisms in all seasons. All 2856 can be in play during winter. The attenuation process must leave significant amounts of only four nuclides

(H1, H2, He3, He4) at the end of winter and only infinitesimal amounts of the other nuclides—the desired initial state of the universe.

I will explain choice (1). The summer universe is filled with electron-flavor neutrinos, but the second and third generation neutrinos are rare. During winter, a $\nu(e)$ inflight cannot initiate the attenuating process of Eq. (7.3) *all the time* if U_{FM} is not diagonal, thus requiring a longer winter. (2): The choice of 30 Mev makes $\nu(e)$ heavy enough so that *none of the 2856 nuclides can undergo either positron decay or beta decay during winter*—only the processes of Eq. (7.3) can occur: (3) and (4). These changes make the cross section for the processes that can occur many orders of magnitude larger in winter—shorter physical time to arrive at the initial state. (5): The Z interaction causes scattering events that drain needed energy from any $\nu(e)$ inflight during winter—keep the Z cross section weakly small.

I have chosen the following gravitational changes in winter including five new universal constants ($Q_{GC}(q,1)$) tabulated in Appendix Z:

$$\begin{aligned}
&Q_{GC}[1,\mathrm{E}(\phi_{ep})] = [1-\mathrm{K}_G(\phi_{ep})] + \mathrm{K}_G(\phi_{ep})Q_{GC}(1,1),\\
&Q_{GC}[2,\mathrm{E}(\phi_{ep})] = [1-\mathrm{K}_G(\phi_{ep})] + \mathrm{K}_G(\phi_{ep})Q_{GC}(2,1),\\
&Q_{GC}[3,\mathrm{E}(\phi_{ep})] = [1-\mathrm{K}_G(\phi_{ep})] + \mathrm{K}_G(\phi_{ep})Q_{GC}(3,1),\\
&Q_{GC}[4,\mathrm{E}(\phi_{ep})] = [1-\mathrm{K}_G(\phi_{ep})] + \mathrm{K}_G(\phi_{ep})Q_{GC}(4,1),\\
&Q_{GC}[5,\mathrm{E}(\phi_{ep})] = [1-\mathrm{K}_G(\phi_{ep})] + \mathrm{K}_G(\phi_{ep})Q_{GC}(5,1),\\
&\mathrm{K}_G(\phi_{ep}) = 0.5\left(1-\tanh\{\Gamma_G[\mathrm{E}(\phi_{ep})-\mathrm{E}_G]\}\right),
\end{aligned} \tag{7.5}$$

where $\mathrm{E}(\phi_{ep})$ is developed leading to Eq. (2.17), Note that I have chosen to provide the possibility of a slightly different time and rate for gravity changes versus the weak interactions.

The timing and order of Eq. (7.4) and Eq. (7.5) have been chosen to *marginalize the effects of the bubble era*. In both cases, the value of constants of interest are nearly the same on both sides of the bubble wall.

C. Reverse nucleosynthesis

RN is extremely complex—so much so that a simplified model is necessary. During winter, the stable nuclides and free neutrons present at the start of winter must be converted by the end of winter into H1, He4, relic amounts of H2 and He3, and very tiny amounts of heavier nuclides. Furthermore, electron flavor neutrinos, and antineutrinos must be attenuated into relic amounts. The heavier nuclides are eliminated at the beginning of winter. The remainder of winter is devoted to converting He4 into H1.

The strong interactions will be unchanged in winter, so nuclear physics and the properties of the nuclides will be important. A good source is the website for the Brookhaven National Nuclear Data Center (NNDC), which has an interactive chart of all 2856 studied nuclides. The details of RN will be outlined in the following sub sections.

1. Attenuation model

The rate of attenuation of nuclear species in winter requires knowledge of the neutrino and antineutrino densities (#/cubic meter), their energy spectrums, and the densities of each of the 2856 nuclides that could exist during the process everywhere in space. This requirement overwhelms us from the start. Only the crudest estimates of these factors are available at present, and one has no idea about their values 42 billion years in the future when winter will begin. Also needed are 2856 neutrino-initiated reaction cross sections, of which only a few have been calculated (for summer). A precise evolution of the attenuation process will require super-computer computations and many years of research. Simplifying assumptions are needed now.

First, neglect antineutrinos and free neutrons. Those densities are likely small compared to others, and their neglect will halve the number of nuclides in play. The determination of relic H2 will be lost in this approximation. Next, construct an initial abundance of stable nuclei for the start of winter, which mimics present day estimates but with a bias toward more neutrons. Then neglect many of the smaller entries. Figure 6 illustrates the start of winter abundance that will be used. The model will have 54 stable species instead of 273, and 406 nuclides in play. Furthermore, all these model nuclides will be assumed to reside within canisters.

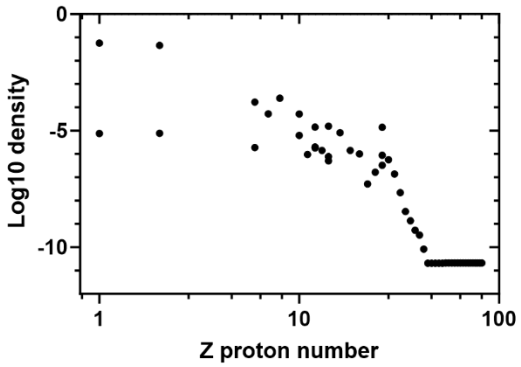

Figure 6. Log10 of the number of nuclides per cubic meter versus proton number, Z, at the start of winter.

It is important that attenuation is not influenced significantly by the random distribution of canisters in space. That result can be obtained by having the attenuation process take place over a sufficiently long physical time. In that case, even the slowest heavy neutrino can travel through a collection of neutron rich canisters. I have chosen 300 billion years for each winter per cycle for this model. A major simplification results—the densities will only depend on physical time.

A winter neutrino will travel at the slowest velocity outside of canisters and then speed up considerably in transit across an intercepted canister. All the neutron rich canister mass is concentrated within or near the MDGO at the center of the canister (a radius of roughly 2 million light-years). The transiting neutrino will follow an orbit within the canister that has a nearest approach to the center. Attenuation may only occur when the nearest approach is within the central MDGO—a specific range of impact parameters. Even then, attenuation may not occur. If attenuation does not occur the neutrino will exit the canister at a deflected angle without loss of kinetic energy. Thus, the path of a winter neutrino is a random walk through a density of randomly situated canisters until it is absorbed. I believe that the random walk justifies the attenuation model of uniform nuclide density, which then implies uniform winter neutrino flux.

The universal constants of Eq. (7.2) can be used, e.g., the initial neutron density associated with Figure 6 is $0.385N_{RN}$, *and the initial neutrino density for this model must be* $0.260N_{RN}$. The proton/neutron ratio of Figure 6 is 1.597 (end of red or blue fall) compared to 7.0 (start of red or blue spring).

2. Neutrino model

The electron-flavor neutrino spectral-densities can be approximated by a series of delta functions as in the following profile:

$$n_\nu(E_\nu,\tau) = N_{RN}\sum_{k=1}^{K} \mathrm{P}_k(\tau)\,\delta(E_\nu - E_{\nu k}),$$
$$N_\nu(\tau) = N_{RN}\sum_{k=1}^{K} \mathrm{P}_k(\tau), \qquad (7.6)$$

where $E_{\nu k} = k\Delta E_\nu$, $\Delta E_\nu = (20.0/K)$ Mev in summer, and N_{RN} is the universal constant of Eq. (7.2). I have assumed that a neutrino in-flight during summer will have the same momentum in winter—the mass change will alter only the energy. Therefore, the winter values of neutrino energy will be $E_{\nu k} = [(k\Delta E_\nu)^2 + (m_{\nu e}^W c^2)^2]^{1/2}$. $\mathrm{P}_k(\tau)$ is dimensionless and continuous across red or blue spring or fall transitions. The start of winter corresponds to $\tau = 0$, and $N_\nu(0)/N_{RN} = 0.260$ as described above. A suitable model would have $K = 500$, and $\mathrm{P}_k(0)$ would rise to a peak at $k = 10$, (approximating the pp branch for solar neutrinos) followed by an exponential decline $\propto \exp(-\chi k)$ thereafter. The attenuation model uses $\chi = 0.018$, and Figure 7 shows $\log_{10}\mathrm{P}_k(\tau)$ at the start and end of winter. The higher energy neutrinos are exhausted to a much greater extent due to the energy dependence of the reaction cross section for He4.

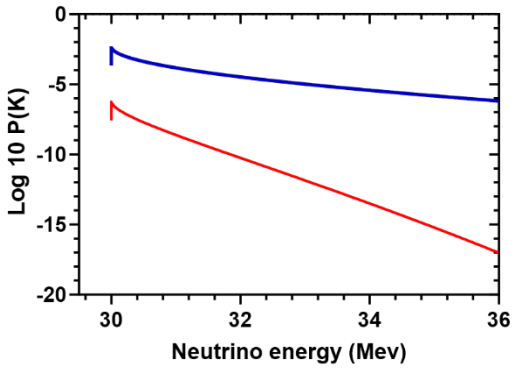

Figure 7. Log10 of the dimensionless neutrino spectral density defined in Eq. (7.6) versus the total winter neutrino energy. The blue curve is at the start of winter and red is at the end of winter.

3. Neutrino initiated processes

A general electron-flavor neutrino-initiated process (NIP) can be represented as follows:

$$\begin{aligned} &\nu(e)+[A,Z]_0 \rightarrow \\ &[A-a,Z-z+1]_j+\{a,z\}+e^- \end{aligned} \tag{7.7}$$

where [..] are nuclides, the subscript 0 is the ground state, and $j \geq 1$ would be an exited state. The ejected state {..} in what follows can be nothing ($a = z = 0$), one or more protons, or He4 (alpha particle). The high energy of the winter neutrino makes the probability of the electron in Eq. (7.7) being captured negligible.

The reaction cross section for Eq. (7.7) is important for RN, but it has only been calculated for a few NIPs [11], otherwise the calculations are extremely difficult. There will be an important NIP, $\nu(e) + \text{He4} \rightarrow \text{He3} + p^+ + e^-$, that illustrates the problem. This NIP is the inverse of the theoretical *hep* process, one branch of the proton cycle in stars. Two decades of theoretical work were required to get a convergent *estimate* for the *hep* process [12], but this research is not useful for RN.

There is a subset of Eq. (7.7) that can be calculated with reasonable accuracy, the case where {} = 0. If the positron decay half-life in summer of the final state is known—the inverse of the NIP, $[A,Z+1]_j \rightarrow [A,Z]_0 + e^+ + \nu_e$ —then the corresponding NIP ($\nu_e + [A,Z]_0 \rightarrow [A,Z+1]_j + e^-$) is known. The underlying assumption is that the nuclear matrix elements are independent of energy and are the same for NIP and inverse NIP, and that *the probabilities and energy dependence of transitions are dominated by the density of final states*. See the first half of Appendix I for more details about NIPs.

4. General attenuation

Dimensionless nuclide densities can be defined, $Y_j(\tau) = N(j,\tau) / N_{RN}$, where *j* corresponds to an entry in a table of the 2856 nuclides having positive binding energy. There is a specific atomic number, A_j, and proton number, Z_j, for each entry. The second half of Appendix I has details about the physical time evolution of the $Y_j(\tau)$ set. The figures below are based on the following requirements,

$$\begin{aligned} &N_\nu(\text{winter-end}) / N_\nu(\text{winter-start}) = 10^{-4}, \\ &\left(g_W^W m_W^S / g_W^S m_W^W\right) = 4.3404\text{x}10^5. \end{aligned} \tag{7.8}$$

Figure 8 shows the number of nuclides having $Y > 10^{-20}$ as a function of time. This number quickly grows to 404 as nuclides start moving down their attenuation chains, but they must funnel through an ever-smaller set of recipient nuclides. All must pass through C10, and then after 819 million years only H1, He3, and He4 are left along with an extremely tiny amount of relic nuclides heavier than He4. That phase represents only 0.27% of winter.

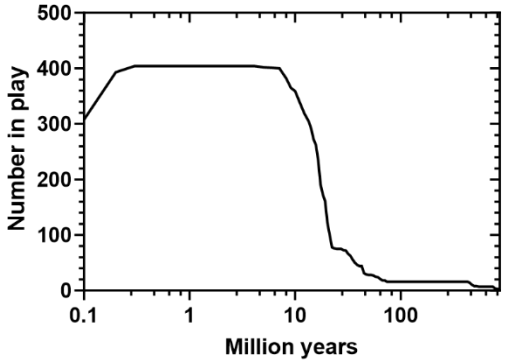

Figure 8. Number of nuclides undergoing attenuation versus time

Figure 9 shows details for three important nuclides—C10, C12, and O16. C12 and O16 are stable and plentiful at the start of winter but are eliminated very quickly. C10 has a smaller reaction cross section than C12, and it serves as the last storehouse for heavier nuclides before they are converted to He4.

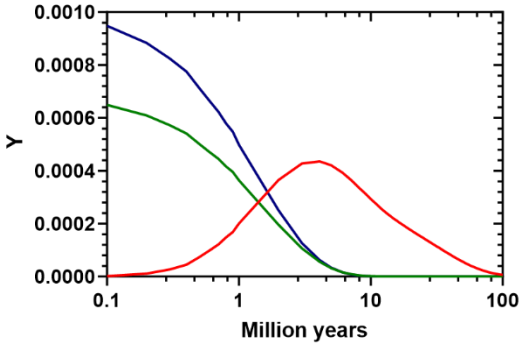

Figure 9. Dimensionless density functions, Y (defined before Eq. (I.5)), for three nuclides versus time. C10 is the red curve, O16 is blue, and C12 is green.

Figure 10 shows the slow attenuation of He4 and neutrinos over the entire winter. Throughout the later part of this period $Y(\mathrm{He3})/Y(\mathrm{He4}) = 6.07\times10^{-5}$. The relic density of He3 depends on the relative size of the reaction cross sections for both He3 and He4. For this model He4 was estimated and He3 was chosen to give the asymptotic ratio above. The actual ratio is poorly known, but it is thought to be of the order shown. The asymptotic density of He4 corresponds to a proton/neutron ratio of seven at the end of winter as required for this model.

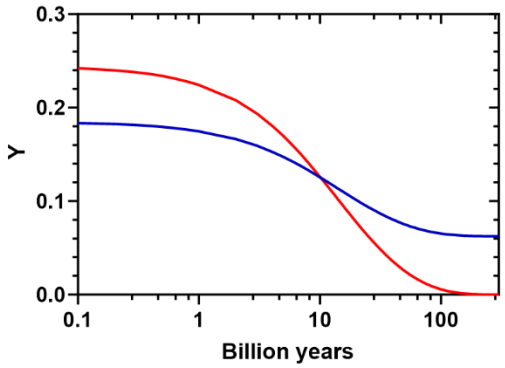

Figure 10. Dimensionless density functions, Y, for He4 (blue) and neutrinos (red) versus time.

Every aspect of reverse nucleosynthesis in this model is governed by the assumption that the reaction cross section for He4 is significantly smaller than those of the nuclides that have high neutrino-energy thresholds for their NIPs. The estimation process of Sec. VII(C3) bears out this assumption for those few nuclides that are well known.

D. Distribution of matter during winter

The model of subsection C above has been simplified by treating matter as being distributed uniformly in winter. That model served a useful purpose, how much time is required to return the universe to the desired early summer state? One has discovered that almost all of winter is used to convert helium into hydrogen—both widely distributed. However, some nuclides are distributed in a lumpy fashion during summer (and winter as well), e.g., iron. What is their fate during winter? Section VII (C.1) justifies using the average flux of winter neutrinos to study the fate of specific lumps of nuclides.

NCNG has a new sequestration of matter featuring canisters on the largest scale. A ghostly MDGO accounts for a significant portion of the canister mass. I have no clue what the average mass density is for the universe. The number I have used (Appendix Z) is unreliable (based on LCDM). Worse yet, the currently concordant universal abundance of nuclides is unreliable as well. In the next subsection, the fate of stars and stellar cinders will be studied. This subsection will study the winter fate of lumpy relics from summer (subject to the uncertainties of unreliable constants).

What are lumpy summer objects? They are planets, planetary cinders, asteroids, and small objects that I will call rocks. When a star dies, its planets can be gasified if close enough. If farther away, only the core of the planet may survive (planetary cinders). Asteroids seem to be big rock piles weakly held-together by local gravity in summer. Summer rocks are distantly associated with stars, but when the star dies, the rocks will eventually disperse. All these summer types will be distributed throughout inter-stellar space.

The second event in the fall transition is turning off local gravity. Any stellar systems created late in summer will disassemble after the transition, and their planets will disassemble and cool as well. Asteroids will disperse as rocks. An early winter galaxy will consist of a vast amount of gas, a sparse collection of large planetary core parts, and a vast collection of rocks, and dust (molecular

size rocks). The first event in the fall transition is changing the weak interactions—RN gets a slight head start before winter starts.

The fate of lumpy galactic constituents in winter is extremely complex. An example will clarify the process. Imagine an iron (Fe56) sphere of radius R_{LUMP} at the start of winter. The properties of metallic iron will hold the lump together despite the lack of gravitational binding. This lump will be bombarded by a uniform (very faint) flux of heavy neutrinos (ν_e) for billions of years—RN in progress. Each ν_e will initiate a NIP within the lump. The mean free path for the most common winter neutrino that collides with the iron ball immediately after the second transition is only 6 millimeters. Furthermore, the reaction of this winter neutrino will leave behind an Fe55 nuclide, a proton, and an energetic electron. The energetic electron will heat the locale and eventually join the proton to form a hydrogen atom in the locale. The incident neutrino can strike the ball surface from any angle, so the average penetration would be less than 6 millimeters. A scenario emerges.

The fate of a winter lump is determined by the NIPs generated in a thin zone at the surface of the lump. *The probability that a ν_e will be absorbed is a decreasing function of distance from the surface (depth)*. Thus, each lump will have a profile of nuclide constituents versus depth that is *time dependent*. The profile consists of nuclides that are on the attenuation chain for the material at that depth at the start of winter. The nuclide at the surface will move lower in the attenuation chain (toward C10) with time, whereas the nuclide at the depth of the zone remains unchanged. When the surface nuclide reaches a point where the surface lump structure will disassemble into gas and dust, *the surface will start moving inward*. That point (lower than or equal to A40) is inevitable since there are many lower nuclides that are gaseous. Furthermore, hydrogen trapped in the lump would weaken the structural integrity of the lump material.

The fate of lumps clearly depends on size. Planetary core parts will survive winter almost intact. Small rocks will be converted to gas and dust. Larger rocks will shrink but survive winter depending on their initial size and composition.

Rocks play an important role in NCNG. The MDGO in every canister generates Xray radiation in all seasons (Appendix F). The energy of the Xray photons is of order 1000 ev and they form a universal Xray background. The only way a background Xray photon can be destroyed is by being stopped in matter of sufficient thickness. There must be an equilibrium between the endless creation of canister Xray photons and the endless destruction of these photons by matter. The luminosity of the background is faint, so the destruction must use matter efficiently. A large lump is overkill. A tiny lump will not stop the Xray. *A rock of sufficient size is best, and there must be a significant numerical density of them throughout the universe*.

E. The fate of boundary and stellar-cinder objects in early winter

All galactic stars are created during the period extending from turning on local gravity (at the end of winter) to turning off local gravity (at the beginning of winter). During that period a star can die and create three types of stellar cinders (WD, CCNS, CCBO) and gas. That topic was discussed in section VI(E). At the beginning of that duration, a single CCBO near the galactic center will grow during the duration to become a MBO at the center of the galaxy. That topic was discussed in section VI(G). During the summer, light-weight lumpy objects can form, and their fate during winter is discussed in section VII(D).

In this subsection, the fate of major objects existing when local gravity is turned off will be discussed (star, CCBO, CCNS, WD, and MBO). Recall that *fusion is turned off just before the end of the duration*.

Any star that exists at the off local gravity transition will disperse into a diffuse gas in winter—star evaporates. In what follows, evaporation means that the constituents of the object are dispersed sufficiently so that the constituent matter is efficiently recycled by RN into hydrogen during winter. *The information about the object does not survive winter*.

A WD cinder consists of electron degenerate matter (EDM) which *retains the identity of the constituent elements that formed it* since the nuclides remain intact. The off local gravity transition for a WD will disperse diffuse constituent gases (largely carbon and oxygen)—WD evaporates.

A CCNS is a mixture of EDM (iron) and denser neutron-soup. The mixture has EDM (iron) on the surface, soup at the center, and a combination between. The soup has lost the identity of the matter that formed it. The local gravity transition for a CCNS will disperse into iron and a diffuse neutron gas. During winter, neutrons are efficiently recycled into hydrogen. The mixture of iron and neutrons depends on the mass of the CCNS. Heavier objects will have less iron and this iron will likely be diffuse. Light objects will have fewer neutrons, and the iron could be somewhat chunky rather than diffuse. In either case, little iron will survive RN during the winter, so the object-information is lost—CCNS evaporates.

The source of a *recently created* CCBO is similar to a CCNS in composition— EDM on the surface, neutron soup at the center, and a combination between. However, the mixture is the reverse of the CCNS object. The lightest CCBO has the least iron, and the iron content increases with mass. The boundary disappears at the end of the off local gravity transition, so the fate of a CCBO is much the same as a CCNS—CCBO evaporates.

The fate of a MBO is extremely complex. Section VI(G) describes the MW MBO composition at the end of summer. I will use that model as a guide to the fate of MBOs in general in this section.

The off local gravity transition lasts about a thousand years—practically instantaneous. The boundary and the hydrostatic pressure that holds the MBO source together will vanish at once, but the radiation pressure will not. The radiation pressure is only significant in the iron zone. The reduced pressure cannot support EDM material.

Suddenly, the MBO source (several hundred thousand km in radius) becomes a ball of hot static material. The ball has two parts. The inner part is the iron zone which consists of an iron supercritical fluid. The outer part consists of all the other zones and phases. The outer part will eventually disperse into a gas that will be efficiently recycled by RN.

The evolution of this system can only be expansion and cooling. The expansion will be driven by iron zone radiation pressure until cooling favors thermodynamic expansion. The thermodynamic expansion will be adiabatic, and the work done will be the increase of kinetic energy of all the expanding material.

What will be the final state of the MBO in winter, and will it be efficiently recycled by RN? There is no problem for the layer gases (hydrogen, helium, oxygen, carbon) since they will eventually disperse completely into an ultra-diffuse state.

The fate of the iron zone material is important but not obvious. The pressure, density, and temperature (PDT) of the iron zone material will all decline toward zero during the expansion. However, the PDT *must not intersect a change of phase* during the expansion to a sufficiently diffuse final state (a very cold and very diffuse atomic-iron perfect gas). An intersection would lead to large blobs of solid iron in the final state (*not efficiently recycled*).

The expansion of the iron zone can be divided into three eras. The first era is the radiation expansion (RE), the second era is the thermodynamic supercritical expansion (TSE), and the final era is the thermodynamic gas expansion (TGE).

The RE era starts when local gravity is turned off and ends when the partial pressure of the radiation can be neglected relative to the partial pressure of the iron supercritical fluid (P_{ISF}), e.g., $P_{Rad} > 0.01 P_{ISF}$. The pressures follow:

$$\begin{aligned} P_{Rad} &= (4/3)\sigma c^{-1} T^4, \\ P_{ISF} &= \mathrm{f}(\rho_{ISF}, T), \end{aligned} \tag{7.9}$$

where $\sigma = 5.6686\,\mathrm{x}10^{-8}$ and T is the temperature (MKS and degree kelvin units). ρ_{ISF} is the MKS density of the iron supercritical fluid. For the RE and TSE eras, the properties and thermodynamics of iron supercritical fluid are unknown (the function f is not known). Even the iron critical pressure and density are not well established.

The TSE era starts when RE ends, and Eq. (7.9) represents an initial condition for TSE. The TSE era must end when the pressure (P_{iron}) is small enough so that the supercritical iron fluid is well approximated by a perfect atomic iron gas,

$$P_{iron}(\text{TSE end}) = \alpha P_{critical} \ , \tag{7.10}$$

where alpha is small, and it is thought that $P_{critical} = 8.750\,\mathrm{x}10^{8}$ mks $\pm 13\%$.

The TGE era starts when TSE ends. TGE ends at the final state, e.g., $T_{final} = 5\ ^{\circ}$ kelvin . During the TGE era the iron zone will undergo adiabatic expansion of a perfect monatomic gas. Eq. (7.10) provides a constraint on the initial condition,

$$k N_{TGS} T_{TGS} = \alpha P_{critical} \ . \tag{7.11}$$

The expansion relation, $N = N_{final}(T/T_{final})^{(\gamma-1)^{-1}}$ (where $\gamma = 1.67$), gives the final density as a function of the temperature at the beginning of the TGE era as follows,

$$N_{final} = \alpha P_{critcal} k^{-1} T_{final}{}^{-1} (T_{TGE}/T_{final})^{-2.4525}. \tag{7.12}$$

The resulting final density is best illustrated by a ratio ($\chi = N_{final}/N_{lab}$), where $N_{lab} = 8.476\,\mathrm{x}10^{28}$ meters^{-3} is the density of iron in my laboratory. If $\chi << 1$, then one should expect that the probability of a large lump of iron surviving winter (observable in the following summer) is negligible. As an example, if $\alpha = 0.01$, $T_{final} = 5\ ^{\circ}$, and $T_{TGE} = 10^{5}\ ^{\circ}$. Then $\chi = 2.85\,\mathrm{x}10^{-11}$.

The development of a MBO fate so far has served to establish a plausible initial temperature profile and a plausible distribution of nuclides and their thermodynamic state (supercritical fluids).

An actual calculation of the evolution would produce a specific value of χ for a specific model. However, the uncertain properties of the supercritical fluids prevent such a calculation.

Any type of debris from the expansion would eventually end up with a *substantial radial velocity*. Lacking any local gravity, the constituents of the expansion would move apart until their radial velocity is stopped. I believe that fact alone is sufficient to prevent the MBO debris forming any observable iron lumps that would survive winter.

VIII. SPECIAL TOPICS

There are two special topics that are important to GRLCDM, cosmic microwave background and gravitational waves. There are two special topics that are important to NCNG, stability and tests of validity.

A. Cosmic microwave background

There is cosmic microwave background (CMB) radiation in NC and anisotropies (CMBA) as well. The NC version of CMB and CMBA will be developed in this section. CMB radiation consists of relic photons that have traveled since the preceding winter. The observed CMB radiation today has a black body frequency distribution corresponding to $2.725\ ^{\circ}\mathrm{k}$. Today is $z=0$, where z is the NC cosmological redshift. The histories of Appendix C give z as a function of *A* (the apex field). One can discover that $z=0$ also when $A=1.00667$, very near the end of the preceding winter. Thus, the temperature today is $2.725\ ^{\circ}\mathrm{k}$ because the temperature was $2.725\ ^{\circ}\mathrm{k}$ in late winter about 20 billion years ago—*beyond our ability to observe or calculate*.

CMBA depends on the path and timing of a CMB photon (γ_{cmb}) relative to the brief early spring turning on of local gravity (τ_{on})—the same time everywhere in the universe. Appendix N develops the details of this subject.

One will discover that the NCNG version of CMBA results from a net gravitational wavelength (temperature) shift of a relic γ_{cmb} passing through or near a canister at $\tau=\tau_{on}$. A canister is a vast and massive collection of matter and an associated gravitational field. The universe is filled with canisters. τ_{on} was about 20 billion years ago, so only the subset of canisters which are close to 20 billion light years away will exhibit a small temperature shift.

It should be possible to observe a sky map of these special canisters (as described in Appendix N). Once done, all of the basic aspects of NCNG could be proven. The internal tensions of GRLCDM have passed the breaking point, and JWST observations will likely increase the tensions. Therefore, *it is time to create new observatories to test alternatives to* GRLCDM.

B. Gravitational waves

The early observations of LIGO were described by many as proof that general relativity was the only correct theory. That belief was not true, and “proof” evolved into “consistent with”. Any viable gravitational theory will support gravitational waves, and NCNG is no exception. Section IV(B), Eq. (4.13) shows a solution which is a transverse (tensor) plane wave with the same cosmological redshift as electromagnetic waves. These plane waves are what LIGO observes. The difference between NCNG and GR is billions of light years away where the waves are created.

Gravity is so weak that waves cannot be observed unless the distant source is an event that provides a catastrophic amount of energy to be carried away in waves. The best event occurs when two black holes come together to form one black hole. In NCNG the black holes are replaced by CCBOs. Calculations of such events are incredibly complicated for both versions (beyond the scope of this document).

The GR version requires the simultaneous solution of more than 400 nasty equations. The black holes spiral inward toward each other moving at very high velocities (phase1). After the two event horizons come in contact, the two will have only one event horizon (phase 2). LIGO sees phase1 as a wave form of increasing frequency and amplitude. Phase 2 is a wave form of faint frequency and vanishing amplitude. The two phases make a recognizable pattern that denotes an event (if observed by both LIGO observatories).

The NCNG version is similar and every bit as complicated, but for different reasons. The wave formation process is much easier since it will be like electromagnetic waves. The two boundaries will replace event horizons. However, *now one needs to calculate the behavior of the two* CCBO *sources all the way from beginning to end of their wild ride*! There are many scenarios. During phase1 for example, a CCBO source will be subject to centrifugal distortion which would deform the boundary as well. It is even possible that such a distortion would destroy the source and cause it to evaporate.

The main difference between GR and NCNG is that NCNG will have a wider range of recognizable patterns than GR. Thus, LIGO will not recognize and record some portion of actual events (using the GR version criterion).

C. Universal stability

Stability is all about energy densities, so a review of this topic is useful. Energy densities are averaged over sufficiently large volumes. There are only three energy densities: $U_{ax}(\tau)$ for the apex field, $U_{ep}(\tau)$ for the epoch field, and $U_M(\tau)$ for "matter" (everything else). There is a universal constraint,

$$U_{ax}(\tau)+U_{ep}(\tau)+U_M(\tau)= \text{ univeral constant.} \tag{8.1}$$

The apex and epoch fields are discussed at length in section II. Matter is discussed at length throughout NCNG. Only the most common particles are included: electrons, electron-flavor neutrinos, neutrons, protons, nuclides, photons in flight, and gravitons in flight. Electromagnetic and gravitational fields are also included. The apex and epoch energy densities are negative and matter is positive. There is a basic hierarchy,

$$\left|U_{ax}(\tau)\right| > \left|U_{ep}(\tau)\right| >> U_M(\tau), \tag{8.2}$$

where $U_M(\tau)$ is thought to be 250 Mev per cubic meter today (suspect value). $U_M(\tau)$ has a positive lower limit (a frozen universe), but there is no upper limit (an infinite temperature universe). Eq. (8.1) is the ultimate guarantor of stability, but that is not what this subsection is about. Here, one wants to know if the NCNG universe can run off the tracks?

Derailment means that there is a persistent imbalance which causes the apex and epoch energy densities to steadily become more negative and the matter energy density to steadily increase toward infinity—a disastrous outcome consistent with Eq. (8.1). I have evaded this question till now by insisting that the magnitude of the apex and epoch fields energy density is very much larger than the energy density of matter—an imbalance would take many cycles to derail. To avoid this outcome, it is necessary to study the complex network of energy transfers in NCNG.

An example will illustrate the network. The apex field is the ultimate storehouse of energy, and the epoch field is an important but lesser storehouse. Eq. (2.22) shows that energy can move between the two storehouses only for a very brief period (controlled by Γ_{ep}) when $|A| = A_{ep}$. Γ_{ep} and A_{ep} are universal constants tabulated in Appendix Z. This connection only occurs four times in every cycle, so the epoch-field storehouse must handle requirements without help for billions of years.

The epoch field connects with matter via the epoch factor, $\mathrm{E}(\phi_{ep})$, defined by Eq. (2.17). The epoch factor appears in the LDM for matter via Eq. (3.1), and the connections are manifested by Eq. (7.4) and Eq. (7.5). Thus, any transfer of energy between the epoch field and matter can only occur during brief periods (controlled by Γ_W or Γ_G) when $\mathrm{E}(\phi_{ep}) = \mathrm{E}_W$ or $\mathrm{E}(\phi_{ep}) = \mathrm{E}_G$. Γ_W, Γ_G, E_W, and E_G are universal constants tabulated in Appendix Z. Both the weak and gravity energy transfers occur four times in each cycle. These specific connections all occur during spring or fall. In spring, the first event is the apex-epoch connection (AE). The second event is the bubble era (not an energy transfer) 2.35 million years later (based on the constants of Appendix Z). The third event is the epoch-gravity connection 5.58 million years after AE. The fourth event is the epoch-weak connection 6.46 million years after AE. In fall, the order is reversed. Thus, the epoch field must endure four matter connections before connecting to the apex field again.

The apex field is also connected directly to matter at all times. The apex field can subtract energy from photons and gravitons in flight via cosmological redshift—$\mathrm{U}_{ax}(\tau)$ increases. Energy can be added via cosmological blueshift—$\mathrm{U}_{ax}(\tau)$ decreases. In section III, one learns that the apex field also constantly interacts with all types of matter to empower the (excellently approximated) illusion of special relativity.

This subject is extremely complex (beyond the scope of this document). There are many ways that the apex field can gain or lose energy. Furthermore, the interactions between different types of matter will add even more complications. To move forward, one must estimate the relative importance of the mechanisms and build a model using the most important ones for study. A concordant model will arise from studies. This subject is important, so I believe that a constraint on the universal constants of Appendix Z may be required. It is also possible that some new physics might be required as well.

D. Tests of validity

There are only three universal theories that should be of interest (GRLCDM, MOND, and NCNG). I believe that MOND can be discarded for the following reason. Assume that MOND is a correct theory.

If MOND is a correct theory, then dark matter does not exist. Without dark matter the LCDM cosmology collapses. The minimum requirement for a viable cosmology is the prediction of a correct value of the Hubble constant (accurately known). Therefore, MOND must generate a *new*

cosmology to replace LCDM. I believe that MOND cannot be made to predict the Hubble constant—MOND is not a correct theory.

There are many observations that could compare NCNG predictions with GRLCDM predictions. Unfortunately, most of these observations require equipment that does not exist presently.

JWST may eventually provide some of these observations. NCNG has a maximum cosmological redshift during very early red summer (Appendix C). The oldest JWST object observed as of late 2022 has $z = 13.2$ [18]. I believe that the accurately determined maximum z will not be much larger than this observation.

There is one important subject which has used existing equipment, spiral-galactic rotation (refer to Appendix D). One will realize that NCNG is the only survivor.

IX. BIBLIOGRAPHY

[1] Adam G. Riess *et al*., Astrophys. J. **876**, 85 (2019)
[2] Jacques Colin *et al*., Astronomy & Astrophysics **631**, L13 (2019)
[3] S. Coleman, Phys. Rev. D **15,** 2929 (1977)
[4] C. G. Callan Jr. and S. Coleman, Phys. Rev. D **16,** 1762 (1977)
[5] W. J. G. de Blok *et al*., Astronomical Journal, 136:2648-2719, 2008 December
[6] J. F. Navarro, C. S. Frenk, and S. D. M. White, Astrophys. J. **490**, 493 (1997)
[7] K. G. Begeman, A. H. Broeils, and R. H. Sanders, Mon. Not. R. astron. Soc. **249**, 523 (1991)
[8] E. Corbelli and P. Salucci, Mon. Not. R. astron. Soc. **311**, 441 (2000)
[9] F. Douchin and P. Haensel, 2001arXiv:astro-ph/0111092v2
[10] Patrick Cote *et al*., 1991arXiv:astro-ph/9907003v1
[11] J. N. Bahcall, Phys. Rev. **135**, B137 (1964)
[12] E. G. Adelberger *et al*., Rev. Mod. Phys. **83**, 195 (2011)
[13] L. Landau and E. Lifshitz, in *The Classical Theory of Fields,* translated by M. Hammermesh (Addison-Wesley, Reading MA, 1951), pp. 312-316
[14] Martin Schwarzschild, in *Structure and Evolution of the Stars,* (Dover Publications, Inc., New York, 1965), pp. 52-62
[15] G. Gentile *et al.,* A&A, 554 A125 (2013)
[16] R. Schodel *et al.,* A&A, 609 A27 (2018)
[17] Laurent Chemin *et al*., The Astrophysical Journal, 705:1395-1415, 2009 November 10
[18] Cosmin Ilie *et al.*, arXiv:2304.01173v2 [astro-ph.CO] 12 Apr 2023

APPENDIX A: REFLECTIONS ON HISTORY

Strange as it might seem, I believe Einstein is the hero of this story. Einstein was the first (and possibly the last) researcher to understand that there was something seriously awry with GR—pathological exact solutions. Both the Friedmann metric tensor and the Schwarzschild metric tensor give rise to troubling infinities. Einstein tried to save general relativity by eliminating the most troubling pathology through the introduction of a cosmological constant (the opposite sign from what we call dark energy today). A few years later, Hubble's observations (and their erroneous interpretation as a doppler shift) would wreck Einstein's repair job and perversely tarnish his reputation.

Decades later (when it became clear that GR by itself could not agree with observations), there was a reversal of fortune. Two fudge factors (dark matter and dark energy) were added to physics so that we could pretend that GR is a correct theory—posthumous reputation restored.

There followed decades of research developing GRLCDM, and *the pathologies became entrenched*. Einstein and the researchers who followed cannot be blamed for following this sterile path. Their toolbox was nearly empty.

GR is based on nineteenth-century math and physics. Since GR is a geometric theory, it has more in common with the axiomatic theories of the ancient Greeks than with modern physics, e.g., the standard model of particle physics.

Since my teens, I have been very interested in attempts to eliminate the expanding universe pathology. As a freshman at Cal Tech (class of 1960), I attended a luncheon featuring Fred Hoyle. His steady-state universe model was an addition to the Einstein attempt—a (dubious) explanation for cosmological redshift. This attempt failed also for lack of a mechanism to steadily create the hydrogen required for stellar fusion. There were other ideas that failed, e.g., the unit of electric charge is a function of time. Without realization, my interest left a seed. Mechanisms (for control of nucleosynthesis and the draining of energy from photons in flight) would be necessary for a successful attempt.

Some years later as a graduate student at Harvard, my thesis advisor was Walter Gilbert. Walter did pioneer work on Higgs fields (considered to be a rabbit hole at that time). He also taught a course on Quantum Field Theory which I audited. *That was the first time that I saw a self-supporting (scalar) field*. At that time there was a research associate (several offices away from Walter) that I recognized from Cal Tech, Sydney Coleman. Sydney tutored me about the eight-fold way one summer, and I recognized that he would be important in the future.

At Harvard one was expected to do field theory using Green's functions, but at Cal Tech one used Feynman's path-integral method. Green's functions are poorly suited for finding a successful attempt, but Feynman's method could be applied to many different problems (including classical fields). Years later, [3] and [4] would provide *tools for another path toward a successful attempt*. My toolbox was no longer empty, but I was no longer interested in attempts. I went down a different rabbit hole.

I would return to the quest forty years later. During that period, I had developed an interest in the recurring ice ages. I found a chaos theory model that featured sudden transitions between lengthy stable climates (ice or no ice). Furthermore, propagating disturbances in the neutral Higgs field had been observed (Higgs bosons). Thus, the idea (of a self-supporting field pervading all of space and time could exist) was solidified. Sydney Coleman's idea of sudden vacuum transitions

was the final tool required. My toolbox was full, and section II in NCNG followed. *The idea of relativity died on the day that the Higgs boson was observed*.

I followed a path that was akin to a Forrest Gump adventure—at the right place at the right time. The final irony is that Einstein could have eliminated the pathologies only by destroying general and special relativity.

APPENDIX B: SPRING BUBBLE FORMATION

The formation of bubbles is described in [3] and [4]. The probability of a bubble forming within a space-volume V and an evolution-duration Δx^0 is $P_{form} = p_B V \Delta x^0$. In red spring, p_B is given with sufficient accuracy in [4] as

$$p_B = (L_{ep}^{-4} / 4\pi^2)\theta^2 e^{-\theta}. \tag{B.1}$$

The exponent (θ) is a function of $\lambda(A)$, a_{ep} , and $\mathcal{N}_{ep}$ (calculated using the thin wall approximation of [3])

$$\theta = 2\pi^2 \mathcal{N}_{ep} 27 S^4 \varepsilon^{-3}, \tag{B.2}$$

$$\begin{aligned} \varepsilon &= V_{ep}(\phi_{\text{false}}) - V_{ep}(\phi_{\text{true}}), \\ S &= \int_{\phi_{\text{false}}}^{\phi_{\text{true}}} d\phi \{V_{ep}(\phi) - V_{ep}(\phi_{\text{true}})\}^{1/2}. \end{aligned} \tag{B.3}$$

$$\begin{aligned} \phi_{\text{true}} &= \{-\lambda(A) + [a_{ep}{}^2 + \lambda(A)^2]^{1/2}\} / 2a_{ep}{}^2, \\ \phi_{\text{false}} &= \{-\lambda(A) - [a_{ep}{}^2 + \lambda(A)^2]^{1/2}\} / 2a_{ep}{}^2. \end{aligned} \tag{B.4}$$

L_{ep} will be a fraction of a meter, whereas the typical expanding bubble radius (R) will be measured in light-years, so the bubble wall will be extremely thin compared to R.

The average energy density of matter in the universe (as defined at the start of section III) is thought to be about 250 Mev per cubic meter. This number comes from GR and ΛCDM, so the value is suspect, but I will use this value throughout this paper. Thus $\left|U_{ep}^{S}\right| = \chi_{ep} U_{matter}$, where $\chi_{ep} >> 1$ (by hypothesis). Eq. (2.18) then leads to the relation,

$$\mathcal{N}_{ep} = \chi_{ep} (L_{ep} / L_m)^4 \left|V_{ep}(\phi_S)\right|^{-1}, \tag{B.5}$$

where $L_m = 1.70306 \times 10^{-4}$ meters.

To develop an understanding of the bubble formation era, a cubic space-volume of interest is defined in terms of a length ($V = L_V{}^3$). The universe is filled with these cubes. L_V must be large compared to the radius of the largest bubble that is likely to form within a specific cube during the chaotic period, e.g., $L_V = 10^4$ ly.

There is a simple constraint that accurately governs (ultra-thin wall) bubble-formation—*a new (valid) bubble cannot form within an existing bubble*. P_{form} is ignorant of this constraint, but it can

be used to calculate the probability of an *attempt* at bubble formation. It is useful to express the probability in terms of the apex field instead of x^0

$$d\,\mathrm{P}_{form} / d\,\mathrm{x} = -(dA / dx^0)_{A_d}{}^{-1}\,\mathrm{L_V}{}^3 (4\pi^2\,\mathrm{L}_{ep}{}^4)^{-1}\theta^2 \exp(-\theta), \tag{B.6}$$

where $A = A_d - \mathrm{x}$ and $\mathrm{x} \geq 0$. The quantities of interest for $\mathrm{x} \to 0$ are as follows:

$$\begin{aligned}
&\varepsilon = \mathrm{x}\,\Gamma_1\,,\\
&\Gamma_1 = (100/96)(\beta_{ep}\Gamma_{ep} / a_{ep}{}^3)[1-(\lambda_{ep}/\beta_{ep})^2],\\
&\mathrm{S} = 0.25502\; a_{ep}{}^{-2},\\
&\theta = \Lambda_\theta\,\mathrm{x}^{-3},\\
&\Lambda_\theta = 54\pi^2\,\mathrm{S}^4\,\Gamma_1{}^{-3}\chi_{ep}(\mathrm{L}_{ep}/\mathrm{L}_m)^4\left|\mathrm{V}_{ep}(\phi_S)\right|^{-1},\\
&DA = 0.5\,(\mathcal{F}_S(A_d) + \mathcal{F}_W(A_d)),\\
&(dA/dx^0)_{A_d} \simeq -DA\,\mathrm{L}_{ax}{}^{-1}.
\end{aligned} \tag{B.7}$$

The average number of attempts made prior to x is as follows:

$$\begin{aligned}
&NA(\mathrm{x}) = \Pi\int_0^{\mathrm{x}} d\,\mathrm{x}'(\mathrm{x}'^{-6})\exp(-\Lambda_\theta\,\mathrm{x}'^{-3}),\\
&\Pi = DA^{-1}\,\mathrm{L}_{ax}\mathrm{L_V}{}^3(4\pi^2\,\mathrm{L}_{ep}{}^4)^{-1}\Lambda_\theta{}^2.
\end{aligned} \tag{B.8}$$

The leading term of Eq. (B.8) as $\mathrm{x} \to 0$ results,

$$\log(NA) = \log(\Lambda_\theta{}^{-1}\Pi/3) - 2\log(\mathrm{x}) - (\log(e))\Lambda_\theta\,\mathrm{x}^{-3}. \tag{B.9}$$

If $NA(\mathrm{x}_1) = 1$ (the first bubble in V), then there will be *explosive growth* in *NA* thereafter if $\log(e)\Lambda_\theta\,\mathrm{x}_1{}^{-4} >> 1$. Eq. (B.9) has limited usefulness since Π depends on the arbitrary volume of the cube. There is a more useful metric that is independent of cube volume,

$$\Delta(\mathrm{x}) = \mathrm{L}_V{}^{-3}(-(dA/dx^0)_{A_d})^{-3}\int_0^{\mathrm{x}} d\,\mathrm{x}'(4\pi/3)(\mathrm{x}-\mathrm{x}')^3(d\,\mathrm{P}_{form}/d\,\mathrm{x}'). \tag{B.10}$$

Delta is a ratio--the (approximate) volume of the bubbles created within the cube divided by the volume of the cube. Delta ignores the bubble validity constraint and the fact that bubbles can overlap. One could define the *end of the bubble era* (x_{end}) by choosing $\Delta(\mathrm{x}_{end}) = 1$. This estimate will be a *lower bound* of x_{end} for the following reason. The integrand in Eq. (B.10) represents an over-estimate of the true bubble volume since it includes non-valid bubbles and ignores bubble overlap. Thus, the integration reaches 1 at a lesser value of x than the true value for x_{end}. The

explosive growth of bubble attempts insures that $\log(\Delta)$ can be neglected in what follows. The leading term of Eq. (B.10) as $\mathrm{x} \to 0$ follows:

$$\begin{aligned} \Delta(\mathrm{x}_{end}) &= \Xi\, \mathrm{x}_{end}{}^{10} \exp(-\Lambda_\theta\, \mathrm{x}_{end}{}^{-3}), \\ \Xi &= (2/81\pi)(\mathrm{L}_{ax}/\mathrm{L}_{ep})^4 DA^{-4}\Lambda_\theta{}^{-2}. \end{aligned} \tag{B.11}$$

Eq. (B.11) is equivalent to

$$\begin{aligned} &Y^{-3} - 10\log(Y) = F, \\ &\mathrm{x}_{end} = [\Lambda_\theta \log(e)]^{1/3} Y, \\ &F = \log(\Xi) + (10/3)\log[\Lambda_\theta \log(e)]. \end{aligned} \tag{B.12}$$

It is a simple matter to find Y given F. The factors in Eq. (B.12) are dominated by $\mathrm{L}_{ax}/\mathrm{L}_m >> 1$, $\mathrm{L}_m/\mathrm{L}_{ep} >> 1$, and $\chi_{ep} >> 1$. It is useful to isolate these factors. F can be rewritten in order of size,

$$F = 4\log(\mathrm{L}_{ax}/\mathrm{L}_m) + (4/3)[\log(\chi_{ep}) - \log(\mathrm{L}_m/\mathrm{L}_{ep})] + F_0. \tag{B.13}$$

The value ($\mathrm{L}_{ax} = 9\mathrm{e}9$ l.y.) will be established in Appendix C. Thus, $4\log(\mathrm{L}_{ax}/\mathrm{L}_m) = 118.80$. The second and third terms govern the energy density of the epoch field, but they are constrained by limits on the size of x_{end}. If $\log(\chi_{ep}) = 8$, and if L_{ep} is the Compton wavelength of a one electron-volt mass particle (plausible values), then the second and third terms equal 7.849. The last term is due to numerical factors and a swarm of factors from Eq. (B.7). A generic set of epoch field constants gives $F_0 = -5.599$. Therefore, the last three terms of F contribute 2.25 (less than 2% of the total). The value $F = 121$ corresponds to $Y = 0.20615$. Using Eq. (B.12), one finds

$$\mathrm{x}_{end} = 0.1561\, \Lambda_\theta{}^{1/3}. \tag{B.14}$$

In practice, x_{end} will be fixed by the (small) portion of spring that the bubble era is allotted. In that case, Eq. (B.14) will be a constraint on the relation between χ_{ep} and L_{ep}. The allotment will also fix the scale of bubble size. Furthermore, x_{end} will be very small and the explosive bubble-formation criterion will be met. The fall transition has a bubble era, and the same considerations as above are valid. For all transitions, $\mathrm{x}_{end} > 0$. For red transitions, $A_{end} = A_d - \mathrm{x}_{end}$, and for blue, $A_{end} = A_d + \mathrm{x}_{end}$.

On average, nearly all the physical time allotted to x_{end} is spent waiting for the first bubble to form. Once formed, explosive growth will end the era within several thousand years. The model of Appendix Z will allot 736,000 years for the era.

APPENDIX C: MODEL HISTORIES OF THE APEX FIELD AND PHYICAL TIME

A model history is a tabulation of three variables of interest versus the Apex field over a (red branch) range of interest using the universal constants of Appendix Z. The variables are z (cosmological red shift relative to now), the epoch parameter E, and the elapsed physical time relative to an edge of the range. Appendix Z is a work in progress. New observations and deeper research will require periodic updates of the model and thus *change these histories*.

The equations that govern the variables are the following set. E(A) is given by Eq. (2.12) through Eq. (2.17). The relation of physical time and the Apex field is as follows:

$$\begin{aligned} &G_{ax}(A) = d_1^{ax}A^2 + d_2^{ax}A^4 + d_3^{ax}A^6, \\ &dA/cd\tau = -\mathrm{L}_{ax}^{-1}\,\mathcal{F}(A)\;\mathrm{J}(A,\mathrm{E}(\phi_{ep}(A)))^{1/2}, \\ &\mathcal{F}(A) = \left[1+\xi(A)-G_{ax}(A)\right]^{1/2}, \\ &\xi(A) = (\alpha_W^{ax}/2)\{1+\tanh[2A_{ep}\Gamma_{ep}(A-A_{ep})]\}, \end{aligned} \tag{C.1}$$

where J is given by Eq. (3.29). The cosmologic red shift is zero at earth (now), and z is defined as follows:

$$\begin{aligned} &z = \mathrm{J}(A,\mathrm{E}(\phi_{ep}(A)))^{-1/2}\,\mathrm{J}(A_0,\mathrm{E}(\phi_{ep}(A_0)))^{1/2} - 1, \\ &\mathrm{L}_{ax} = 0.5\,\mathrm{L}_H(1-A_0)^{-1/2}[1-G_{ax}(A_0)]^{1/2}, \\ &\mathrm{L}_H = 13.26\,\mathrm{x}\,10^9 \text{ light-years}, \end{aligned} \tag{C.2}$$

where A_0 is the value of A today (not a universal constant). Use the lower members of Eq. (C.2) to calculate A_0, then use the upper member to obtain z.

Each history requires (the same) knowledge of some of the universal constants of Appendix Z—five apex constants, five epoch constants, three clock constants, and x_{Bera}—a total of fourteen. If there was a set of precise standard-candles (for a wide range of z), the fourteen constants could be determined from observations, but that is not the case. However, there are consistency constraints to be imposed. Furthermore, the effect of a variation of each constant on the history can be quantified.

Several constraints are obvious. *All histories will have a maximum value of* z—necessarily larger than the most distant observations to date. All histories must have a (blue to red) winter lasting at least 300 billion years—in accordance with the reverse nucleosynthesis model. There are also some constraints that control what can be seen for z near the maximum.

The maximum value of z is largely dependent on β_{cl}. I have chosen the values of Appendix Z so that $z_{\max} \sim 15$ (a spec for the JWST). The constants of this document yield $z_{\max} = 14.9213$. The most recent (oldest) observation for this edition is galaxy JADES-GS-z13-0 [18]. That value is $z_{\max} = 13.2$, the current candidate. Since JWST can go to higher z, one should expect that future

observations will clarify if JWST can establish $z_{\max}$. Note that obtaining a value for z from JWST data is arcane—possibly leading to controversy.

There is another complication in NCNG. There are *two different distances* for $z = 13.2$ which bracket the maximum. Which distance is JADES-GS-z13-0? Using the constants of this edition, the oldest distance occurs about 496,000 years after local gravity is turned on, but 378,000 years before fusion is turned on (Fig. C5). The older version of JADES-GS-z13-0 would consist of only Kelvin contraction stars and gas, The more recent version of JADES-GS-z13-0 would occur 418,000 years after the older version (after fusion is turned on). One should expect that the newer version would have greater luminosity than the older version—more time to convert gas into stars and hotter fusion stars compared to Kelvin contraction stars. I believe that JADES-GS-z13-0 is the older, dimmer version. This object is erroneously identified as a *supermassive dark star* [18], but it is actually a normal galaxy in very early red summer.

Many of the astronomical observations (during my lifetime) have been interpreted through the filter of the suspect GRLCDM theory—suspect conclusions requiring re-examination. Some of the rungs in the ladder of distance will survive and some will require a new expression. The goal will be a coherent model of distance versus cosmological red shift ($d(c\tau)/dz$) derived from an ultimate version of Appendix Z. The first step is outlined below using the version of the standard model of Appendix Z in this document.

The apex field (*A*) varies between 1.043716 and -1.043716 between midwinter extremes. Thus, the value of *A* for a point within a cycle is a long decimal—inconvenient for an axis of a figure. One can use Eq. (C.2) to obtain the now parameter, $A_0 = 0.8150217$. Then, I have chosen the following definition:

$$A = A_0 - \Delta A \alpha, \tag{C.3}$$

where $\Delta A = 2.36 \text{x} 10^{-5}$. Some of the figures below will be versus alpha less a starting offset (instead of *A*). Several markers of interest can be tabulated; $z_{MAX} = 14.9213$ at $A = 0.9992719$, and the turning point at the middle of (blue to red) winter $A_W = 1.0413716$ (maximum value of *A*).

Fig. C1 (below) shows the shape of E in the range 0.999 (winter) to 0.001 (summer) versus alpha less an offset. The bubble discontinuity is at $A = 0.9992856$ (alpha = 7807.788). Physical time is increasing toward the left of the figure, i.e., the right side is the oldest value.

The history will follow one quarter of a cycle from $A = 0$ to $A = A_W$ on the red branch. The first segment (Fig. C2) is from the middle of red summer to now ($0 < A < A_0$)—in the future. The duration of this segment is 12.685 billion years.

The next segment (Fig. C3) is from now to the past physical time when $z = z_{MAX}$ (completely in red summer). The duration of this segment is 19.972 billion years (in the past).

The next brief segment goes from maximum z ($A = 0.9992719$) to the summer side of the E-discontinuity ($A = 0.9992855$). The duration of this brief segment is 17.534 million years.

The last segment (Fig. C4) is from the winter side of the E-discontinuity at $A = 0.9992856$ to $A_W = 1.0413716$. The duration of this lengthy segment is 150.192 billion years. This quarter lasts 182.867 billion years and a complete cycle will be 731.466 billion years. Winter will amount to 82.2 % of the cycle. Note that z is negative (cosmological blue shift) for the first 367 million years of Fig. C4 (late winter).

Fig. C3 is important since it involves only four universal constants ($d_1^{ax}, d_2^{ax}, d_3^{ax}$, and L_{ax}) because $\mathrm{E} = 0$. A ladder of distances can be established by observing Cepheid variables and multi-image gravitational lensing of more-distant type 1a supernovae events (a tall order). The ladder is equivalent to Fig. C3 and the four constants can be established from observations. Thus, one can improve Appendix Z and improve the accuracy of NCNG.

Fig. C5 has detail for events of interest when z is earlier than maximum z. Local gravity is turned on at $z = 12.9532$ and offset alpha = 0.6398. Fusion is turned on at $z = 13.4303$ and offset alpha = 0.6102.

All the details in these figures will only be accurate in the future if JWST will eventually establish that the maximum value of z is very close to 14.9213, and the fourteen constants of Eq. (C.1) and Eq. (C.2) are not different than the values of this edition. Otherwise, recalculations will be necessary.

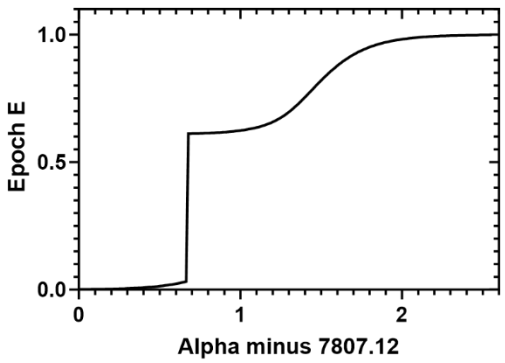

Figure C.1. The epoch field function E defined in Eq. (2.17) versus a linear function of the apex field defined above.

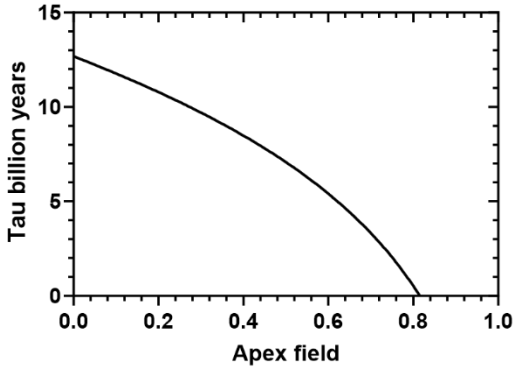

Figure C.2. Physical time in the future moving left from now till *A* is zero (the half point of the red branch).

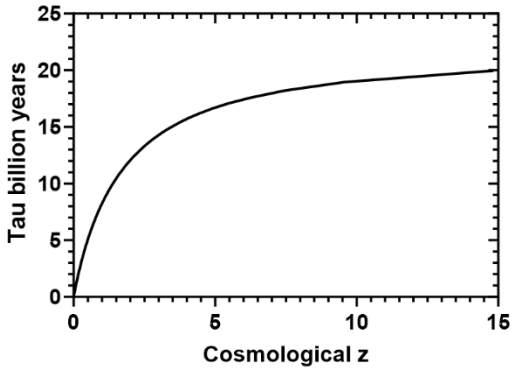

Figure C.3. The age (distance/c) of a luminous object versus z from now back to the maximum value of z.

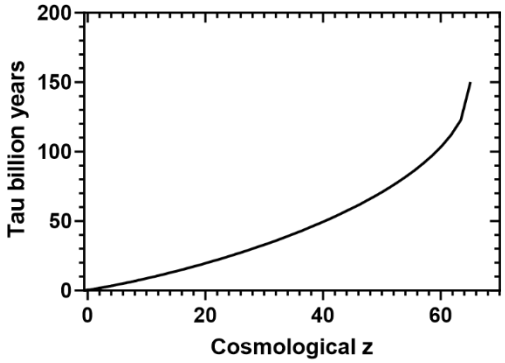

Figure C.4. This figure adds a major segment of the age of a cycle, and z gives the temperature of CMB in winter (cold).

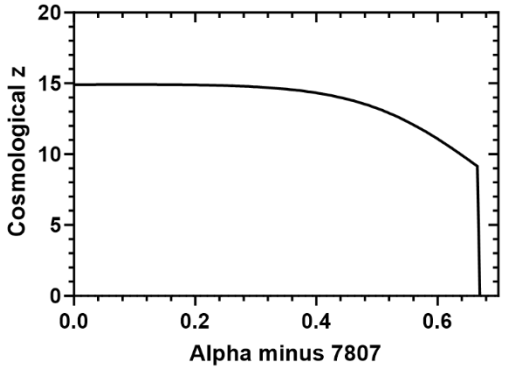

Figure C.5. This figure covers the oldest portion of early red summer—a (brief) eventful era.

APPENDIX D: SPIRAL GALAXY ROTATION

The main purpose of this appendix is to compare NCNG with GRLCDM as per section VIII(D). Eq. (5.5) forms the basis for obtaining the NG rotational velocity profile from a given distribution of neutral matter. The mass distribution of a suitable flat disc galaxy in Cartesian coordinates is *approximated*,

$$\rho(\mathbf{x}) = \sigma(R)\delta(z), \tag{D.1}$$

where $R^2 = x^2 + y^2$ and δ is the Dirac delta function. Next, take the Fourier transform of both $\mathcal{A}_N(\mathbf{x}, q)$ and $\rho(\mathbf{x})$ to obtain the relation between transformed functions using Eq. (5.5),

$$\begin{aligned} \bar{\mathcal{A}}_N(\mathbf{p}, q) &= -4\pi G Z_q \bar{\rho}(\mathbf{p})\left\{\mathbf{p}^2 + \mathrm{L}_q^{-2}\right\}^{-1}, \\ \bar{\rho}(\mathbf{p}) &= \int d^3x \rho(\mathbf{x}) \exp(i\mathbf{x}\cdot\mathbf{p}). \end{aligned} \tag{D.2}$$

The expression for $\bar{\rho}$ can be simplified through a tedious series of steps manipulating the integration in the x-y plane,

$$\bar{\rho}(\mathbf{p}) = 2\pi \int_0^\infty R dR\, \sigma(R)\mathrm{J}_0(aR) \equiv \bar{\rho}(a), \tag{D.3}$$

where $a^2 = p_x^2 + p_y^2$ and J is the Bessel function of indicated order. Take the inverse Fourier transform of Eq. (D.2) to obtain $\mathcal{A}_N$,

$$\begin{aligned} \Phi(R, q) &\equiv \mathcal{A}_N(x, y, z = 0, q) \\ &= -GZ_q \int_0^\infty a da \frac{\bar{\rho}(a)\mathrm{J}_0(aR)}{\left(a^2 + \mathrm{L}_q^{-2}\right)^{1/2}}. \end{aligned} \tag{D.4}$$

Next, obtain the rotational velocity by using Eq. (5.5) along with the assumptions that pressure gradients and viscosity can be ignored,

$$v_{rot}^2(R) = R\sum_{q=1}^{N_q} \frac{d\Phi(R, q)}{dR}. \tag{D.5}$$

The last step introduces dimensionless variables to simplify Eq. (D.5):

$$\begin{aligned} R &= \eta R_0, \\ a &= \chi R_0^{-1}, \\ M_G &= \xi M_0, \\ \sigma(R) &= M_0 R_0^{-2} \Lambda(\eta), \\ \lambda_q &= R_0 / \mathrm{L}_q, \\ v_0 &= \left(G M_0 R_0^{-1}\right)^{1/2}, \end{aligned} \tag{D.6}$$

where

$$\begin{aligned} R_0 &= 10^3 \text{ light-years}, \\ M_0 &= 10^9 \text{ solar masses}, \\ v_0 &= 118.5 \text{ km/s}. \end{aligned} \tag{D.7}$$

The equations simplify as follows:

$$\int_0^\infty \eta d\eta \Lambda(\eta) = \xi / 2\pi, \tag{D.8}$$

$$\Delta(\chi) = 2\pi \int_0^\infty \eta d\eta \Lambda(\eta) \mathrm{J}_0(\chi\eta), \tag{D.9}$$

$$v_{rot}^2(\eta) = v_0^2 \eta F(\eta), \tag{D.10}$$

$$F(\eta) = \int_0^\infty \chi^2 d\chi \Delta(\chi) \Psi(\chi) \mathrm{J}_1(\chi\eta), \tag{D.11}$$

$$\Psi(\chi) = \sum_{q=1}^{N_q} \mathrm{Z}_q (\chi^2 + {\lambda_q}^2)^{-1/2}. \tag{D.12}$$

Eq. (D.12) is constructed from *universal constants and it is the same for all spiral galaxies*. The delta function is governed by the distribution of mass for each spiral galaxy.

One suitable model for the delta function is akin to a Laplace transformation,

$$2\pi\Lambda(\eta) = \sum_{k=1}^{N} \alpha_k^2 \xi_k \exp(-\alpha_k \eta), \tag{D.13}$$

in which case,

$$\Delta(\chi) = \sum_{k=1}^{N} \xi_k \alpha_k^3 \left(\alpha_k^2 + \chi^2\right)^{-3/2}. \tag{D.14}$$

The total mass of the galaxy is $\xi = \sum_{n=1}^{N} \xi_n$. Note that ξ_n must be positive.

There is another relation that connects the density of galactic mass directly with the rotation profile;

$$F(\eta) = \int_0^\infty d\eta' \eta' 2\pi\Lambda(\eta') K(\eta,\eta'), \tag{D.15}$$

$$K(\eta,\eta') = \int_0^\infty \chi^2 d\chi \Psi(\chi) \mathrm{J}_1(\chi\eta) \mathrm{J}_0(\chi\eta'). \tag{D.16}$$

The *K* function is *the same for all galaxies* and needs only to be calculated once.

The universal function, Ψ, is featured in Fig. D.1 below.

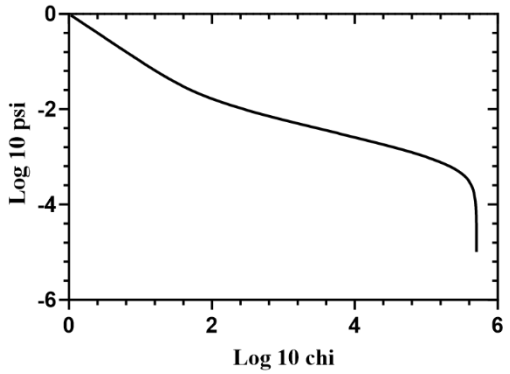

Figure D.1. Graph of Eq. (D.12) using the standard model universal gravitational parameters of Appendix Z.

The primary plague of astronomy (unreliable ladder of distances) infects this study. Astronomers are wise enough to tabulate rotation observations in arc minutes or seconds (an angle relative to the center of the galaxy). In that case, the problems of the distance ladder are side-stepped. At this point, it is useful to convert the equations above to angles instead of distances. That is accomplished by using the relation ($\eta \to \Gamma_D \omega$) in Eq. (D.10) and Eq. (D.11) or Eq. (D.15), where $\Gamma_D = \mathrm{D}_{MPC} / 63.24$ and D_{MPC} is the distance to the center of the spiral galaxy from earth in units of Mpc, and ω has units of arc seconds.

The rotation velocities for *all galaxies* subject to equations (D1) to (D16) have a common feature, a finite radius beyond which $dv_{rot}(\omega)/d\omega > 0$ out to vast radii. This feature is the hallmark of NCNG. The two competing theories (GRLCDM or MOND) always have asymptotic rotation velocities where $dv_{rot}(\omega)/d\omega \le 0$. Thus, rotation velocities at large radii are of great interest.

Rotation velocities at larger radii are best observed using radio telescope arrays (relative doppler shift of 21 cm radiation from H1). Only two (VLA and Westerbork) have been used for this purpose. VLA has 1.93 times the maximum collection-area versus Westerbork—an advantage for VLA. The signal to noise error for an array governs the maximum radius for observable velocities.

The subject of signal versus noise for radio telescopes is very arcane. For rotation velocities, the 21 cm doppler shift (signal) at the earthly array collectors is extremely weak and the large collection of noises is extremely strong by comparison. It is necessary to reduce the noise.

A single collector (dish) illustrates the technique. The collector focuses electromagnetic waves on an antenna which converts this information into a time dependent voltage. The voltage has both a weak signal and strong noise. The noise voltage has an average of zero. The voltage is subject to a series of steps.

Step one is a band-pass filter that passes only frequencies close to 1.489 GHZ (bandwidth $\Lambda\nu \sim$ 6 MHZ). Next, the voltage is squared. This leaves the resulting voltage with three parts: the square of the signal (average = constant with time), the square of the product of the signal and noise (average = 0), and the square of the noise (a random value between 0 and a large positive number). The final step is the integrator which is the average of the sum of the square voltages with time. The result is a voltage that equals the signal plus an error, where the error is proportional to $(\Delta\nu t)^{-1/2}$. One can find an integrating time (t) that produces a sufficiently small error compared to *any* signal. The error bars for the observations of [7] are obtained from the known integration errors.

The only suitable large radii observations are found in references [5], [7], and [15]. Reference [7] studied NGC 3198 and 2841 (observed in spring of 1982 using a primitive version of Westerbork). Reference [15] concerns only NGC 3198 but provides several data points at larger radii than [7] (using an upgraded Westerbork). Reference [5] provides higher resolution rotational velocity profiles for many galaxies including those of interest using VLA (but not larger radii than the Westerbork observations).

NGC 3198 and 2841 are important because [7] shows increasing velocities at largest radii for both (favoring NCNG). Furthermore, [7] velocity fits at largest radii for GRLCDM are mediocre. Nevertheless, the data of [5], [7], and [15] is not yet sufficient to decide which theory is correct. It may be necessary to observe rotation velocities for larger values of η for NGC 3198 and 2841. VLA should be able to do this by using a longer integration time. These two galaxies also share the benefit of very accurate distances due to the detection of cephid variables using the Hubble space-telescope.

A supercomputer is necessary to study the observations of [5], [7], and [15] in detail. However, there is a simple spiral-galaxy model which has $N=1$ in Eq. D.14—a single value α_1. In that case, a pc can calculate the rotation velocity profiles. The one-a model has a simple relation for the rotation velocity profile,

$$v(\omega, \mathrm{D}_{MPC}; \alpha_1, \xi) = (\xi / \xi_0)^{1/2} v(\omega, \mathrm{D}_{MPC}; \alpha_1, \xi_0), \tag{D.17}$$

where $\eta = \omega \mathrm{D}_{MPC} / 63.24$. Eq. (D.13) gives the density of H1 for large radii for this model and allows an estimate of required integration time for necessary accuracy.

A one-a model for a *hypothetical galaxy* (that mimics NGC 3198) would require $\mathrm{D}_{MPC} = 14.4$, $\alpha_1 = 0.07,$ and $\xi_0 = 55.$ This hypothetical galaxy is used below to illustrate and compare the larger radii behavior of the rotation velocity profiles for NCNG and GRLCDM.

The GRLCDM version of the hypothetical galaxy results from the following set of equations:

$$\begin{aligned}
&\Delta(x) = \xi_{GR}\,\alpha_1^3\left(\alpha_1^2 + x^2\right)^{-3/2},\\
&v_{GR}(\eta) = [v_M(\eta)^2 + v_H(\eta)^2]^{1/2},\\
&v_M(\eta)^2 = {v_0}^2\eta\int_0^\infty dx\, x\Delta(x)\,\mathrm{J}_1(x\eta),
\end{aligned} \tag{D.18}$$

where v_0 is found in Eq. D.7 and v_H below.

The spherically-symmetric dark matter halo is defined by the mass density, $\rho(r) = \rho_0[1+(r/R_c)^2+\gamma(r/R_c)^4]^{-1}$, where R_c is measured in kly and $v_{H0} = (4\pi G\rho_0 {R_c}^2)^{1/2}$ is a velocity measured in km/s. The dimensionless constant γ causes the dark matter halo to have a finite mass. Note that [7] uses $\gamma = 0$ (infinite halo mass). The halo equations are as follows:

$$\begin{aligned}
&\kappa = R_0 / R_c\\
&{v_H(\eta)}^2 = {v_{H0}}^2(\kappa\eta)^{-1}\,\mathrm{H}(\kappa,\gamma,\eta),\\
&\mathrm{H}(\kappa,\gamma,\eta) = \int_0^{\kappa\eta} dy\, y^2[1+y^2+\gamma y^4]^{-1},\\
&\xi_H = \kappa^{-1}(v_{H0}/v_0)^2\,\mathrm{H}(\kappa,\gamma,\infty),\\
&\mu = \xi_H / \xi_{GR},
\end{aligned} \tag{D.19}$$

where ξ_H is the *finite* mass of the dark matter halo in units of one billion solar masses and κ is dimensionless ($R_0 = 1$ kly). It is thought that the universal ratio of dark matter mass to ordinary matter mass is 5.6 in the LCDM cosmology. One should not expect that μ for this model would radically differ from 5.6.

The NCNG version of the hypothetical galaxy rotation velocity profile has three parameters: D_{MPC}, ξ_0, and α_1. The GRLCDM velocity profile has six parameters: D_{MPC}, α_1, κ, v_{H0}, ξ_{GR}, and ξ_H. The two profiles cannot be the same, so the only path forward is to use the extra parameters of GRLCDM to fit the two profiles to coincide for small radii and see where they diverge. This task requires defining an error function,

$$1 + \mathrm{E}(\eta) = v_{GR}(\eta) / v_{NCNG}(\eta), \tag{D.20}$$

where $\mathrm{E}(\eta_0) = 0$ for the smallest observed radius (η_0). Manipulations of Eq. (D.18) and Eq. (D.19) show that $\mathrm{E} = \mathrm{E}(\mu,\kappa,\gamma,\eta)$. Thus, the task requires finding the set of parameters (μ,κ,γ) that give the smallest E values for small radii. A tedious calculation of E gives the following result:

$$\begin{aligned}
&1 + \mathrm{E} = \mathrm{v}_{NCNG}(\eta_0)\,\mathrm{v}_{NCNG}(\eta)^{-1} M(\mu,\kappa,\gamma,\eta)^{1/2}\, M(\mu,\kappa,\gamma,\eta_0)^{-1/2},\\
&M(\mu,\kappa,\gamma,\eta) = G(\eta)I(\gamma) + \mu\eta^{-1}H(\kappa,\gamma,\eta),\\
&I(\gamma) = H(\kappa,\gamma,\infty),\\
&G(\eta) = \eta\int_0^\infty dx\, x\,\alpha_1^3\left(\alpha_1^2 + x^2\right)^{-3/2}\,\mathrm{J}_1(x\eta),
\end{aligned} \tag{D.21}$$

where $v_{NCNG}(\eta)$ is calculated using Eq. (D.1) through Eq. (D.17)—recall that $D_{MPC} = 14.4$, $\alpha_1 = 0.07$, $\xi_0 = 55$ for this hypothetical galaxy.

Eq. (D.21) gives $E(\mu,\kappa,\gamma,\eta_J)$ for each value of eta, where $\eta_J = 0.22770(j+1)\Delta\omega$ and $\Delta\omega = 30$ arc seconds. The three parameters (μ,κ,γ) need to minimize the errors for small values of eta. The error is automatically zero for 30 arc seconds. Three more constraints are needed,

$$0 = E(\mu,\kappa,\gamma,60'') = E(\mu,\kappa,\gamma,90'') = E(\mu,\kappa,\gamma,120''). \tag{D.22}$$

Eq. (D.22) is beyond my pc, so I have used $\kappa = 0.05$ and $E(\mu,0.05,\gamma,60'') = 0$ for the figures below.

FIG. D.2 below illustrates the rotation velocity profiles for NCNG and GRLCDM for this hypothetical galaxy. If NCNG is a correct theory, then *one would have observed* (using the 1982 Westerbork) the (solid) velocity profile. If GRLCDM is a correct theory, then *one would have observed* (using the 1982 Westerbork) the (dash) velocity profile for an (absurdly heavy) dark matter halo ($\mu = 200$), or the (dash-dot) velocity profile for a more reasonable halo ($\mu = 5.6$).

The two theories start diverging at 210 arc seconds—small compared to the 660 arc second limit of the 1982 Westerbork signal to noise ratio for this hypothetical galaxy. The NCNG profile is very similar to the actual 1982 NGC 3198 observations found in the source of [7]. Therefore, one can only realize that GRLCDM is a complete failure for NGC 3198.

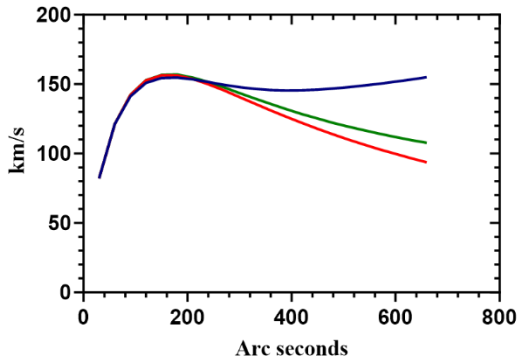

Figure D.2. Rotation velocities: (blue) NCNG, (green) GRLCDM mu = 200, (red) GRLCDM mu = 5.6.

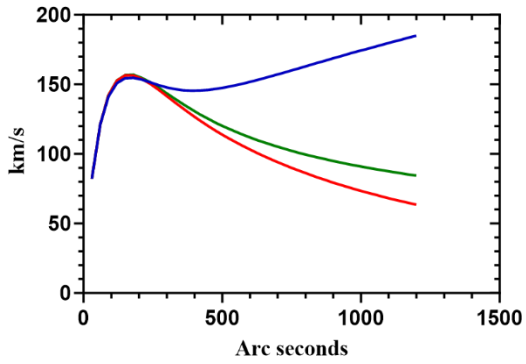

Figure D.3. The model of rotation velocities in FIG. D.2 extended to larger distances (not observable in 1982).

The equations above show that all NCNG rotation-velocity profiles will trend upward as η increases. However, GRLCDM profiles with finite-mass dark matter haloes will all trend downward. The surprise for me is that the two curves start diverging at a relatively small η. Furthermore, the GRLCDM profile dives while the NCNG profile creeps upward. One should expect that other galaxies will repeat this result. The original rational for dark matter was to flatten out the rotation-velocity profiles. I believe *that goal has not been met*, and GRLCDM should be discarded as a viable theory.

The equations above are an ideal model for a spiral galaxy—cylindrical symmetry and a thin disk of matter. Real spiral-galaxies are messy. They have bars, arms, lumps, bulges, warps, and so on. Suitable galaxies for study (using the equations above) are hard to come by.

The most important requirements (for a suitable galaxy) are an accurate distance (D_{MPC} determined using cephid variables) and an accurate rotation profile extending well beyond the likely theory-divergence point. One should discard near face-on or edge-on galaxies. As mentioned above, only two of the ten galaxies studied in [7] are suitable. NGC 3198 (Sb) has a faint bar and many faint arms wrapped around the galactic center—a reasonable model for cylindrical symmetry. Furthermore, there is very little warping except for the outermost observed η. I believe that the model for FIG, D.2 is sound.

Eventually, it will be necessary to extend rotation profiles beyond the limits of 1982 since the rate of upward trend is an important constraint on the universal constants of Eq. D.12.

APPENDIX E: CLASSICAL ORBIT EQUATIONS

The classical limit of Eq. (4.16) is found by substituting $\phi = \exp\left(R + i\hbar^{-1} I\right)$ into Eq. (4.16) and keeping only the largest terms in powers of $\hbar$. The result is the relativistic version of the Hamilton-Jacobi equation,

$$0 = -G^{\mu\nu}\left(\partial_\mu I\right)\left(\partial_\nu I\right) + m^2 c^2. \tag{E.1}$$

The weak-field limit for *G* is given by Eq. (5.14) and Eq. (5.15),

$$\begin{aligned} G^{00} &= (1 - br^{-1})^{-1}, \\ G^{rr} &= -(1 + br^{-1})^{-1}, \\ G^{\theta\theta} &= -r^{-2}, \\ G^{\phi\phi} &= -r^{-2}\sin^{-2}\theta. \end{aligned} \tag{E.2}$$

With no loss of generality, the orbit can lie in the plane where $\theta = \pi/2$, and Eq. (E.1) becomes,

$$0 = \left(1 - br^{-1}\right)^{-1} c^{-2}\left(\partial I/\partial\tau\right)^2 - \left(1 + br^{-1}\right)^{-1}\left(\partial_r I\right)^2 - r^{-2}\left(\partial_\phi I\right)^2 - m^2 c^2. \tag{E.3}$$

Hamilton's principle function, *I*, is as follows:

$$I = E\tau + A\phi + \mathrm{f}\left(r, E, A\right), \tag{E.4}$$

where *E* is the conserved total energy of the particle, and *A* is its conserved angular momentum. There are three conditions:

$$\begin{aligned} &\partial I/\partial E = 0 = \tau + \partial\,\mathrm{f}/\partial\,\mathrm{E}, \\ &\partial I/\partial A = 0 = \phi + \partial\,\mathrm{f}/\partial A, \\ &\left(1 + br^{-1}\right)^{-1}\left(\partial_r\,\mathrm{f}\right)^2 = \left(1 - br^{-1}\right)^{-1} c^{-2}E^2 - A^2 r^{-2} - m^2 c^2. \end{aligned} \tag{E.5}$$

Set $\sigma = r^{-1}$, and then a series of manipulations gives the orbit equation,

$$\left(d\sigma/d\phi\right)^2 = A^{-2}\left(1 + b\sigma\right)^{-1}\left[\left(1 - b\sigma\right)^{-1} c^{-2}E^2 - A^2\sigma^2 - m^2 c^2\right]. \tag{E.6}$$

Eq. (E.6) is accurate for $b\sigma << 1$—the weak-field condition.

To calculate the weak-field orbit from Eq. (E.6), expand the right-hand side as a power series in σ keeping terms only up to the first order in *b*. Then take the ϕ derivative to obtain the following:

$$d^2\sigma / d\phi^2 = R^{-1} - \sigma + \alpha\sigma^2, \tag{E.7}$$

where $R = A^2\left(GMm^2\right)^{-1}$ and $\alpha = \frac{3}{2}b = 3GMc^{-2}$. An approximate solution of Eq. (E.7) follows:

$$r^{-1} = R^{-1}\{1 + \varepsilon\cos[\phi\left(1 - \alpha R^{-1}\right)]\}. \tag{E.8}$$

Eq. (E.8) is the usual Newtonian orbit but with a small advance of perihelion per cycle. This advance is exactly the same as the famous general relativity prediction.

The path of a light ray through a central field is described by Eq. (E.7) as well by taking the limit where $m = 0$,

$$d^2\sigma / d\phi^2 = -\sigma + \alpha\sigma^2, \tag{E.9}$$

A weak-field solution to Eq. (E.9) yields

$$r^{-1} = R^{-1}\cos\phi + \beta\left(1 + \sin^2\phi\right), \tag{E.10}$$

where $\beta = \frac{1}{3}\alpha R^{-2}$ and $\phi = 0$ corresponds to perihelion (R is the impact parameter of scattering theory for the photon—the radius of the sun for an observation). The asymptotes of the path described by Eq. (E.10) are bent at a relative angle of $\Delta\phi = \frac{4}{3}\alpha R^{-1}$—the same as the famous GR prediction. The general relativity versions of the equations of this appendix are developed in [13].

There is another effect of interest, gravitational red shift. Consider a transverse electromagnetic wave-train moving radially outward in a central gravitational field. The wave-train will consist of 2N peaks within an expanding (thin) shell in a vacuum, The solution of Eq. (4.19) for the vector potential ($\mathrm{A}_\theta(\tau, r) = r^{-1}\sin(\psi)$) follows,

$$G_0^0 c^{-2}\partial^2\,\mathrm{A}_\theta / \partial\tau^2 = r^{-2}\partial_r(r^2 G_r^r \partial_r\,\mathrm{A}_\theta), \tag{E.11}$$

where $G_0^0 = (1 - br^{-1})^{-1}$ and $G_r^r = (1 + br^{-1})^{-1}$. The interpretation of Eq. (E.11) will follow the reasoning of section III(D). The argument of the potential can be defined as follows,

$$\psi(\tau, r) = 2\pi\lambda(r)^{-1}\xi(\tau, r)\,, \tag{E.12}$$

where $\xi = r - c\tau$ near the center of the wave train ($\xi = 0$). Substitute the potential into Eq, (E.11), and keep those terms which could survive in the limit ($\xi \to 0$),

$$
\begin{aligned}
&0 = G_r^r \partial_r^2 \psi + (\partial_r G_r^r)\partial_r \psi, \\
&\partial_r \psi = \lambda^{-1} - (\lambda^{-2}\partial_r \lambda)\xi \to \lambda^{-1}, \\
&\partial_r^2 \psi = -2\lambda^{-2}\partial_r \lambda + order(\xi) \to -2\lambda^{-2}\partial_r \lambda, \\
&2\partial_r \ln \lambda = \partial_r \ln G_r^r, \\
&\lambda(\infty)/\lambda(R) = (1+bR^{-1})^{1/2} \to (1-bR^{-1})^{-1/2} \text{ weak field.}
\end{aligned}
\tag{E.13}
$$

Eq. (E.13) is the usual weak-field result. $\lambda(\infty)$ is the observed wavelength (at an infinite distance from the origin) for a photon that was emitted with wavelength $\lambda(R)$ at a distance *R* from the origin. Furthermore, Eq. (E.12) indicates that observers at any distance from the origin will see the wave train moving with velocity c. Following the analysis of III(D), the shell contains a fixed number of photons (photons cannot be created or destroyed in flight through a vacuum). The result of Eq. (E.13) is *valid for an individual photon*. GR agrees with NG for local weak-field situations, but not for distal or strong field situations.

APPENDIX F: CANISTER DETAILS

Physics for the MDGO plasma is complicated by the extremely high temperature and extremely low density. One would find only a few thousand hydrogen and helium nuclei per cubic meter and an equal number of electrons—the mean free path for collisions between particles would be on the order of light year fractions. The high temperature (roughly 1 Kev energy) generates soft Xray photons (thermal bremsstrahlung) which interact with matter via Compton scattering. The photons will lose more energy in collisions with electrons compared to hydrogen or helium. Thus, the opacity of the gas is dominated by free electrons, but the tiny density of electrons causes the gas opacity to be nearly zero—a telescopic photograph of the gas will show an Xray expanse.

The energy source for the MDGO has four possible components, proton-proton fusion (in red or blue summer), gravitational Kelvin contraction (in all seasons), The NG version of a super-massive black-hole heat source within the MDGO, or shock waves from a collision between MDGOs in a container.

In a MDGO (free of shock waves), Kelvin contraction rules. That situation is studied below. A NG version of a super-massive black hole has a negligible effect on the MDGO, but it is much brighter and hotter than the Kelvin radiation of the MDGO. The Chandra Wolter-1 telescope had ten times better resolution compared to the best of the three Wolter-1s of the Newton observatory spacecraft. The Kelvin radiation can be obscured by a poorly resolved (active) black hole source in a Newton Xray camera shot of a distant canister. By comparison, a Chandra camera shot can show the Kelvin radiation more clearly. The radius of the MDGO (radius of the Kelvin radiation) is important below, so the limited number of Chandra camera shots is the only source of information about the size of MDGOs.

Kelvin contraction is a diffuse energy source. Thus, the three modes of heat transfer (conduction, convection, radiation) become marginalized (confined to eliminating local micro-imbalances). There are negligible gradients of pressure, temperature, and density within the MDGO. A good approximate model for MDGO density is $\rho(r,\tau)=\rho_0(\tau)$ for $r<\mathrm{R}_E(\tau)$ (else = 0), where τ is physical time and derivatives of $\rho_0(\tau)$ and $\mathrm{R}_E(\tau)$ are very small.

A solution for Eq. (5.5) uses the following functions:

$$
\begin{aligned}
b(q,r,\tau) &= \int_0^r dr' r' \rho(r',\tau)\sinh(r'\,\mathrm{L}_{gq}{}^{-1}),\\
c(q,r,\tau) &= \int_r^\infty dr' r' \rho(r',\tau)\exp(-r'\,\mathrm{L}_{gq}{}^{-1}),\\
B(r,\tau) &= \sum_{q=1}^{N_q} \mathrm{Z}_q\,\mathrm{L}_{gq}\,b(q,r,\tau)\exp(-r\,\mathrm{L}_{gq}{}^{-1}),\\
C(r,\tau) &= \sum_{q=1}^{N_q} \mathrm{Z}_q\,\mathrm{L}_{gq}\,c(q,r,\tau)\sinh(r\,\mathrm{L}_{gq}{}^{-1}),\\
\mathcal{A}_N(r,\tau) &= -4\pi G r^{-1}[B(r,\tau)+C(r,\tau)],\\
\mathrm{V}_{00}(r,\tau) &= 2c^{-2}\mathcal{A}_N(r,\tau).
\end{aligned}
\tag{F.1}
$$

There is a constraint for Eq. (F.1),

$$\begin{aligned} &\mathrm{M} = 4\pi\int_0^\infty r^2 dr\,\rho(r,\tau) = (4\pi/3)\rho_0(\tau)\,\mathrm{R}_E(\tau)^3, \\ &\partial_\tau \ln\rho_0(\tau) = -3\partial_\tau \ln \mathrm{R}_E(\tau). \end{aligned} \tag{F.2}$$

Eq. (F.1) can be solved in closed form,

$$\begin{aligned} &B(r,\tau) = \rho_0 \sum_{q=1}^{N_q} \mathrm{Z}_q\,\mathrm{L}_{gq}{}^3\,\mathrm{f}_q(r)\exp(-r\,\mathrm{L}_{gq}{}^{-1}), \\ &\mathrm{f}_q(r) = (r\,\mathrm{L}_{gq}{}^{-1})\cosh(r\,\mathrm{L}_{gq}{}^{-1}) - \sinh(r\,\mathrm{L}_{gq}{}^{-1}) \ \text{ for } r < \mathrm{R}_E(\tau), \\ &\mathrm{f}_q(r) = (\mathrm{R}_E(\tau)\,\mathrm{L}_{gq}{}^{-1})\cosh(\mathrm{R}_E(\tau)\,\mathrm{L}_{gq}{}^{-1}) - \sinh(\mathrm{R}_E(\tau)\,\mathrm{L}_{gq}{}^{-1}) \ \text{ for } r \ge \mathrm{R}_E(\tau), \\ &C(r,\tau) = \rho_0 \sum_{q=1}^{N_q} \mathrm{Z}_q\,\mathrm{L}_{gq}{}^3\,g_q(r)\sinh(r\,\mathrm{L}_{gq}{}^{-1}), \\ &g_q(r) = (1 + r\,\mathrm{L}_{gq}{}^{-1})\exp(-r\,\mathrm{L}_{gq}{}^{-1}) - (1 + \mathrm{R}_E\mathrm{L}_{gq}{}^{-1})\exp(-\mathrm{R}_E\mathrm{L}_{gq}{}^{-1}) \ \text{ for } r < \mathrm{R}_E(\tau), \\ &g_q(r) = 0 \ \text{ for } r \ge \mathrm{R}_E(\tau), \\ &\mathcal{A}_N(r,\tau) = -4\pi G r^{-1}[B(r,\tau) + C(r,\tau)]. \end{aligned} \tag{F.3}$$

The radius of an equilibrium MDGO (R_E) is an observable since it can be inferred from soft Xray photography. The gravity field of this type of MDGO becomes a function of M and R_E. The velocity dispersion for galaxies orbiting within the field determined by Eq. (F.1) and Eq. (F.3) should provide a method for estimating M. As shown in section V(B), the virial theorem is unreliable for gravitating objects of galactic size or larger, so a new approach is required (beyond the scope of this document).

The gravitational potential of the mass within an equilibrium MDGO,

$$\mathcal{E}_G(\tau) = 4\pi\rho_0(\tau)\int_0^{\mathrm{R}_e(\tau)} r^2 dr\,\mathcal{A}_N(r,\tau), \tag{F.4}$$

can be calculated in closed form using the equations above. Furthermore, the power balance for Kelvin contraction is as follows,

$$d\mathcal{E}_G / d\tau = -\varsigma_X L_{sun}, \tag{F.5}$$

where the MDGO Xray luminosity is proportional to solar luminosity (L_{sun}). The dimensionless factor ς_X is an observable. The potential energy is as follows,

$$
\begin{aligned}
&\mathcal{E}_G = -9G\,\mathrm{M}^2\mathrm{R}_E^{-1}\sum_{q=1}^{3}\mathrm{Z}_q x_{Eq}^{-5} I(x_{Eq}),\\
&I(x_{Eq}) = a(x_{Eq}) - b(x_{Eq})\exp(-2x_{Eq}),\\
&a(x_{Eq}) = 0.5 + (x_{Eq}^{\,3}/3) - (x_{Eq}^{\,2}/2),\\
&b(x_{Eq}) = 0.5 + x_{Eq} + (5x_{Eq}^{\,2}/8),
\end{aligned}
\qquad \text{(F.6)}
$$

where $x_{Eq} = \mathrm{R}_E \mathrm{L}_{gq}^{-1}$. Plausible units are needed to estimate the rate of contraction for a heavy MDGO:

$$
\begin{aligned}
&\mathrm{M}_{GB} = 10^{14} \text{ solar masses},\\
&\mathrm{R}_{GB} = 10^{6} \text{ light years},\\
&\mathrm{M} = \varsigma_M\,\mathrm{M}_{GB},\\
&\mathrm{R}_E(\tau) = \varsigma_R(\tau)\,\mathrm{R}_{GB},\\
&\tau_{GB} = G\,\mathrm{M}_{GB}^{\,2}\mathrm{R}_{GB}^{\,-1} L_{sun}^{\,-1} = 2.310\ \mathrm{x}10^{22} \text{ years},\\
&\mathcal{E}_G \equiv -\varsigma_M^{\,2}\tau_{GB} L_{sun}\,\mathrm{F}_{GB}(\mathrm{R}_E).
\end{aligned}
\qquad \text{(F.7)}
$$

The equations above lead one to a Xray luminosity relation for this type of MDGO,

$$
\varsigma_X = \varsigma_M^{\,2}(\tau_{GB}/\Delta\tau)[\mathrm{F}_{GB}(\mathrm{R}_E - \Delta\mathrm{R}_E) - \mathrm{F}_{GB}(\mathrm{R}_E)], \qquad \text{(F.8)}
$$

where $\Delta\tau$ is a duration of interest ($\Delta\mathrm{R}_E$ is the shrinkage). For example: use Eq. (5.10), $\Delta\tau = 6.4\mathrm{x}10^{10}$ years (summer duration), $\varsigma_M = 1$, $\varsigma_R = 2$, and $\Delta\varsigma_R = 2\mathrm{x}10^{-6}$, then $\varsigma_X = 8.66\,\mathrm{x}10^{10}$ ($\varsigma_X = \Delta\varsigma_R\, 4.33\mathrm{x}10^{16}$).

Contraction is an extremely slow mechanism that produces a vast amount of energy for gravitating objects of canister size and huge mass—MDGOs being the most massive objects in the universe. Contraction will be revisited in section VIII about NCNG stability.

Using the same parameters as the preceding example, the red summer solution of Eq. (F.1) gives some important characteristics for a single heavy MDGO canister. The size of the canister is $\mathrm{R}_{nul} = 11.78$ MLY. The height of the (summer) repulsive barrier corresponds to 1480 km/s—only objects with radial velocities greater than 1480 km/s can enter the summer canister. A negligible amount of matter will enter during summer. The gravitational redshift at the center of the MDGO relative to the outside of the canister is $\mathrm{z}_{gravity} = 0.00202$. The escape velocity for matter located at R_E is 15013 km/s (0.050 *c*). It is obvious that negligible matter can enter or escape this canister in summer. These values show that *this gravitational well is very deep*. The doppler red shift of galaxies in the canister will be of order $\mathrm{z}_{gravity}$, so one must account for the radial distance of galaxies when studying velocity dispersion. The study of dispersion is complicated by the fact that our earthly observer is in a canister of unknown position, size, or depth. Note that velocities are directly proportional to MDGO mass (other factors being equal). In some cases where there is

more than one MDGO in a canister, I believe that the solution above can be used to obtain a canister field that is the superposition of the separate MDGO fields.

APPENDIX G: FILAMENT DETAILS

The fact that V_{00} is a function of two variables dooms any possibility for familiar or easy to calculate orbits. There are only two special cases ($r=0$ or $z=0$) which yield (complicated) results that don't require a super-computer. The probability of a special case is negligible.

The canister-sources are assumed to be near the bottoms of their gravitational wells—small orbits with small velocities. V_{00} is proportional to the source mass, (ξ_S solar) and for this example, $\xi_S = 10^{12}$, a modest mass. The special cases follow.

For $r=0$, one has the following:

$$\begin{aligned} &V_{00}(0,z) = V_{00}(0,0) + \alpha z^2, \\ &\alpha = 1.6576 \text{x} 10^{-19} \text{ ly}^{-2}, \\ &\partial_t^2 z(t) = -.5c^2(\partial_z V_{00})_{z=z(t)} = -\omega^2 z(t), \\ &\omega^2 = c^2\alpha, \\ &period = 2\pi c^{-1}\alpha^{-1/2} \text{ years}, \\ &V_{00}(0,0) = -4.590 \text{x} 10^{-6}, \end{aligned} \quad , \qquad \text{(G.1)}$$

where z has units of light-years. The period is 15.43 billion years. A similar calculation for $z=0$ yields a period of 1.24 trillion years. These results indicate that canister-sources in the frame chain are weakly bound.

A rogue passing near a canister-source will have a greater velocity than the canister-source. This meeting will provide an impulse to the canister-source—a new velocity in some random direction. Dislodgement of a canister-source can only be the result of a random walk. The orbits of rogues within the chain gravity need to be calculated to establish the mean time between dislodgements for a canister-source. This problem is hopelessly complex. For example, one must include the collisions between orbiting rogues (more likely than a collision with a canister-source).

There is another complication. It is possible for a durable equilateral triangle of canister-sources to form on a chain—one of the triangle sides are two pre-existing members of the chain with one new outlier canister-source. The outlier can be the start of a new chain heading in a random direction (a kink). The probability of such a formation is very small, but there are eons available to wait. *There is no end to the complexity of this topic*.

APPENDIX H: SOURCE MASS SPECTRUM DETAILS

It is necessary to convert Eq. (6.7) into dimensionless form for a numerical solution. MKS units of density (ρ_c) and pressure (P_c) are required. They can be arbitrary, but it is useful if they correspond to a specific point in the EOS that will be used (Table 3 and Table 5 of [9]). I have chosen the following MKS values,

$$\begin{aligned} \rho_c &= 1.0748 \,\mathrm{x}\, 10^{18}, \\ \mathrm{P}_c &= 1.6930 \,\mathrm{x}\, 10^{34}. \end{aligned} \tag{H.1}$$

The following dimensionless set will be used:

$$\begin{aligned} & r = R_c x \ , \\ & \rho = \rho_c \theta(x) \ , \\ & R_c^{-2} = 8\pi G \rho_c c^{-2}, \\ & \mathrm{P} = \mathrm{P}_c \psi(x) \ , \\ & \chi_c = \mathrm{P}_c / \rho_c c^2 \ , \\ & \mathrm{M}_c \equiv 4\pi \rho_c R_c^{\ 3} = \kappa_c \ \text{(solar masses)}. \end{aligned} \tag{H.2}$$

The numerical values follow:

$$\begin{aligned} R_c &= 7.0606 \text{ km}, \\ \kappa_c &= 2.3908, \\ \chi_c &= 0.17526 \ . \end{aligned} \tag{H.3}$$

The dimensionless form for Eq. (6.7) follows:

$$\begin{aligned} & Q(V) \equiv 1 + H(V), \\ & U = -x(\partial V / \partial x), \\ & (\partial V / \partial x) = -x^{-2} \int_0^x dx' \, x'^2 \theta(x') (\partial Q^{-1} / \partial V)_{x'} \ , \\ & \partial \ln\theta / \partial x = -[2\chi_c (\partial \psi / \partial \theta)]^{-1} (\partial V / \partial x)[Q(-U)^{-1} (\partial Q / \partial V)] \ , \\ & M_{gravity}(x) = \kappa_c (x^2 \partial V / \partial x) \ \text{ solar masses}. \end{aligned} \tag{H.4}$$

The EOS information is confined to $\partial\psi / \partial\theta$ (a function of θ). There are three EOS regions of interest that allow $\partial\psi / \partial\theta$ to be formed into a connected function of theta. The lowest density region consists of EDM—EOS defined by Eq. (8.5), Eq. (8.15), and Eq. (8.16) of [14]. The middle density region consists of neutron star matter—EOS defined by table 3 and table 5 (cgs units) of

[9]. The (hypothetical) highest density region consists of a quark-gluon phase outlined in [15]. There are changes of phase between each region, so $\partial\psi / \partial\theta$ will have discontinuities between the regions. The quark-gluon phase would only play a role in the source for an MBO of incredible mass ($> 3\text{x}10^{10}$ solar masses). Such objects are thought to exist (possibly at the center of a very massive MDGO within a heavy canister).

The boundary conditions are $U(0) = 0$, $V(0) = V_0$, and $\theta(0) = \theta_0$. A trial solution is generated using V_0 and θ_0. A correct solution is found for that value of θ_0 for which $0 \le 1 - (U(x_{edge}) / V(x_{edge})) < \varepsilon$, where I have chosen $\varepsilon = 10^{-6}$. The numerical solutions use the constants of Eq. (6.13). The gravitational mass of an object is evaluated at the edge, $M = M_{gravity}(x_{edge})$.

Numerical solutions yield the following set of figures for three types of (cold) summer sources. In these figures, mass is in units of solar masses, size is in km, and rho0 is the density at the center (kg/m^3). The mass and size are single valued functions of the (negative) gravitational potential at the center (V_0). The bottom end of each figure represents the least negative potential, and the top end is the most negative potential (deepest in the potential well). The lower end of Fig. H.2 is a limit. Both ends of Fig. H.3 are limits. For Fig. H.4 the lightest mass is to the right, and mass increases moving to the left. For MBOs the gravitational mass is equal to the inertial mass.

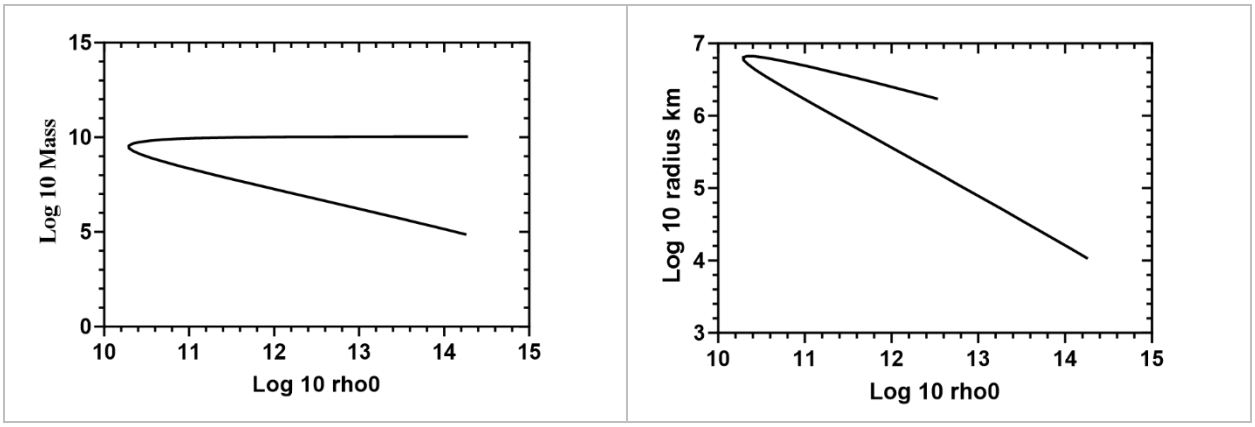

Figure H.1. Gravitational summer mass and source size of a MBO versus central density.

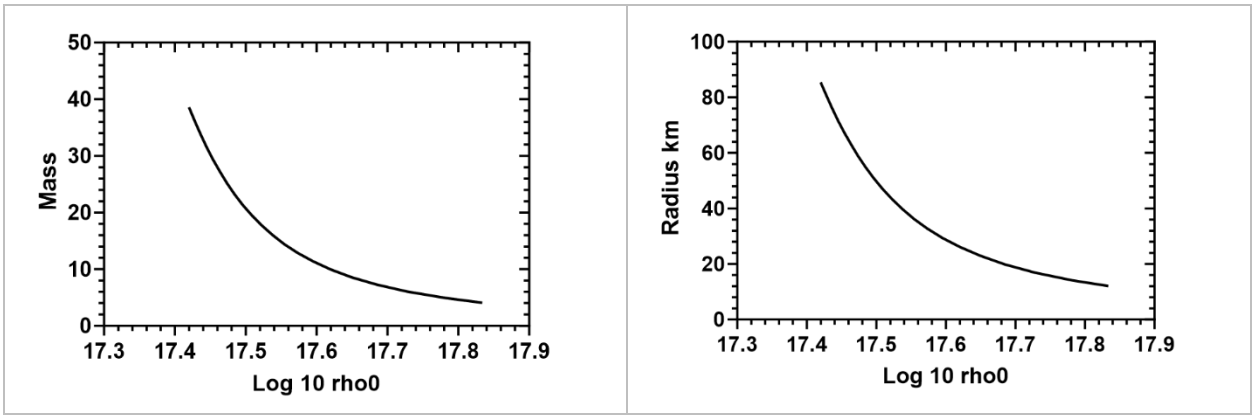

Figure H.2. Gravitational summer mass and size of the source of a CCBO versus central density.

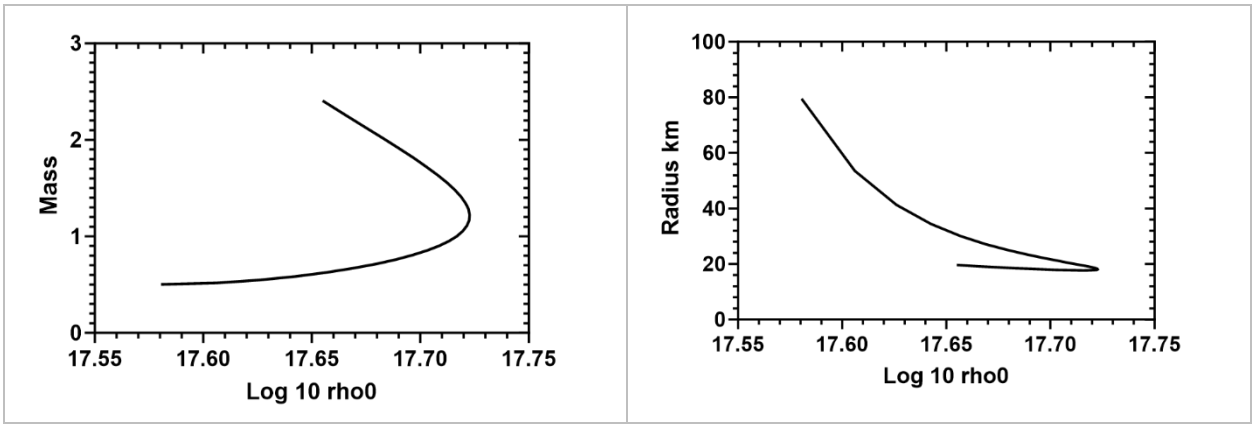

Figure H.3. Gravitational summer mass and size of the source of a CCNS versus central density.

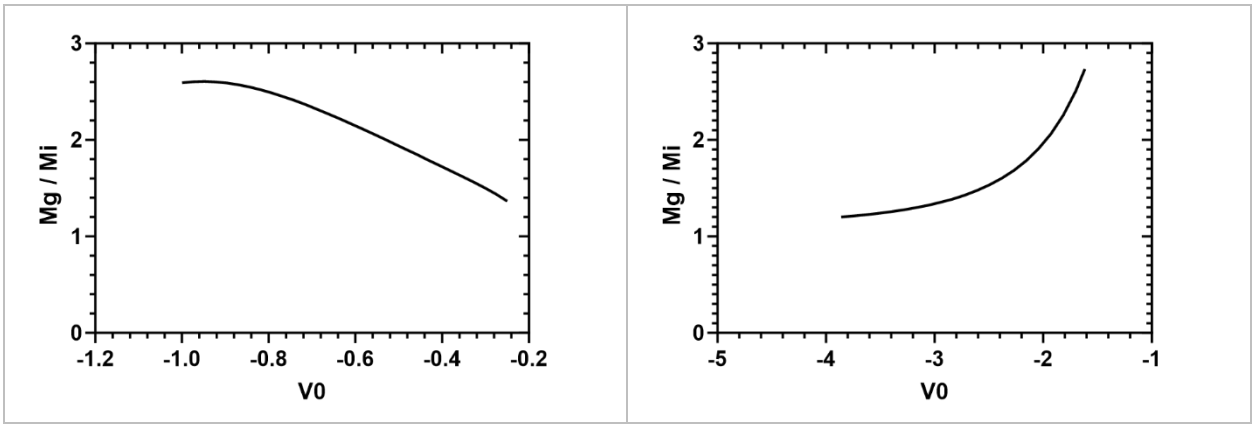

Figure H.4. Gravitational mass/inertial mass versus V0 for CCNS (left) and CCBO (right).

APPENDIX I: NEUTRINO INITIATED PROCESS AND ATTENUATION DETAILS

For the $\{\}=0$ subset of processes, define a dimensional transitional time, T_{fi}, (seconds) in the following manner:

$$\begin{aligned} \tau_{HALF}{}^{-1} &\equiv T_{fi}^{-1} F_S, \\ F_S &= \int_1^{y_m} y dy \left(y^2-1\right)^{1/2} \left(y_m - y\right)^2, \end{aligned} \tag{I.1}$$

where F_S is the dimensionless density of final states function, τ_{HALF} *is the summer half-life of the positron decay for the inverse* NIP (seconds), $y_m = \Delta E / m_e c^2$, and $\Delta E = \left[m(A.Z+1)_j - m(A,Z)_0 \right] c^2$. Coulomb final state effects have been neglected in F_S. The reaction cross section in winter can be derived as follows:

$$\begin{aligned} &\mathrm{v}\left(E_\nu\right)\sigma_{fi}\left(E_\nu\right) \equiv \xi_{RN}\, \mathrm{V}_W\, T_{fi}^{-1} F_0\left(E_\nu\right), \\ &F_0\left(E_\nu\right) = (x-y_m)[(x-y_m)^2-1]^{1/2}, \\ &\mathrm{v}\left(E_\nu\right) = c\left[1-\left(m_{ve}^W c^2 / E_\nu\right)^2\right]^{1/2}, \\ &\xi_{RN} = \left(g_W^W m_W^S / g_W^S m_W^W\right)^4, \end{aligned} \tag{I.2}$$

where E_ν is the *total* energy of the massive neutrino, v is the massive neutrino velocity, $\mathrm{V}_W = 2\pi^2 \left(\hbar / m_e\, c\right)^3$ is a characteristic volume, F_0 is the dimensionless density of states function, $x = E_\nu / m_e c^2$, y_m is the same as in Eq. (I.1). In summer, $\xi_{RN} = 1$, but in winter it will need to be extremely large.

For initial target states that are stable, there is experimental data for some of the lighter nuclei that allows the determination of T_{fi}. Consider the important NIP, $\nu_e + \mathrm{C12} \rightarrow \mathrm{N12} + e^-$, where $\Delta E = 16.827$ Mev, $\tau_{HALF} = 0.01163$ s, and then $T_{fi} = 14940$ s for use in Eq. (I.2). For proton-rich states unstable in summer, the experimental data is sparse, so estimates are necessary.

In the case where {} corresponds to the final state H1 or He4, the reaction rate is given by Eq. (I.2) with F_0 replaced by F_1 defined as follows:

$$F_1 = \int_0^y dx(1+x)(y-x)^{1/2}[(1+x)^2-1]^{1/2}, \tag{I.3}$$

where $y = (E_\nu - \Delta E) / m_e c^2$, and $\Delta E = [m(A-a, Z-z+1) + m(a,z) + m_e - m(A,Z)]c^2$. Until more accurate calculations are made, these approximations can be used. The density of states function

is known given E_ν, leaving T_{fi} as the only unknown for each NIP. Note that the T_{fi} for the F_1 group are not directly comparable to the T_{fi} for the F_0 group since they represent different processes.

There is an approximation for all the NIPS that is useful—intermediate states. The NIP can be separated into two sequential steps:

$$\begin{aligned} &\nu_e + [A,Z]_0 \rightarrow [A,Z+1]_j + e^- \rightarrow \\ &[A-a,Z-z+1]_0 + \{a,z\} + e^-. \end{aligned} \tag{I.4}$$

Here, it is assumed that the intermediate state is created via Eq. (I.2) and then, if the intermediate state is unstable against proton emission, one or more protons are emitted (possibly in a cascade) until a nuclide stable against proton emissions results. Only the reaction cross section of the first step is needed for attenuation since any subsequent strong decays occur instantly on the cosmic time scale. There is no experimental data for positron decays of proton emitters in summer, since the extremely rapid strong decay dominates, i.e., T_{fi} in Eq. (I.1) is unknown. In many cases the nuclear spin and parity are known for target and intermediate state, so one can estimate T_{fi} based on whether the decay would be favored, allowed, or forbidden.

An important NIP is the attenuation of He4 (ground state = 0+ spin/parity). In that case, the intermediate state is Li4 (ground state = 2- spin/parity) and a transition would be first forbidden and not favored. Li4 has an excited state at 0.320 Mev (1- spin/parity), and that transition would be first forbidden and favored—100 times smaller T_{fi} than the ground to ground transition. First forbidden T_{fi} is typically 10^4 times the favored value. Thus, a reasonable estimate for the excited intermediate transition is $T_{fi} = 5\times10^7$ seconds and $\Delta E = 22.71$ Mev to be used in Eq. (I.1). The resulting cross section is *smaller than for all other target nuclides*, and that is why He4 is the only significant neutron-bearing nuclide left when the neutrinos are exhausted.

Using the chart of nuclides, it is possible to obtain the attenuation chain for the ground state of any nuclide. One follows the path of the first half of Eq. (I.4) until a proton emitter is encountered, then drop down a path of constant neutron number, (A-Z), to a proton non-emitter. No entry on the chart of nuclides counts as a proton emitter since that would be a state of negative binding energy. These chains are independent of the cross sections. By absorbing one neutrino, a specific target nuclide can be converted into only one specific resulting nuclide, but more than one target nuclide can contribute to a specific resulting nuclide. Two important chains will illustrate this process: O16-O15-O14-O13-C10-C9-He4 (summarized by $6\nu(e) + \mathrm{O16} \rightarrow \mathrm{He}\,4 + 12p^+ + 6e^-$) and C12-N12- C10-C9-He4. C10 can be made from both O13 and N12.

The intermediate state approximation has unknown accuracy, but it is a reasonable guide to the *relative* sizes of some of the cross sections—important for the overall attenuation pattern. There are many steps along the chains for which there is insufficient chart-data to use this approximation—one must use generic cross sections instead.

The physical time evolution during winter of the set, $Y_j(\tau) = N(j,\tau)/N_{RN}$, is as follows:

$$\begin{aligned} dY_j / d\tau &= -Y_j / \mathrm{T}_j + \sum_n \mathrm{B}_{jn} Y_n / \mathrm{T}_n , \\ \mathrm{T}_j(\tau)^{-1} &= \int_0^\infty dE_\nu \; n_\nu(E_\nu, \tau)\, \mathrm{v}\left(E_\nu\right) \sigma_j\left(E_\nu\right). \end{aligned} \tag{I.5}$$

The combining matrix, B_{jn}, has either one or two nonzero entries $(=1)$ determined from the attenuation chains for each nuclide. The time constant, $\mathrm{T}_j(\tau)$, is measured in seconds and depends on physical time. It can be simplified using Eq. (7.6) as follows:

$$\mathrm{T}_j(\tau)^{-1} = \Gamma T_{fi}(j)^{-1} \sum_{k=1}^{K} \mathrm{P}_k(\tau)\, F\left(j, E_{\nu k}\right), \tag{I.6}$$

where the parameters defined after Eq. (I.2) are used to obtain $\Gamma = \xi_{RN}\, \mathrm{V}_w\, N_{RN}$, a dimensionless scaling factor for time duration. $F\left(j, E_{\nu k}\right)$ is either $F_0\left(E_{\nu k}\right)$ as in Eq. (I.2), or $F_1\left(E_{\nu k}\right)$ as in Eq. (I.3) depending on the final state of the attenuation of nuclide *j*. The evolution of the neutrino spectrum is as follows:

$$d\mathrm{P}_k / d\tau = -\mathrm{P}_k \Gamma \sum_j Y_j\left(\tau\right) T_{fi}(j)^{-1} F\left(j, E_{\nu k}\right), \tag{I.7}$$

where $F = F_0$ or F_1 as in Eq. (I.6).

The coupled set, Eq. (I.5) and Eq. (I.7), can be solved numerically subject to the following boundary conditions: (1) P_k and Y_j are continuous across (red or blue) spring or fall transitions. (2) The set, $E_{\nu k}$, are changed when $m_{\nu e}$ changes. (3) $Y_j\left(0\right)$ is determined by the abundance of stable nuclides at the end of red or blue fall. (4) The relic neutrino density ratio, $RNDR = N_\nu\left(\text{winter-end}\right) / N_\nu\left(\text{winter-start}\right)$, constrains the duration of winter. The proton and neutron densities are of interest:

$$\begin{aligned} N_p &= N_{RN} \sum_j Z_j Y_j , \\ N_n &= N_{RN} \sum_j \left(A_j - Z_j\right) Y_j . \end{aligned} \tag{I.8}$$

Although it is not obvious, Eq. (I.5) and Eq. (I.7) satisfy Eq. (7.2), so there are two constraints when antineutrinos are neglected:

$$\begin{aligned} 1 &= \sum_j A_j Y_j , \\ \vartheta_{RN} &= \sum_j \left(A_j - Z_j\right) Y_j - \sum_k \mathrm{P}_k . \end{aligned} \tag{I.9}$$

I have chosen $\vartheta_{RN} = 0.125$ and $RNDR = 10^{-4}$ for this model. A numerical solution of Eq. (I.5) and Eq. (I.7) has been carried out for the model and parameters described above.

The results are summarized in four figures that appear in section VII(C.4), but the main observation is simple enough—*almost all of winter is spent attenuating* He4 and He3. All other nuclides could be neglected to a good approximation. The poorly known universal constant, N_{RN}, has no real impact on the pattern of evolution. This model requires $\xi_{RN} N_{RN} = 8.873 \times 10^{21}$, so if $N_{RN} = 0.25$, then $\xi_{RN} = 3.549 \times 10^{22}$. The parameter ξ_{RN} represents a constraint on two of the new universal constants (m_W^W and g_W^W).

APPENDIX J: SOURCES FOR EQ. (4.22)

I will concentrate on a non-relativistic scalar boson source defined by Eq. (4.16) in this appendix. For that case, the LDM will be as follows for cartesian coordinates,

$$\begin{aligned}
&\mathcal{L}_M = \mathcal{L}_M{}^{\mathrm{T}} - \mathcal{L}_M{}^{\mathrm{V}},\\
&\mathcal{L}_M{}^{\mathrm{T}} = \mathcal{N}\, G^{\alpha\beta}\partial_\alpha\phi(x)\partial_\beta\phi(x)^*,\\
&\mathcal{L}_M{}^{\mathrm{V}} = \mathcal{N}\, \mathrm{L}^{-2}\,\phi(x)\phi(x)^*,\\
&\mathrm{L}^{-1} = mc/\hbar\ ,
\end{aligned} \tag{J.1}$$

where $\mathcal{N}$ is a normalization constant. $\mathcal{L}_M$ has dimensions of energy density divided by *c*. The energy density for this non-relativistic particle is dominated by $c\mathcal{L}_M{}^{\mathrm{V}}$, and the following results,

$$\int d^3x \mathcal{N}\,\mathrm{L}^{-2}\left|\phi(x)\right|^2 = mc. \tag{J.2}$$

The Schrodinger wave function comes from $\phi\left(x_0,\mathbf{x}\right)=\psi\left(\tau,\mathbf{x}\right)\exp\left(ix_0\,\mathrm{L}^{-1}\right)$, where $x^0 = c\tau$. The *weak field* source for Eq. (4.22) is then as follows,

$$J_{00}(q,\tau,\mathbf{x}) = -Q_{GC}(q,\mathrm{E})\kappa_q\{\mathcal{N}\,\mathrm{L}^{-2}\left|\psi(\tau,\mathbf{x})\right|^2\}, \tag{J.3}$$

where *the other components of* $J_{\mu\nu}$ *are negligible*. The mass of the "particle" could have any value—an electron, a stellar mass object, or even a galaxy. The classical limit for a source (being treated as a point) is given by using Eq. (J.2) and Eq. (J.3),

$$\{\mathcal{N}\,\mathrm{L}^{-2}\left|\psi(\tau,\mathbf{x})\right|^2\} \to mc\delta^3(\mathbf{x}-\mathbf{X}(\tau)), \tag{J.4}$$

where δ^3 is the three-dimensional Dirac delta function, and $\mathbf{X}(\tau)$ is the vector position of the point source as a function of physical time. Thus, Eq. (4.22) for a point source in cartesian coordinates is given by,

$$\nabla^2\,\mathrm{v}_{00}(q,\tau,\mathbf{x}) - \mathrm{L}_{gq}^{-2}\mathrm{v}_{00}(q,\tau,\mathbf{x}) = 8\pi G mc^{-2}Q_{GC}(q,\mathrm{E})\,\mathrm{Z}_{gq}\,\delta^3(\mathbf{x}-\mathbf{X}(\tau)), \tag{J.5}$$

where *G* is the Newtonian gravitational constant. $Q_{GC}(q,\mathrm{E})$ is defined in section IV(D) and Z_{gq} is defined in section V(B). The S_0 and N_0 terms of Eq. (4.22) cancel out the time derivatives of v_{00} and the time derivatives of other components will be ignorable for most problems of interest. An exception would be the generation of strong gravitational waves from matter in accelerated paths.

Eq. (J.5) is linear so a collection of N point sources with different positions will generate a gravitational field which is the sum of the individual solutions of Eq. (J.5).

APPENDIX K: CANISTER CENTRAL FIELD ORBITS

The goal of this Appendix is to find a static central-field solution of Eq. (4.22) when the source is a MDGO. Inhomogeneous solutions for all four diagonal potentials are required for orbit calculations. The canister fields will be strong enough so that orbits will have significant advance of the radial turning points.

One starts with the inhomogeneous solutions of the polar coordinate version of Eq. (4.22), using the following components:

$$\begin{aligned} V(q,r) &\equiv \mathrm{v}_0^0(q,r), \\ U(q,r) &\equiv -\mathrm{v}_r^r(q,r), \\ W(q,r) &\equiv -\mathrm{v}_\theta^\theta(q,r), \\ Z(q,r) &\equiv -\mathrm{v}_\phi^\phi(q,r). \end{aligned} \tag{K.1}$$

One must have no off-diagonal components, so $Z = W$. A tedious calculation using Eq. (4.20) leads to three independent equations:

$$J_0\theta = r^{-2}\partial_r(r^2\partial_r V) - \mathrm{L}_{gq}^{-2} V, \tag{K.2}$$

$$\begin{aligned} J_0\theta &= -\partial^2{}_r V - 2r^{-1}\partial_r U - \mathrm{L}_{gq}^{-2} U + 2\partial^2{}_r W + 4r^{-1}\partial_r W, \\ J_0\theta &= -r^{-1}\partial_r V - r^{-1}\partial_r U - 2r^{-2}U + \partial^2{}_r W + 4r^{-1}\partial_r W + (2r^{-2} - \mathrm{L}_{gq}^{-2})W, \end{aligned} \tag{K.3}$$

where J_0 is a constant and $\theta = 1$ for $r < \mathrm{R}_E$ and $\theta = 0$ for $r > \mathrm{R}_E$. In what follows, the unit of length will be 10^6 light-years, and the mass of the MDGO will be in solar masses. The potentials *V, U,* and *W* are dimensionless, and the radial length (*r*) in the equations above is in the 10^6 light-years unit. The source term is given as follows:

$$\begin{aligned} J_0 &= \kappa \mathrm{M} Z_{gq} \mathrm{L}_{gq}{}^2 \mathrm{R}_E{}^{-3}, \\ \kappa &= 9.374432 \,\mathrm{x}\, 10^{-19}, \end{aligned} \tag{K.4}$$

where M is in solar masses, Z_{gq} is dimensionless, and both L_{gq} and R_E are in the 10^6 light-year units. The boundary conditions for these equations are as follows:

$$\begin{aligned} &U(0) = W(0), \\ &\partial_r V(0) = \partial_r U(0) = \partial_r W(0) = 0, \\ &V(\infty), U(\infty), W(\infty) \to 0. \end{aligned} \tag{K.5}$$

Eq. (K.2) is solved in closed form using the techniques of Appendix F. Substitute Eq. (K.2) into the set of Eq. (K.3)—eliminate J_0. One discovers a simple solution,

$$V(q,r) = U(q,r) = W(q,r). \tag{K.6}$$

Is Eq. (K.5) the only solution? The answer is yes, but not easy to prove. Introduce two functions f and g (where $U = \mathrm{f}\,V$ and $W = gV$) into Eq. (K.3). A numerical solution for the resulting equations for f and g shows that f and g can be of order unity at a (growing) finite value of r only if they are (shrinkingly) infinitesimally close to $\mathrm{f} = \mathrm{g} = 1$. For example, if $r = 15\,\mathrm{L}_{gq}$ then f and g must be less than 10^{-15} away from 1 otherwise f and g become very large.

Orbit calculations require the techniques of Appendix E plus Eq. (4.14). The Hamilton-Jacobi equations for the orbit of a non-zero mass object (an electron or a galaxy) moving under the influence of the gravitational fields above are modified in the following manner. Eq. (E.2) for the weak field becomes the following:

$$\begin{aligned} &\mathrm{V}(r) \equiv \sum_{q=1}^{N_q} \mathrm{v}_{00}(q,r) \quad \text{summer,} \\ &G^{00} = 1 - \mathrm{V}, \\ &G^{rr} = -(1+\mathrm{V}), \\ &G^{\phi\phi} = -r^{-2}(1+\mathrm{V}). \end{aligned} \tag{K.7}$$

The orbit lies in a plane ($\theta = \pi/2$), and there is no theta dependence. Eq. (E.5) becomes the following:

$$\begin{aligned} &\partial I/\partial E = 0 = \tau + \partial\,\mathrm{f}/\partial\,\mathrm{E}, \\ &\partial I/\partial A = 0 = \phi + \partial\,\mathrm{f}/\partial A, \\ &\left(\partial_r\,\mathrm{f}\right)^2 = (1-\mathrm{V})\left(1+\mathrm{V}\right)^{-1} c^{-2}E^2 - A^2 r^{-2} - m^2c^2\left(1+\mathrm{V}\right)^{-1}. \end{aligned} \tag{K.8}$$

A series of manipulations leads to the following result:

$$\begin{aligned} &(dr/d\phi)^2 = r^4 R_a^{-2}[\alpha^2(1-\mathrm{V}) - 1](1+\mathrm{V})^{-1} - r^2, \\ &d\tau/d\phi = r^2 \alpha R_a^{-1}(1-\mathrm{V})(1+\mathrm{V})^{-1}, \end{aligned} \tag{K.9}$$

where $\alpha = \mathrm{E}/mc^2$ and $R_a = A/mc$. Alpha is dimensionless, tau has a unit of 10^6 years, and both R_a and r have units of 10^6 light-years,

Any orbit for a given gravitational field (V) is completely determined by α and R_a. Orbits of interest will be bounded since the escape velocity at $r = 2$ for a typical canister is $0.05c$ (radial component of orbital velocity). Thus, $\alpha < 1$. It is convenient to define $\alpha = 1 - \varepsilon$ where $0 < \varepsilon << 1$. An orbit will have turning points, $R_{OUT} \geq r \geq R_{IN}$. If $R_{OUT} \neq R_{IN}$ (not circular) the orbit will not close, and the orbiting object will never revisit a specific point in space.

Fig. K1 illustrates the complexity of a non-circular orbit. The specifications for FIG. K1 are as follows:

$$
\begin{aligned}
&\mathrm{M} = 10^{14} \ \text{ see Fig. 1,}\\
&\mathrm{R}_E = 2,\\
&\varepsilon = 0.0007,\\
&R_a = 0.06,\\
&R_{IN} = 1.416,559,\\
&R_{OUT} = 2.429637,\\
&\text{period } = 426.52 \text{ million years,}\\
&\text{advance = } 53.8804 \text{ degrees.}
\end{aligned}
\qquad \text{(K.10)}
$$

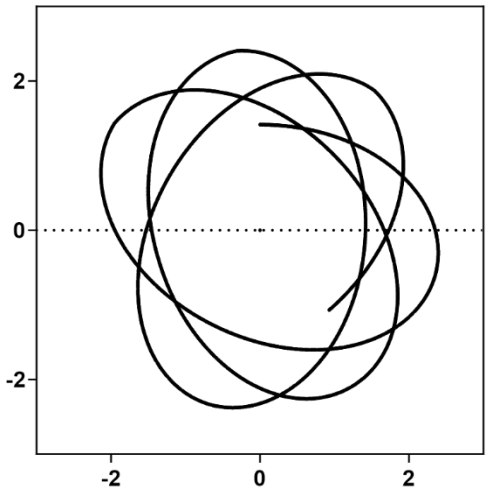

Figure K.1. Advance of galactic orbits within the MDGO of a canister.

The advance is the difference of phi for any two *nearest* points where $r = R_{0UT}$. The period is defined as the elapsed physical time for an object to travel along the orbit between the two advance points. I believe that the advance will vanish in the limit where $R_{IN} \to R_{0UT}$ (difficult to establish using numerical techniques).

The orbit for a photon moving in the gravitational field defined above is a subject of interest—gravitational lensing. For a photon, Eq. (K.8) is modified by setting $m = 0$. One can use the techniques of section VI(F) to obtain the orbit equation,

$$d\phi / dr = \pm[r^4 R_{impact}{}^{-2}(1-\mathrm{V})(1+\mathrm{V})^{-1} - r^2]^{-1/2}, \qquad \text{(K.11)}$$

where $A = R_{impact}\,\mathrm{E}\,c^{-1}$ and $\mathrm{E} = h\nu(r=\infty)$. There is a turning point, R_{turn}, where $d\phi/dr = \infty$. The tiny repulsive bump can be neglected, so all the gravitational bending of the photon path would occur for $r < R_0$ where R_0 is a finite radius for which $\mathrm{V}(R_0) = 0$.

V is negligible for $r > R_0$, so the path of a photon is a straight line outside of the canister. A photon (leaving a source at infinity) that intersects the canister has an inbound line. If there was

no gravitational field within the canister, this inbound line would have a point for which the distance to the center of the canister would be a minimum—the impact parameter, R_{impact}. The gravitational field bends the photon path so that it will exit the canister following a straight outbound line (with the same impact parameter) ending at an observer (at infinity). The locations of the source, observer, and the canister-center define a plane on which the photon moves. The angle between the inbound and outbound lines is the deflection angle (θ_D). θ_D is positive when the photon bends toward the canister center.

The deflection angle is calculated in the following manner,

$$\begin{aligned} \psi &= \int_{R_{turn}}^{R_0} dr\left[r^4 R_{impact}{}^{-2}(1-\mathrm{V})(1+\mathrm{V})^{-1} - r^2 \right]^{-1/2}, \\ \omega &= \sin^{-1}(R_{impact} / R_0), \\ \theta_D &= 2(\psi + \omega) - \pi. \end{aligned} \qquad \text{(K.12)}$$

For a given canister gravitation-field, θ_D is a function only of R_{impact}. Eq. (K.12) is accurate to first order of V. That level of accuracy should be sufficient for most applications. Higher accuracy is obtained by using Eq. (4.14). Fig.5 (section VI(F)) illustrates an example solution of Eq. (K.12)

APPENDIX L: ENVIRONMENT OF THE MILKY WAY MASSIVE BOUNDARY OBJECT

This Appendix reviews the information necessary to calculate the evolution model in VI(G). An important topic is the distribution and identity of local matter in the vicinity of the MW MBO (massive boundary object)—the environment. The local matter consists of stars, stellar cinders, and gas. The local matter and the MBO are the source of the local gravitational field, and the MBO grows by ingesting local matter through collisions of local matter with the MBO boundary—described in VI(G).

At the start (local gravity turned on), there is no MBO or cinders, just stars and gas. I believe the following model defines the environment at the start:

$$\rho(r) = \rho_0 \text{ if } r < R_{ENV} \text{ else} = \rho_1(r), \tag{L.1}$$

where $R_{ENV} = 20$ LY and $\rho_1(R_{ENV})$ is small compared to ρ_0. Furthermore, $\rho_1(r)$ trends to zero as *r* increases. The environment is all the matter within R_{ENV}.

The rational for Eq. (L.1) comes from the fact that the orbits of stars within the environment *all have the same period*. Thus, one finds that the mixing time of randomly moving stars can be very brief (several thousand years) if ρ_0 is large enough—excellent mixing inside the environment and poor mixing outside. A star at a specific position in the environment could have come from anywhere within the environment a short time ago. Furthermore, there is little matter moving across the edge of the environment. The mass of matter within the environment is very large compared to the mass of the MBO at the end of summer. Thus, one should assume that the mass of the environment is independent of physical time. Evolution is just the change of the populations of different types of local matter within the environment.

There is scant information about the environment and the MBO. $\mathrm{M}_{MBO}(\tau_{TODAY}) = 4.1\mathrm{x}10^6$ solar and an estimate [16], $\rho_{Stars}(\tau_{TODAY}) = 2.6\mathrm{x}10^7$ solar per cubic parsec. The density of cinders and gas today is unknown—not observable. The census today of star types and masses within the environment is poorly understood.

An evolution model must start with a census of (Kelvin contraction) stars of different masses and an average gas density (hydrogen and helium) shortly after the on transition of local gravity. After fusion is turned on, the census will include oxygen and carbon (gasses) and cinders of all types and masses. One will know the various initial censuses are correct only if the two (today) numbers above are produced—a very weak constraint.

The Newtonian gravitational potential within the environment is well approximated by the following:

$$\mathrm{V}(r,\tau) = -M_{MGO}(\tau) G r^{-1} + 2\pi G \rho_0 r^2 + \text{ constant.} \tag{L.2}$$

Eq. (L.2) is used to define the partial orbits of stars and cinders between random gravitational deflections (when they pass close by other objects). As the MBO grows, the partial orbits of projectiles near the MBO will change so that the probability of the projectiles having tiny angular momentum (necessary for a collision with the MBO boundary) is reduced. This detail is important

because a model that neglects the MBO term of Eq. (L,2) always ends up with all the mass of the environment in the MBO a billion years after today—no stars of cinders left.

The most important evolution factor for stars is their lifetime (a function of the mass of the star). Every star will eventually suffer a spectacular transition into a cinder and gas. The gas will be recycled into (a smaller number of) new stars. During summer, the environment object census will have a growing population of (unobservable) cinders and a shrinking population of stars. The rate of growth of the MBO is different for cinders versus stars. Thus, the changing populations will directly influence the growth of the MW MBO.

This information does not make the model of VI(G) easier to achieve, but it does tell us which topics need the most study.

APPENDIX M: CROSSING THE BOUNDARY

It is very easy for matter to cross the boundary from the inside. In that case, the boundary provides an impulse to increase the radial velocity of particles on the way out. The impulse can be calculated using the techniques of section VI(A). The solution gives the radial velocity for matter crossing the boundary,

$$\begin{aligned} &\beta(V) = \mathrm{v}_r(V)c^{-1}, \\ &\beta(V) = \pm Q(-V)^{-1/2} Q(V)[Q(V)^{-1} - \Delta]^{1/2}, \end{aligned} \tag{M.1}$$

where $Q(V)$ is given by Eq. (6.10) through Eq. (6.13). Δ is well approximated as a constant across the boundary even during the (slow) gravitational transition in spring and fall. Eq. (7.9) leads one to a relation between the velocity on each side of the boundary,

$$\begin{aligned} &\beta_>{}^2 = a + d\beta_<{}^2, \\ &a = \varepsilon_{SL}(2+\varepsilon_{SL})^{-1}[1-\varepsilon_{SL}(1.5\delta_{SL})^{-1}], \\ &d = (2\varepsilon_{SL})^2(3\delta_{SL})^{-2}, \end{aligned} \tag{M.2}$$

where $c\beta_>$ is the velocity on the $V > -1$ side of the boundary, and $c\beta_<$ is the velocity on the $V < -1$ side. The *universal constants*, ε_{SL} and δ_{SL}, are tabulated in Appendix Z. The betas are positive for outbound matter and negative for inbound matter. Since the impulse is a function only of universal constants, Eq. (7.10) can be applied to a wide range of problems. Furthermore, ε_{SL} and δ_{SL} are determined by other considerations, e.g., the mass gap between the heaviest CCNS and the lightest CCBO. In some problems, $\beta_<$ can be neglected and $\beta_> = \pm 0.3590$—a very robust impulse.

A brief review is useful here. Eq. (7.9) results from the Hamilton-Jacobi equations—valid for a *single particle* orbiting in a *static central field*. The boundary thickness is roughly one meter—small compared to the radius of the boundary (approximated by a Dirac delta function). The orbit for a particle at rest at a large distance from the center of the source (R_0) has three outcomes. If the (conserved) angular momentum (A) is larger than a small value (A_0), the particle will simply bounce off of the boundary and return to R_0 (but not where it started). If $A_0 > A > A_1$ (where A_1 is very tiny), the particle will cross the boundary. Once inside, the particle will travel near the boundary and recross the boundary (returning to R_0). If $A_1 > A$, the particle will cross the boundary and collide with the source—be absorbed by the source. The probability of a particle being absorbed is very small (if heading toward the source from outside the boundary). Conversely, the probability of a particle escaping from within the boundary is very good. The radial component of the particle velocity is subject to Eq. (7.9).

The application of Eq. (M.2) depends on the problem. For core collapse, all the matter is moving with a radial velocity across the boundary, so Eq. (M.2) applies to the whole mass. For an accretion of diffuse gas, there would be a *pressure discontinuity across the boundary*.

It is important to note that a boundary is ephemeral if the material source of the gravitational potential is a function of physical time. A boundary can move, disappear, or appear in a new place. If $V_{00}(\tau, x, y, z) = -1$, *then that point lies on a boundary*.

APPENDIX N: CMBA DETAILS

A group of γ_{cmb} are represented by a transverse wave train crossing a canister. The train lies in a plane in polar coordinates that corresponds to $\theta = \pi/2$ (equator). Eq. (4.20) leads one to the equation of motion for the transverse potential in the weak field limit:

$$\begin{aligned} &A_\theta(\tau, r, \phi) = r^{-1} \sin\psi(\tau, r, \phi), \\ &\psi(\tau, r, \phi) = 2\pi\lambda(\tau, r, \phi)^{-1}\xi(\tau, r, \phi), \\ &0 = c^{-2}\partial_\tau[(1-V)\partial_\tau\psi] - \partial_r[(1+U)\partial_r\psi] - r^{-2}\partial^2\psi/\partial\phi^2, \end{aligned} \tag{N.1}$$

Where $\xi = 0$ at the center of the wave train (moving at velocity *c*). The gravitational potential $U = V$, and use Eq. (F.3) to get $V(r,\tau) = 2c^{-2}\mathcal{A}_N(r,\tau)$. The time dependence of Eq. (F.3) *for this problem* comes from substituting from Appendix Z the following in the summations of Eq. (F.3): $Z_1 = -958,\ Z_2 = 958,\ Z_3 = 0$ when τ is before the early spring gravitational change, and $Z_1 = -657,\ Z_2 = 958,\ Z_3 = -300$ after. The transition, Eq. (7.5), is completed during a tiny fraction of the millions of years for a γ_{cmb} to travel within a canister, so the transition can be treated as instantaneous. Gravitational fields change everywhere in the universe at the same time.

One can neglect the small deflection of the wave train (and the train is very short compared to the size of the canister), so it is useful to use the approximate coordinates:

$$\begin{aligned} &r = (x^2 + {y_{IP}}^2)^{1/2}, \\ &\partial_r = x\, r^{-1}\, \partial_x, \\ &\partial_\varphi = -y_{IP}\, \partial_x, \\ &\psi = 2\pi\, \lambda(\tau, x)^{-1}\, (x - c\tau), \end{aligned} \tag{N.2}$$

where y_{IP} is a constant (the impact parameter) for a γ_{cmb} moving from $x = -\infty$ to $x = \infty$. The center of the canister is at $x = 0 = y_{IP}$. Next, use Eq. (N.2) to convert polar derivatives into *x* derivatives:

$$\begin{aligned} &\partial_r\psi = x\, r^{-1}\, \partial_x\psi, \\ &\partial_\varphi\psi = -y_{IP}\, \partial_x\psi, \\ &\partial_r(\partial_r\psi) = x^2 r^{-2}\partial_x(\partial_x\psi) + x{y_{IP}}^2 r^{-4}(\partial_x\psi), \\ &\partial_\varphi(\partial_\varphi\psi) = {y_{IP}}^2\partial_x(\partial_x\psi). \end{aligned} \tag{N.3}$$

Next, evaluate the items of Eq. (N.3) in the limit where $x - c\tau \to 0$ (the center of the wave train):

$$\begin{aligned}
&\partial_\tau \psi \to -2\pi c\lambda^{-1},\\
&\partial_\tau(\partial_\tau \psi) \to 4\pi c\lambda^{-2}\partial_\tau \lambda,\\
&\partial_x \psi \to 2\pi\lambda^{-1},\\
&\partial_x(\partial_x \psi) \to -4\pi\lambda^{-2}\partial_x \lambda.
\end{aligned} \tag{N.4}$$

Finally, insert the items of Eq. (N.3) into the third element of Eq. (N.1) and then insert the limits of Eq. (N.4) into that equation to obtain the following,

$$0 = 0.5(c^{-1}\partial_\tau V - \partial_x V) + (1-V)c^{-1}\lambda^{-1}\partial_\tau \lambda + (1+V+{y_{IP}}^2 r^{-2})\lambda^{-1}\partial_x \lambda\ . \tag{N.5}$$

Eq. (N.5) is subject to some constraints. Let τ_{GC} be the universal time when local gravity is turned on in early spring—the same for every canister in the universe. $V(\tau, r)$ is a discontinuous function of r when $\tau = \tau_{GC}$, and λ must be discontinuous as well (otherwise $\partial_\tau V = 0$). Furthermore, Eq. (N.5) is evaluated at the center of the (tiny) wave train, so $\partial_\tau \lambda = c\partial_x \lambda$ (except at the discontinuity).

It is necessary to divide the solution of Eq. (N.5) into two ranges which are connected by the discontinuity. The gravitational potential has two time-independent ranges, $V_<(r)$ and $V_>(r)$. $V_<$ is calculated as described after Eq, (N.1) using the $Z_3 = 0$ set, and $V_>$ uses the $Z_3 = -300$ set. The discontinuity is at $x_{GC} = c\tau_{GC}$ or $r_{GC} = ({x_{GC}}^2 + {y_{IP}}^2)^{1/2}$. $V_<$ is used for $x < x_{GC}$ and $V_>$ after. The time derivative of V is infinite at the discontinuity as is the time derivative of λ. These infinities must cancel, so one requires the time derivatives of Eq. (N.5) to vanish at the discontinuity,

$$0 = 0.5\partial_\tau V + (1-V)\partial_\tau \ln\lambda \quad (\tau = \tau_{GC}). \tag{N.6}$$

Define $\xi = (1+V)^{1/2}$, then Eq. (N.6) is equivalent to $\xi\lambda$ being continuous at the discontinuity. Thus, one finds the following condition across the discontinuity,

$$\lambda_>(x_{GC}) = \lambda_<(x_{GC})(1+V_<(r_{GC}))^{1/2}(1+V_>(r_{GC}))^{-1/2}. \tag{N.7}$$

The equations for λ are as follows,

$$\begin{aligned}
&\partial \ln\lambda_< / \partial x = \left[\ (\partial V_<(r)/\partial x)\{4 + 2{y_{IP}}^2 r^{-2}\}^{-1}\right]\ \ x < x_{GC},\\
&\partial \ln\lambda_> / \partial x = \left[(\partial V_>(r)/\partial x)\{4 + 2{y_{IP}}^2 r^{-2}\}^{-1}\right]\ \ x > x_{GC},\\
&[\ ] \text{ evaluated at } r = ({x}^2 + {y_{IP}}^2)^{1/2}.
\end{aligned} \tag{N.8}$$

The initial condition is $x = -\infty$ and $\lambda_< = \lambda(-\infty)$. The integration continues until $x = x_{GC}$ and $\lambda_<(x_{GC})$ is known. The next initial condition is $x = x_{GC}$ and $\lambda_> = \lambda_>(x_{GC})$—known from Eq. (N.7). The integration continues until $x = \infty$, and $\lambda(\infty) = \lambda_>(\infty)$.

There are only two parameters that determine both $V_<(r)$ and $V_>(r)$, the total mass of the canister (solar masses) and the radius of the MDGO at the center of the canister (light years). There are only two additional parameters y_{IP} (light years) and x_{GC} (light years) required to determine the desired result $T(\infty)/T(-\infty) = \lambda(-\infty)/\lambda(\infty)$.

There is an illustrative exact solution of Eq. (N.8) when $y_{IP} = 0$ as follows:

$$\begin{aligned} &T(\infty)/T(-\infty) = f_> / f_<, \\ &f_< = (1+V_<(x_{GC}))^{1/2} \exp(V_<(x_{GC})/4), \\ &f_> = (1+V_>(x_{GC}))^{1/2} \exp(V_>(x_{GC})/4). \end{aligned} \tag{N.9}$$

Since the gravitational potentials are functions of *r*, it follows that the temperature ratio is a function of $x_{GC}{}^2$ (symmetric). The same holds for the solution of Eq. (N.8).

Numerical solutions of Eq. (N.8) are obtained through a routine program. The temperature ratio, $[T(\infty) - T(-\infty)]/T(-\infty)$, is a function of two parameters for the canister gravitational-potential, and two photon-parameters relative to the location of the center of the canister.

The canister parameters are R_{MGO} (light years) and M_{CAN} (solar masses). The dimensionless potential, *V*, is calculated using Eq. (F.3), where $V = \mathrm{V}_{00} = 2c^{-2}\mathcal{A}_N$, and $\mathrm{R}_E = R_{MGO}$. For use of Eq. (F.2), $\mathrm{M} = M_{CAN}$. The photon parameters are y_{IP} (light years) and x_{GC} (light years). A photon that arrives at my telescope is assumed to travel along a straight line from a distant point much farther away than the center of the canister. y_{IP} is the minimum distance of the photon from the center of the canister along that path (impact parameter). x_{GC} is the distance of the photon along that path (relative to the point of closest approach to the canister center) when the gravitational change occurred. x_{GC} is negative if the gravitational change occurred before the photon reached closest approach, else positive.

Figs. N1 and N2 illustrate some solutions for $M_{CAN} = 10^{14}$ solar masses and $R_{MGO} = 2\mathrm{x}10^6$ light years—the same values used in Fig. 4 for deflections due to gravitational lensing. The temperature ratio is directly proportional to M_{CAN}.

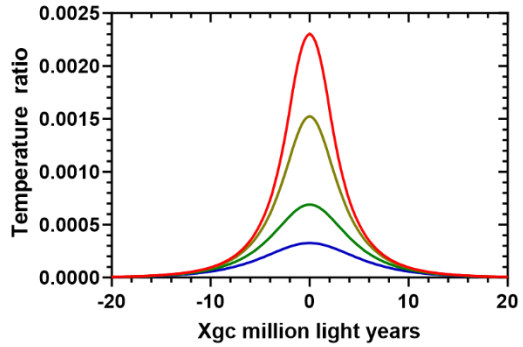

Figure N.1. DeltaT/T for four values of Yip (0 mly red, 2 mly grey, 4 mly green, and 6 mly blue).

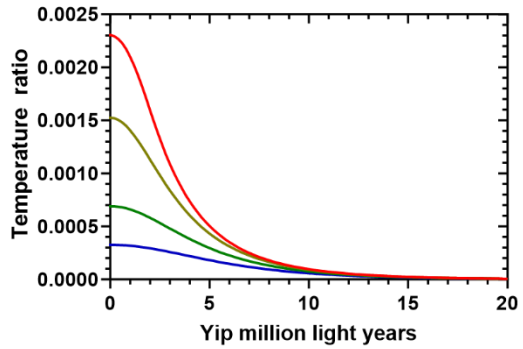

Figure N.2. DeltaT/T for four values of Xgc (0 mly red, 2 mly grey, 4 mly green, and 6 mly blue).

Assume that my telescope can accurately measure the temperature of infrared radiation (T_{OBS}) coming from a sufficiently small area of the sky (excellent resolution and response). In that case, the temperature ratio is $(T_{OBS}/T_{CMB})-1$, where $T_{CMB} = 2.725\ ^{\circ}\mathrm{k}$. The slightly warm object of Fig. N2 is large (diameter about 3.4 arc minutes) compared to a galaxy at that distance. I believe that there would be about 10 of these objects per square degree. A carefully designed collection of baseline interferometers could possibly see these objects behind the foreground point sources. No existing observatory is sufficient. A sky map of these objects would lead to a more accurate value for the average density of matter throughout the universe.

The polarization of the photons (described above) is perpendicular to the plane of photon motion. There are also photons with polarization lying in the plane of motion. The model used above for canister gravitation includes the mass of the canister galaxies (as if they were smeared out in the central gas ball). Thus, the model-canister gravitational potential is a function of *r*, and there would be no net polarization for the whole object.

Galaxies in a canister follow random orbits. A more realistic model would include a gravitational perturbation that reflects the location of the galaxies at the time of interest,

$$V \to V(r) + \delta V(r,\theta,\phi). \qquad \text{(N.10)}$$

The potential of Eq. (N.10) will give rise to a small net polarization for the whole object. A sky map of the object polarizations would not yield any significant information (due to randomness).

A foreground canister is transparent for photons from the object canisters of interest—no change of temperature. However, foreground canisters can deflect photons as per Fig. 4. A bundle of temperature-shifted photons from a small area of the object canister (a pixel) will be subjected to many small random deflections from foreground canisters on their journey to my telescope. The end result is that the size and temperature profile of an object-canister image should be weakly affected by the foreground canisters, but the position of the center of the image could be measurably displaced on the sky map. The apparent position of the center of a canister of interest undergoes a step (in a random walk) with each interception with a foreground canister. This randomness would not affect the average density of universal matter.

APPENDIX Y: ACRONYMS

Acronym	Meaning	Appears
CCBO	Core collapse boundary object	VI(D)
CCNS	Core collapse neutron star	VI(D)
CMB	Cosmic microwave background	III
CMBA	Cosmic microwave background anisotropy	VIII(A)
EOS	Equation of state	VI(D)
EDM	Electron degenerate matter	VI(D)
EM	Electro-magnetic	III(B)
GR	General relativity	Intro
GRLCDM	General relativity-lambda cold dark matter_	Intro
JWST	James Webb space telescope	Intro
LCDM	Lambda cold dark matter	Intro
LD	Lagrangian density	II
LDM	Lagrangian density of matter	III
LIGO	Laser interferometer gravitational-wave observatory	VIII(B)
LSS	Large scale structure	V(D)
LY	Light Years	V(F)
MBO	Massive boundary object	VI(D)
MDGO	Massive diffuse gas object	VI(C)
MLY	Million light years	V
MW	Milky way (galaxy)	VI(G)
MWC	Milky way canister	V(H)
NC	(The) new cosmology	II(C)
NCNG	This document	Intro
NDM	Neutron degenerate matter	VI(D)
NG	(The) new gravity	IV
NIP	(Electron-flavor) neutrino-initiated process	VII(C.3)
PDT	Pressure, density, (and) temperature	VII(E)
PNM	Proton-neutron matter	VI(D)
RE	Radiation expansion (era)	VII(E)
RN	Reverse nucleosynthesis	VII(C)
TGE	Thermodynamic gas expansion (era)	VII(E)
TOV	Tolman, Oppenheimer, Volkoff (equation)	VI(D)
TSE	Thermodynamic supercritical expansion (era)	VII(E)
UDG	Ultra diffuse galaxy	V(J)
VLA	Very large array (Karl G. Jansky very large array)	V(F)
WD	White dwarf (star)	VI(D)

APPENDIX Z: THE STANDARD MODEL OF NCNG UNIVERSAL CONSTANTS

Standard model 10/1/2023

This list is a work in progress, and it will depend upon internal constraints and observations that are not suspect. The model of 10/1/2023 is the first version based on plausible constraints and some reliable observations. There are more than a thousand equations in this document and some of them create a framework of internal constraints. Thus, *the 43 values below are not independent*. Examples of an internal constraint are Eq. (2.25) or Eq. (5.7).

Our ability to make observations about winter will always be extremely limited. One must rely on plausible requirements during the transitions.

Five symbols below have no model value. Three control the magnitude of energy density for the apex and epoch fields relative to the energy density of matter—unknown but must be very large. Two are related to summer values via Eq. (7.8) for use in RN.

Symbol	Association	Appears at	Model Value	Dimensions
L_{ax}	apex field	Eq. (2.3)	9.0	10^9 LY
d_1^{ax}	apex field	Eq. (2.24)	1.400253	
d_2^{ax}	apex field	Eq. (2.24)	-0.9284	
d_3^{ax}	apex field	Eq. (2.24)	0.473062	
$\mathcal{N}_{ax}$	apex field	Eq. (2.2)		
α_W^{ax}	apex field	Eq. (2.24)	0.03	
L_{ep}	epoch field	Eq. (2.10)		meters
$\mathcal{N}_{ep}$	epoch field	Eq. (2.10)		
λ_{ep}	epoch field	Eq. (2.12)	-0.013232	
β_{ep}	epoch field	Eq. (2.12)	0.25	
Γ_{ep}	epoch field	Eq. (2.12)	55700	
a_{ep}	epoch field	Eq. (2.11)	0.35	
A_{ep}	epoch field	Eq. (2.12)	0.99936	
β_{cl}	clock	Eq. (3.29)	118	
κ_{cl}	clock	Eq. (3.29)	0.1	
Γ_{cl}	clock	Eq. (3.29)	10	
N_q	NG	Eq. (4.1)	5	
L_{g1}	NG	Eq. (4.1)	1.118	10^6 LY
Z_{g1}	NG	Eq. (4.1)	-657	
Z_{g2}	NG	Eq. (4.1)	960	

Z_{g3}	NG	Eq. (4.1)	-405.1	
Z_{g4}	NG	Eq. (4.1)	110	
Z_{g5}	NG	Eq. (4.1)	-6.9	
$Q(1,1)$	NG	Eq. (5.9)	1	
$Q(2,1)$	NG	Eq. (5.9)	1.30832	
$Q(3,1)$	NG	Eq. (5.9)	0.99091	
$Q(4,1)$	NG	Eq. (5.9)	-1.59420	
$Q(5,1)$	NG	Eq. (5.9)	0	
Γ_{SL}	Strong limit	Eq. (6.10)	>>1	
ε_{SL}	Strong limit	Eq. (6.12)	0.487	
γ_{SL}	Strong limit	Eq. (6.12)	2.8×10^{-7}	
δ_{SL}	Strong limit	Eq. (6.12)	0.95	
α_{SL}	Strong limit	Eq. (6.12)	-1.9	
N_{RN}	RN	Eq. (7.2)	0.25	meters^{-3}
ϑ_{RN}	RN	Eq. (7.2)	0.125	
m_{ve}^{W}	RN	Eq. (7.4)	30	Mev
m_{W}^{W}	RN	Eq. (7.4)		Mev
g_{W}^{W}	RN	Eq. (7.4)		g_{W}^{S}
x_{Bera}	Bubble era	II(C)	10^{-5}	
Γ_{W}	Weak changes	Eq. (7.4)	10000	
E_{W}	Weak changes	Eq. (7.4)	0.013	
Γ_{G}	Gravity changes	Eq. (7.5)	10000	
E_{G}	Gravity changes	Eq. (7.5)	0.015	